Spring 2010

The stereochemistry of selected supramolecular complexes of cucurbiturils and the effect of homogeneous equilibria and electron transfer of the guest

Arumugam Thangavel

Department: Chemistry

THE STEREOCHEMISTRY OF SELECTED SUPRAMOLECULAR COMPLEXES OF CUCURBITURILS AND THE EFFECT ON HOMOGENEOUS EQUILIBRIA AND ELECTRON TRANSFER OF THE GUEST

by

ARUMUGAM THANGAVEL

A DISSERTATION

Presented to the Faculty of the Graduate School of the

MISSOURI UNIVERSITY OF SCIENCE AND TECHNOLOGY

In Partial Fulfillment of the Requirements for the Degree

DOCTOR OF PHILOSOPHY

in

CHEMISTRY

2010

Approved by

Chariklia Sotiriou-Leventis, Advisor

Nicholas Leventis, Co-Advisor

Pericles Stavropoulos

Jeffrey G. Winiarz

K. Chandrashekhara

ACKNOWLEDGMENTS

I would like to thank all the people who have helped me either directly or indirectly during my graduate study. My special thanks go to my advisor Prof. Chariklia Sotiriou-Leventis and co-advisor Prof. Nicholas Leventis for their guidance during my research. I was motivated by the knowledge and enthusiasm they have towards research. Many times, I was amazed seeing how they approach a problem with an entirely different view, which is a good training for a novice researcher like myself.

Many thanks to Prof. Abdel Monem M. Rawashdeh, visiting scholar to Prof. Chariklia Sotiriou-Leventis's group in the summer of 2007 for his starting me in the cucurbituril project.

I also like to thank Prof. Pericles Stavropoulos, Prof. Jeffrey G. Winiarz, and Prof. K. Chandrashekhara for serving as my advisory committee members.

I owe my thanks to Dr. Bidhu Bhusan Das for his support during my stay at Pondicherry Central University, where I was molded for the position that I have today.

My gratitude goes to Mr. Ravysandirane, Ms. Renuka Ananthakumar, and Ms. Couppammalle who have been my teachers and mentors for many years.

Mr. Joe Counsil, Mr. Mike Meyer, Mr. Dean Lenz, Mr. Dave Satterfield, and my labmates whose direct help on my experiments is greatly appreciated. Also thanks go to Ms. Carol Rodman, Ms. Donna Riggs and Ms. Kathy Eudaly for their help on administrative matters.

My deepest gratitude goes to all my family members. Without their encouragement and support, it would have been impossible for me to finish up this work.

Financial support from NSF, Missouri Research Board and the Department of Chemistry, Missouri S&T is greatly appreciated.

TABLE OF CONTENTS

LIST OF ILLUSTRATIONS

Page

SECTION

LIST OF SCHEMES

Page

LIST OF TABLES

NOMENCLATURE

Symbol	Description
δ	Chemical shift
ε	Molar absorptivity coefficient
ΔA	Absorbance change
Å	Angstrom
A	Absorbance
BP	Benzoyl Pyrydinium
CB[n]	Cucurbit[n]uril
CD	Cyclodextrin
CT	Charge transfer
CV	Cyclic voltammetry
DAAQ	*N.N'*-dimethyl-2,6-diaza-9,10-anthraquinonediium bis(tetrafluoroborate)
DMSO	Dimethyl sulfoxide
DNA	Deoxyribonucleic acid
$E_{1/2}$	Half-wave potential
ESI-MS	Electrospray Ionization Mass Spectrometry
F	Faraday constant
ΔG	Gibbs free energy
J	Coupling constant
λ	Wavelength
M	Molar (mole/liter)
m/z	Mass to charge ratio
MS	Mass Spectroscopy
MV^{2+}	Methylviologen (1.1`-dimethyl-4.4`-bipyridinium)
NMR	Nuclear Magnetic Resonance
ppm	Parts per million
Pylm	Pyrylium
UV	Ultraviolet

SECTION

1. INTRODUCTION

During the early 1970's, D. J. Cram, J. M. Lehn, and C. J. Pedersen conducted research that became a platform for the development of supramolecular chemistry. They were honored with a Nobel prize in 1987 for this contribution.[1-5]

Lehn, Jean-Marie defines supramolecular chemistry as "the chemistry of the intermolecular bond, covering the structures and functions of the entities formed by the association of two or more chemical species." [3,5] Vogtle, Fritz notes that, "In contrast to molecular chemistry, which is predominately based upon the covalent bonding of atoms, supramolecular chemistry is based upon intermolecular interactions (Figure1.1), i.e., on the association of two or more building blocks, which are held together by intermolecular bond." [6,7]

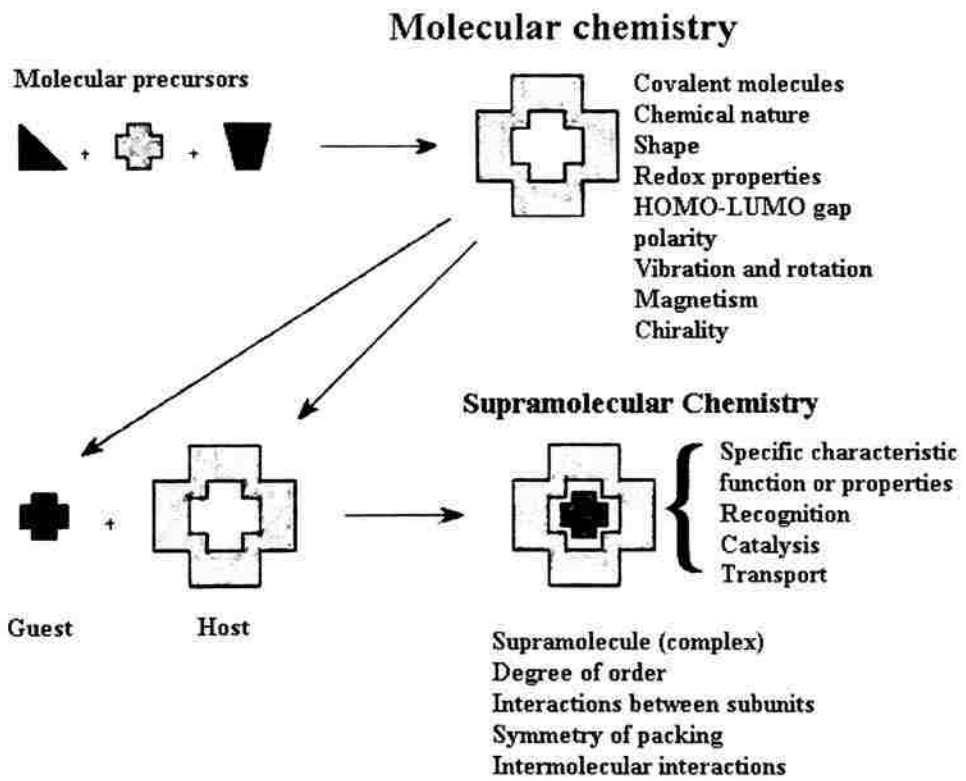

Figure 1.1. Comparison between supramolecular chemistry and molecular chemistry.

Table 1.1. Summary of supramolecular interactions.

Interaction	Strength (kJ mol^{-1})	Example
Ion-Ion	200-300	$Bu_4N^+Cl^-$
Ion-Dipole	50-200	sodium[15]crown-5
Dipole-dipole	5-50	acetone
Hydrogen Bonding	4-120	water
Cation-π	5-80	K^+ in benzene
π- π	0-50	benzene and graphite
Van der waals	<5 but variable depending on surface area	Ar, packing in molecular crystal
Hydrophobic	Related to solvent-solvent interaction energy	cyclodextrin inclusion compounds

1.2.1. Electrostatic Interactions. Electrostatic interactions occur between charged species that may be either attractive between opposite charges, or repulsive between similar charges. Those attractive and repulsive forces play an important role in molecular recognition since their magnitude is higher than those of other noncovalent interactions, and depends on the nature of the medium and the dielectric constant of the molecules. For example, a greater extent of electrostatic interaction is observed in more hydrophobic environments with smaller dielectric constants.

Based on the nature of the charges, electrostatic interactions can be subclassified into one of the following categories:

1.2.1.1. Ion-ion interactions. Ion-ion interactions are nondirectional, and their strength is comparable to the strength of covalent bonding. Examples include sodium chloride, and tetrabutylammonium chloride (Figure 1.2).

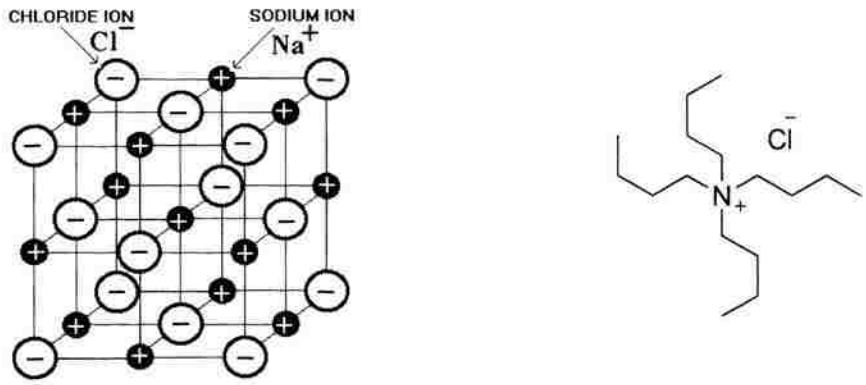

a b

Figure 1.2. a. Sodium chloride ionic lattice; b. tetrabutylammonium chloride.

1.2.1.2. Ion-dipole interactions. Ion-dipole interactions are weaker than ion-ion interactions. They are directional, meaning that the two species that bear the ion and the dipole charges must align favorably to develop such interactions. Examples include hydrated sodium ion, and sodium crown ether complex (Figure 1.3).

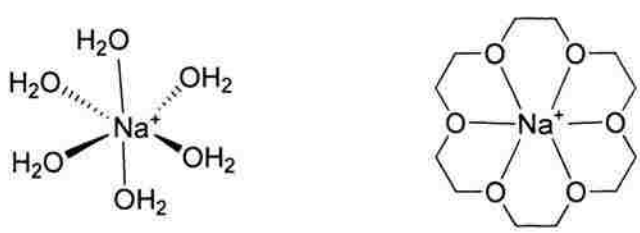

a b

Figure 1.3. a. Hydrated sodium ion; b. Sodium crown ether complex.

1.2.2.3. Weak hydrogen bonding. The strength of weak hydrogen bonding is less than 12 kJ mole-1 and highly nonlinear. It occurs with unconventional donor and acceptor atoms. When such atoms are in the vicinity of highly electronegative atoms, they become more acidic, encouraging weak hydrogen bonding interactions. Examples include the interaction of C-H---N of nitromethane and C-H---O of pyridyl crown ether (Figure 1.7).[13]

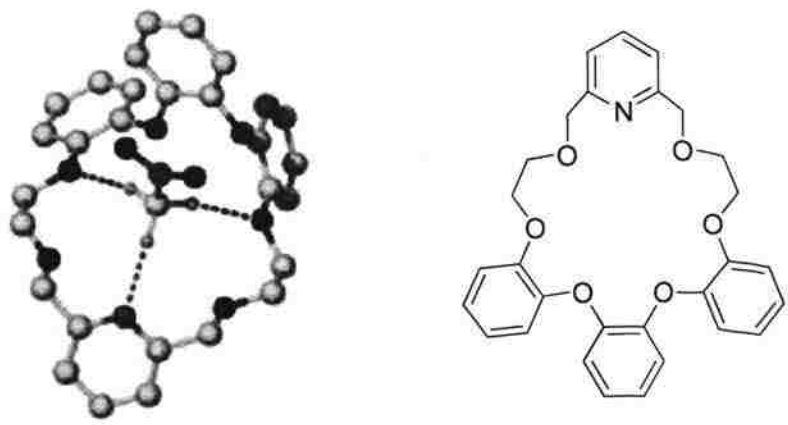

a b

Figure 1.7. a. Crystal structure of pyridyl crown ether and nitromethane; b. Pyridyl crown ether.

1.2.3. Van der Waals Interactions.[14] When two neutral molecules are close to one another, their interaction creates induced dipoles through the uneven distribution of electrons. Those induced dipoles align in such a way that the partial negative charge of one is attracted by the partial positive charge of another. The interaction between those charges creates a London interaction (Figure 1.8). The strength of this interaction depends on the polarizability of atoms, the distance between two molecules, and other factors.

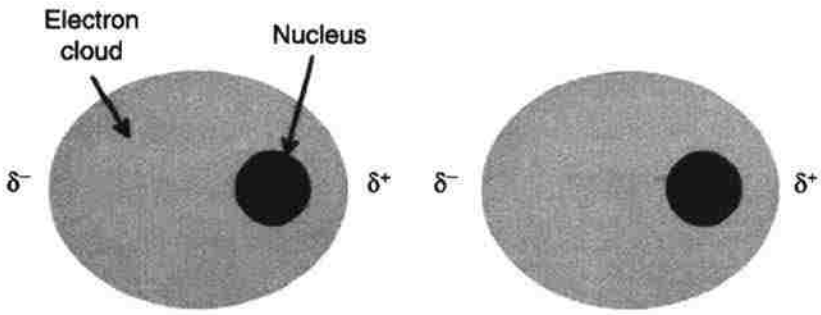

Figure 1.8. A London interaction between two inert atoms.

1.2.4. Hydrophobic Effect.[15] Hydrophobic interactions take place, for example, between hydrocarbons or hydrocarbon-like groups in water. A representative example is chloroform in water. This interaction is responsible for the aggregation of hydrophobic molecules in water. Hydrophobic groups aggregate together to minimize the number of water molecules with which they interact. This interaction plays a vital role in molecular recognition in aqueous media. On the basis of the thermodynamics, hydrophobic interactions can be divided into two types.

1.2.4.1. Enthalpic hydrophobic effect. Most hosts (e.g., cyclodextrins, cucurbit[n]urils, and cyclophanes) have hydrophobic cavities. The water inside then interacts weakly with the cavity. When a guest forms a complex with the host, it expels water from the cavity and interacts strongly with it. The expelled water interacts with bulk water, which is more favorable than the interaction of water with the hydrophobic cavity (Figure 1.9).

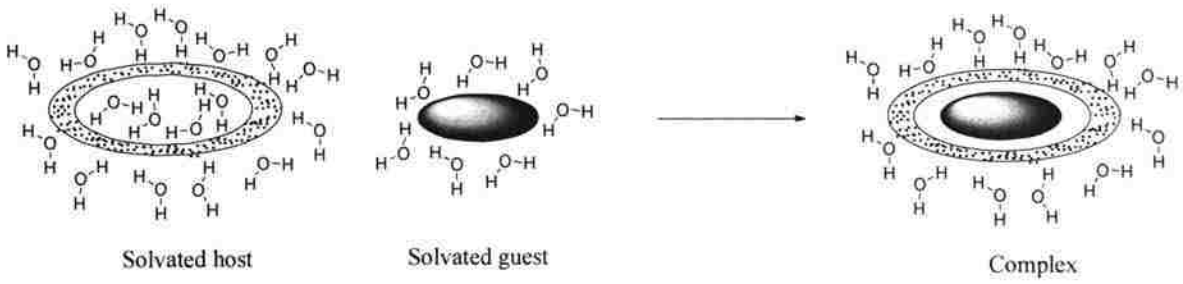

Figure 1.9. Hydrophobic binding of guest and host in aqueous solution.

1.2.4.2. Entropic hydrophobic effect. In bulk water, the host and guest occupy their positions, when they form complex, one of them, either host or guest, leaves its position, which creates a hole or void that is filled by water (Figure 1.10). By minimizing the disruption in the bulk water, creation of such a hole favors the entropic gain, which lowers the overall free energy of the system.

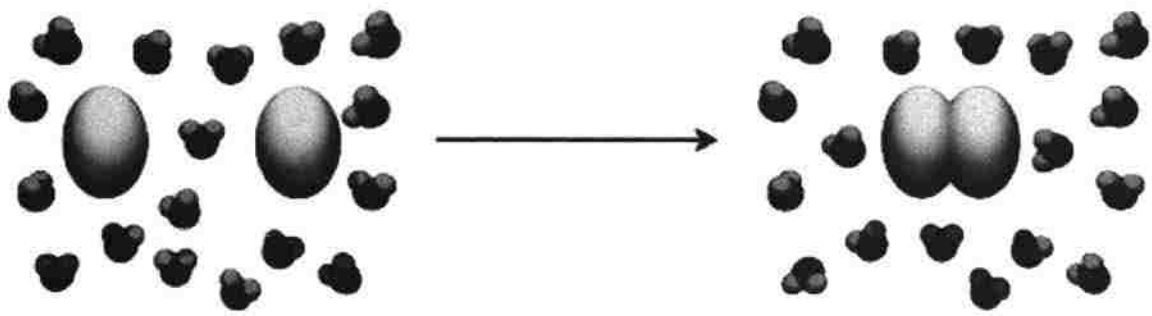

Figure 1.10. Creating hole or void during the complex formation.

1.3. TYPES OF HOST

The host-guest chemistry, which is also refer to as molecular recognition, is the foundation of supramolecular chemistry. The molecule or atom that is recognized is called a guest, and the molecule that recognizes the guest is called a host.[16,17] Examples of hosts include crown ethers, cyclodextrins, calixarenes, and cucurbit[n]urils.

1.3.1 Crown Ethers.[18] Crown ethers were the first artificial hosts developed by Pedersen, when he was working on bisphenol-A, and noted a reaction byproduct,18a which upon examination, showed some interesting chemical properties, for example an ability to increase the solubility of potassium permanganate in benzene. Also the solubility of that compound in alcohol was enhanced in the presence of Na+. Based on those properties, Pedersen postulated a structure in which all the oxygen atoms coordinate with metal and has the shape of a crown (Figure 1.11).

a b

Figure 1.11. a. 18-Crown-6-ether; b. Sodium -18-crown-6-ether complex.

1.3.2. Cyclodextrin.[19,20] Cyclodextrins are naturally occurring macrocyclic host consisting of repeating units of saccharides (Figure 1.12). In nature, they are synthesized from starch, a macrocyclic glycopyranoside, by an enzymatic reaction. Based on the number of repeating units such as six, seven, or eight, it is refered to α, β, or γ cyclodextrin, respectively.

Cyclodextrin has a primary alcohol on the narrow side of the molecule and a secondary alcohol on the wider side. The alcohol functionality of cyclodextrin can be tailored to meet specific requirements, which makes it a versatile host (Figure 1.13). The cavity is hydrophobic as the macrocycle has no polar groups inside. Based on the cavity size (Figure 1.12c), cyclodextrin can accommodate various guests ranging from inorganic ions to gases molecules.[21]

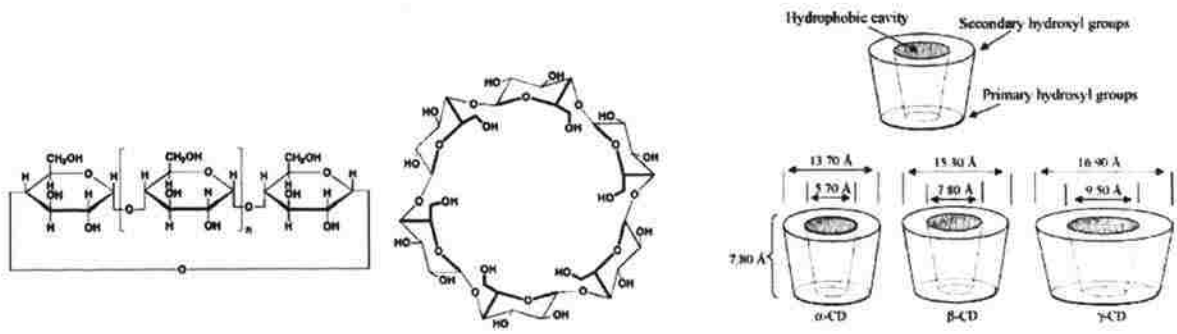

a b c

Figure 1.12. a. α-Cyclodextrin; b. Bird-eye view of α-cyclodextrin; c. Physical properties of cyclodextrin.

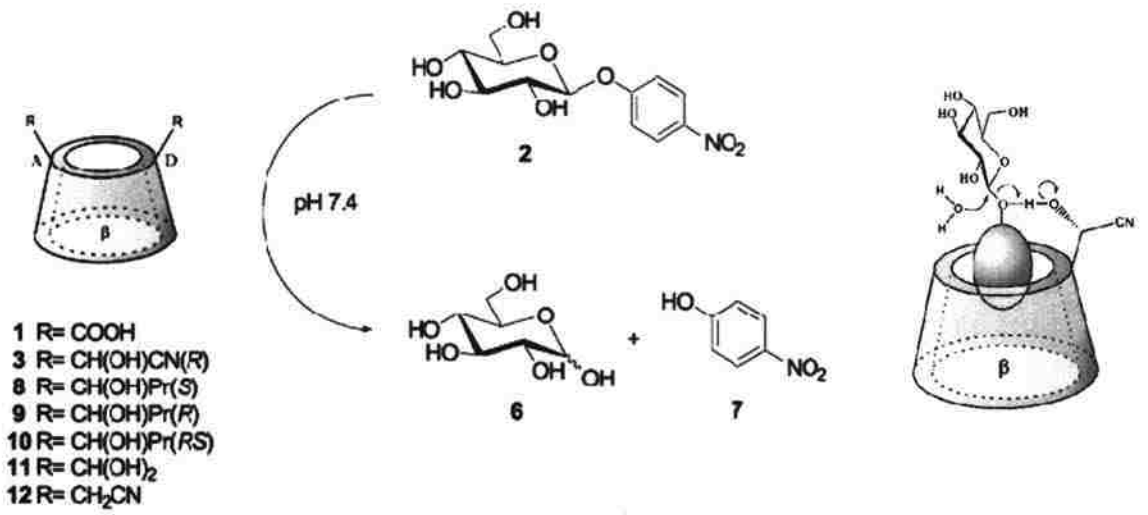

a b

Figure 1.13. a. Glycoside hydrolysis catalysed by the modified-cyclodextrin;
b. Proposed mechanism for the catalysis.

1.3.3. Calixarene.[23] Calixarene, a chalice-shaped molecule (Figure 1.14), was synthesized by interconnecting the phenols with methylene bridges. Calixarene adopts various conformations and its cavity size depends on the number of repeating phenolic groups.

a b

Figure 1.14. a. *Calix carater* shape of *p-t-butyl*-calix[4]arene; b. *p-t-butyl*-calix[4]arene.

A calixarene with four phenolic groups adopts the following conformations (Figure 1.15), each with its own guest selectivity:[24]

- All the phenols point in the same directions, a condition known as cone conformation.
- One phenol points opposite to the others (partial cone structure).
- Alternate phenols point in opposite directions (1, 3 alternative).
- Adjacent phenols point in opposite directions (1, 2 alternative).

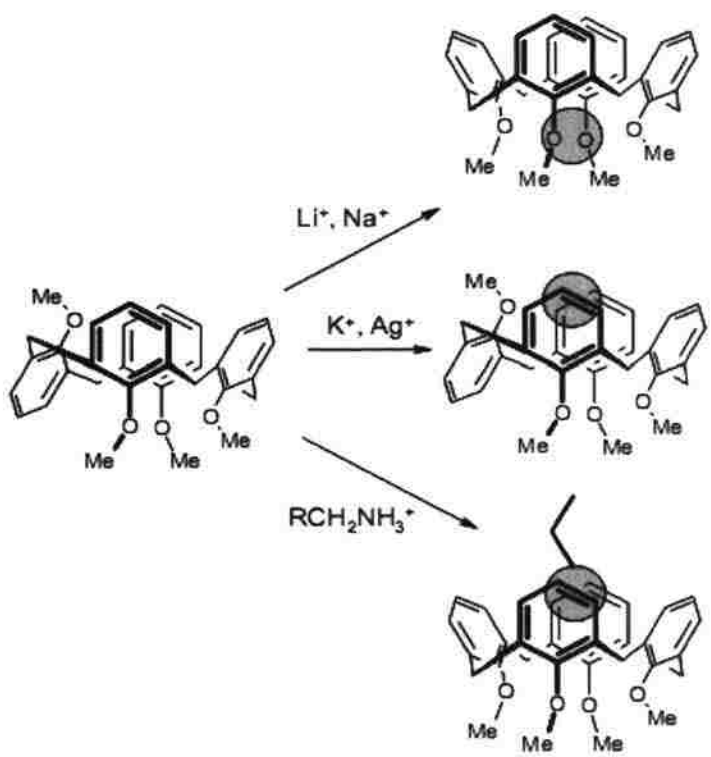

Figure 1.15. Conformational changes with guest selectivity of calixarene.

1.3.4. Cucurbit[n]uril.[25-27] (pronounced 'kyu ker bit yur eel'[25]). Cucurbituril is a self-assembled macrocyclic compound formed from the condensation of formaldehyde and glycoluril. That condensation was first reported in 1905, when Behrend published an article on condensation products of glycoluril and formaldehyde.[28] Due to a lack of suitable analytical methods, Behrend could not characterize the product other than to provide the molecular formula. Later in 1981, Mock et al., characterized the condensation product of glycoluril and formaldehyde and reported the chemical structure by single-crystal X-ray crystallography.[29] The crystal structure revealed a pumpkin-shaped molecule with D_{6h} symmetry and repeating units of six glycolurils and a cavity of approximately 5.5 Å in diameter.[29] That cavity is accessible both sides through the carbonyl portals, which have a diameter of about 4 Å. Although comparable to cyclodextrin in terms of cavity hydrophobicity, and guest binding, cucurbit[n]uril differs in its symmetrical structure with two identical portals.

1.3.4.1. Synthesis. In 2000, Kim et al.,[31] after modifying the original reaction conditions, were able to synthesize cucurbit[n]uril, with n = 5-9. (Scheme 1.1)

Scheme 1.1. Synthesis of cucurbit[n]urils (**CB[n]**).

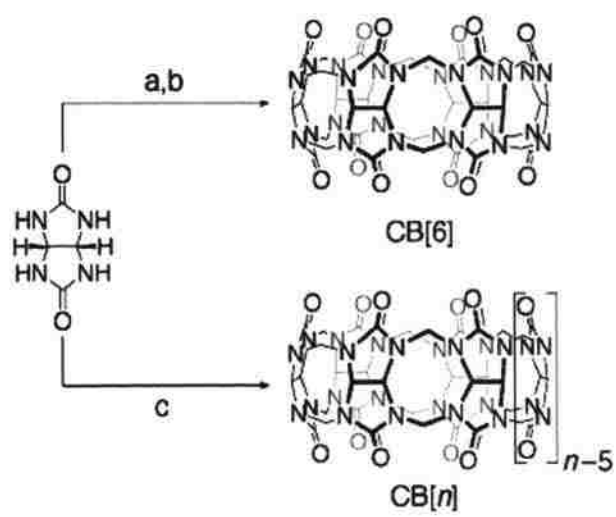

a. CH_2O, HCl, heat; b. H_2SO_4; c. CH_2O, HCl, 100 ^{O}C, 18 h

Based on the reaction conditions (Scheme 1.1), the ratio of homologues such as CB[n], n=6,7,8,10 can be controlled. More drastic conditions like high temperature and higher pH favor cucurbit[6]uril, and milder conditions such as low temperatures and an extended period of heating with dilute acid produce cucurbit[7]uril. Day et al.,[36] investigated the reaction mechanism and the reaction conditions for the optimized synthesis of various homologues. Pure homologues can be separated by repeated recrystallizations.

1.3.4.2. Fundamental properties. [26,27] All homologues of CB[n] have been thoroughly characterized by single X-ray crystallography (Figure1.16), NMR, MS, and other techniques. Table 1.2, shows the physical properties of cucurbiturils in comparison with cyclodextrins.

The properties of reported cucurbit[n]uril were later extensively studied by numerous research groups.[29,31,32,36] The cucurbituril homologues form stable complex with metals, hydrocarbons, protonated alkyl, and aryl amines.[32-35] Although the guest binding properties are comparable to those of other hosts such as crown ethers, cyclodextrins, calixarenes, cucubit[n]uril has its own drawback of poor solubility in most of the common solvents except in neutral or acidified aqueous solutions. Furthermore, it is difficult to functionalize it. These two drawbacks were later addressed by Kim et al.[33]

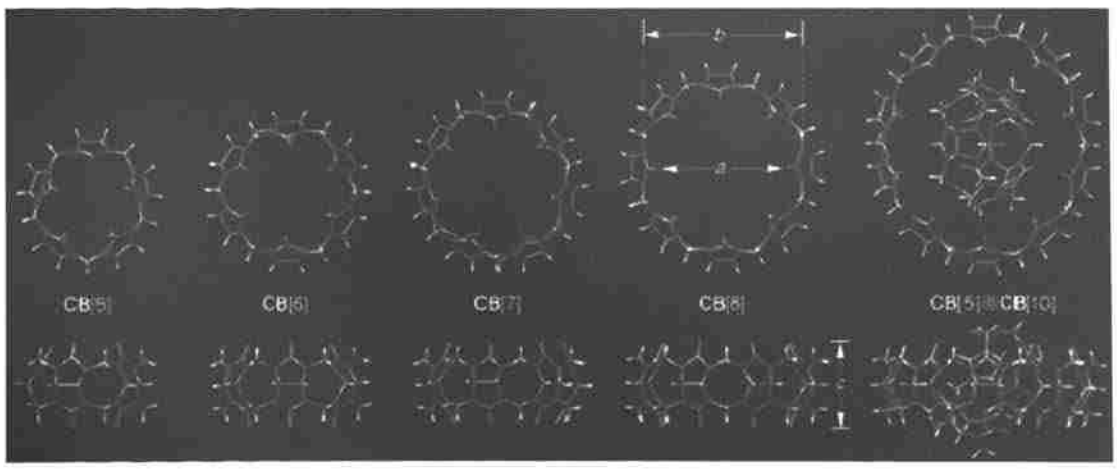

Figure 1.16. X-ray crystallography structures of cucurbituril homologues.

Table 1.2. Physical properties of cucurbituril homologues in comparison with cyclodextrins.

	M_r	a [Å][a]	b [Å][a]	c [Å][a]	V [Å^3]	s_{H2O} [mM]	Stability [°C]	pK_a
CB[5]	830	2.4	4.4	9.1	82	20-30	>420	
CB[6]	996	3.9	5.8	9.1	164	0.018	425	3.02
CB[7]	1163	5.4	7.3	9.1	279	20-30	370	
CB[8]	1329	6.9	8.8	9.1	479	<0.01	>420	
CB[10]	1661	9.0-11.0	10.7-12.6	9.1	-	-	-	-
α-CD	972	4.7	5.3	7.9	174	149	297	12.332
β-CD	1135	6.0	6.5	7.9	262	16	314	12.202
Υ-CD	1297	7.5	8.3	7.9	427	178	293	12.081

[a] The values quoted for a, b, and c for **CB[*n*]** take into account the van der Waals radii of the relevant atoms. [b] Determined from the X-ray structure of the **CB[5]@CB[10]** complex.

1.3.4.3. CB[n] as a host. Cucurbituril homologues have the characteristic features of a hydrophobic cavity and carbonyl groups on both sides of the portals. The polar carbonyl groups are responsible for hydrogen bonding and ion-dipole interactions with the guest. Because of these two interactions, the carbonyl groups interact with positively charged guest molecules. Figure 1.17 shows different binding interactions between **CB[6]** and hexanediammonium ion during the complex formation.

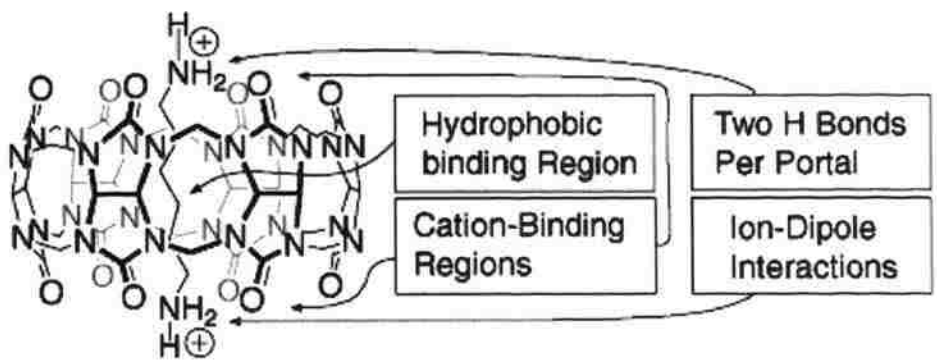

Figure 1.17. Various intercations between **CB[6]** and hexanediammonium ion.

Because of differences in the cavity size, cucurbituril homologues show different binding properties for guest molecules.[37-40] Smaller **CB[5]** cavity promotes binding with relatively small guest molecules, whereas the bigger cavity of **CB[10]** can accept **CB[5]** as a guest.[41] Figure 1.18 lists guest that can be included for each host.

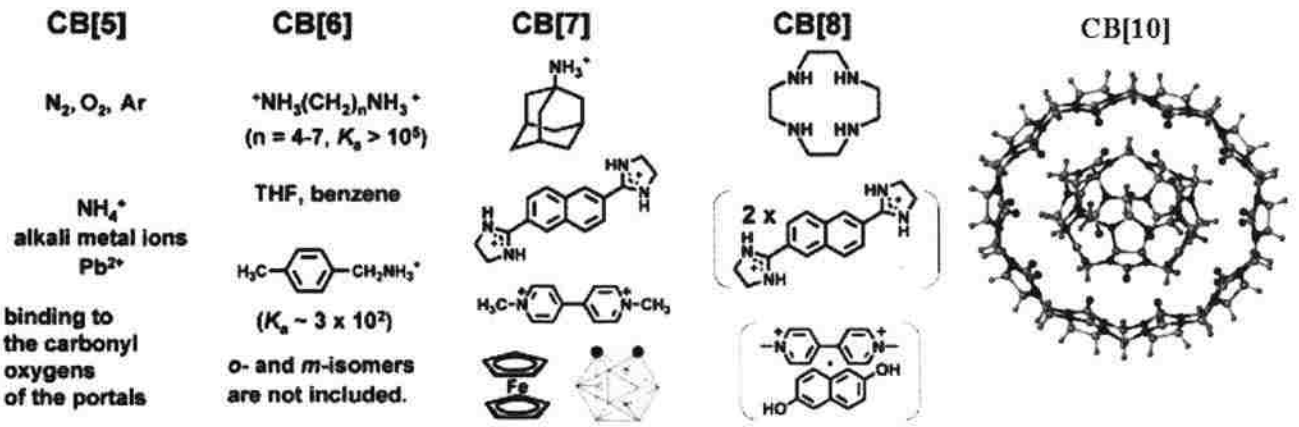

Figure 1.18. List of representative guests for corresponding hosts.

1.3.4.4. Applications of the host-guest chemistry of CB[n]. Recently, many researchers have focused on artificial devices such as molecular machines, and molecular shuttles that can be controlled by external stimulii such as light,[30] heat,[54] pH,[55]and redox process.[56] The following examples show that the inclusion complex of cucurbit[n]uril can also be used for such applications.

Based on the size of the guest, the larger cavity of **CB[8]** can sometimes accommodate two guest molecules.[42-27] For example, Kim et al.,[47,48] reported the formation of a 1:1:1 charge transfer complex between methyl viologen (MV) and 2,6-dihydroxynaphthalene ($Np(OH)_2$). The formation of this complex is favored by the enhancement of the charge transfer between electron-deficient methylviologen and electron-rich 2,6-dihydroxynapthalene inside the hydrophobic cavity of **CB[8]**. This ternary CB[8]:MV:$Np(OH)_2$ complex could be used as a tool to design various supramolecular vehicles, molecular loops, molecular necklace, and so on.

The following example[49] shows that the 1:1:1 complex of CB[8]:MV:$Np(OH)_2$ could be used to design a molecular loop (Figures 1.19 & 1.20), that could be controlled by an external stimuli.

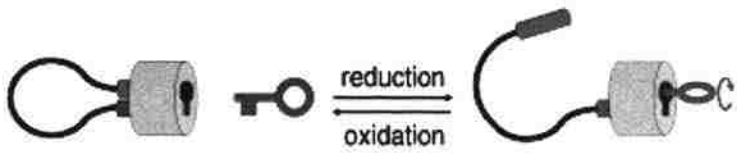

Figure 1.19. Pictorial representation of molecular loop.

Under external redox stimulus, the ternary 1:1:1 complex of CB[8]:MV:$Np(OH)_2$ forms one electron reduced complex of ($MV^{+\cdot}$: $Np(OH)_2$ inside the **CB[8]** cavity (Figure 21a). This complex reacts with free $MV^{+\cdot}$ and undergoes a guest exchange, expelling $Np(OH)_2$ while simultaneously taking up a second $MV^{+\cdot}$ from outside. This simultaneous exclusion of $Np(OH)_2$ and inclusion $MV^{+\cdot}$ leads to the formation of a 1:1:1 $MV^{+\cdot}$: $MV^{+\cdot}$:CB[8] complex.

The redox controlled guest exchange permits the design of molecular machines that can be switched on and off, i.e., locked and unlocked, by external redox stimulus. Figure 21b demonstrates the concept of such redox driven molecular machines.

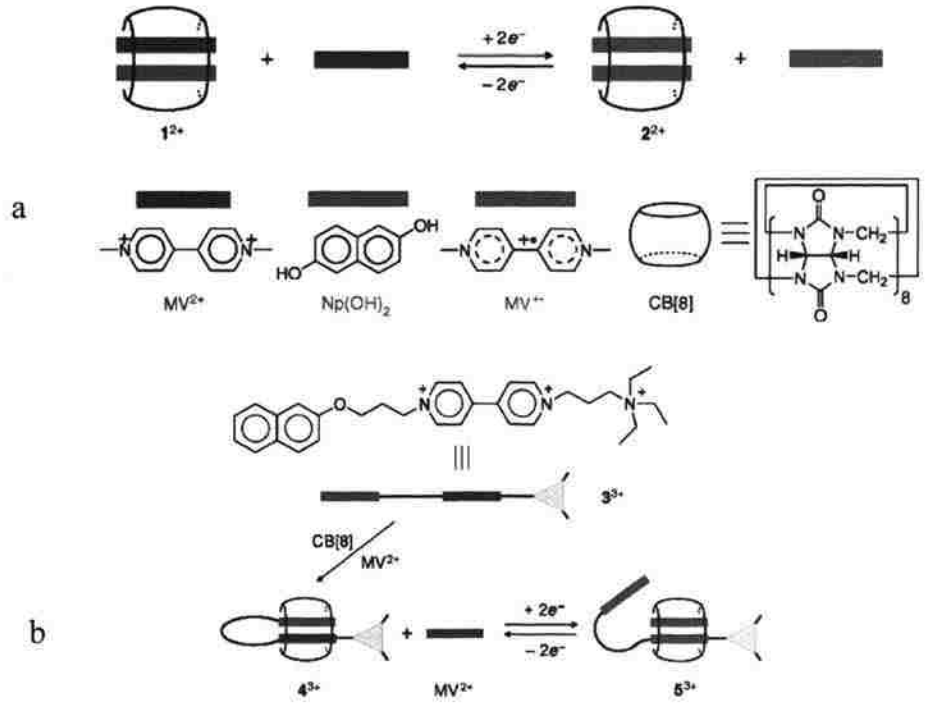

Figure 1.20. a. Redox controlled guest exchange; b. Redox controlled molecular loop.

Sun et al.,[50] reported the first inclusion complex of a molecule (Ru^{2+}-MV^{2+}-$Np(OH)_2$) containing $Ru(bpy)_3$, 2,6-dihydroxynaphthalene and viologen as components with **CB[8]**. The Ru^{2+}-MV^{2+}-$Np(OH)_2$ forms 1:1 complex with **CB[8]** by back folding the naphthalene residue and inserting together with the viologen part of the molecule (Figure 1.21). The back folding of naphthalene and the formation of a complex with viologen is favored due to the charge transfer complex between electron-rich naphthalene and electron-deficient viologen. When this complex is irradiated with visible light, it produces photo induced radical $MV^{+\cdot}$, which becomes a partner radical by accompanying the naphthalene part of the molecule that is stabilized by the **CB[8]** cavity.

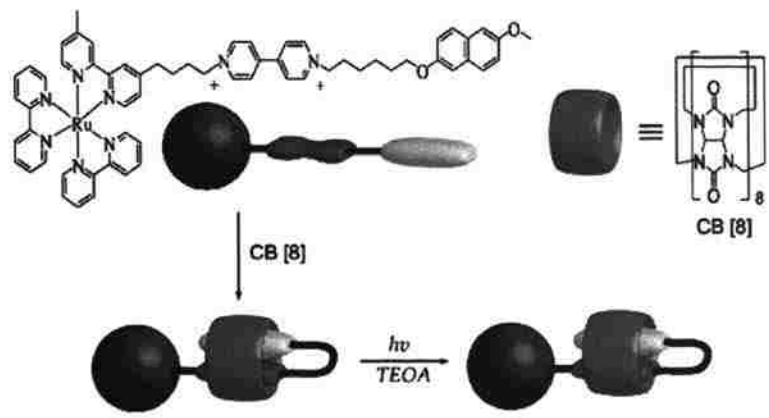

Figure 1. 21. Graphical representation of inclusion of a molecule (Ru^{2+}-MV^{2+}-$Np(OH)_2$) with **CB[8]**.

Aqueous electrochemical studies of free Ru^{2+}-MV^{2+}-$Np(OH)_2$ compound (Figure 1.22) shows that the peak potentials corresponding to the redox couples MV^{2+} /$MV^{+\cdot}$, and $MV^{+\cdot}$ /MV^0 are -0.519 V and -0.841 V, respectively. Following inclusion with **CB[8]**, they changed to -0.66 and -1.23 V, respectively. In addition, the half wave oxidation potential of Ru^{3+}/ Ru^{2+} is shifted from 1.047 to 1.052 V. These studies confirm that when the viologen part of a molecule is inside the **CB[8]**, it experiences stabilization from the cavity, which in turn makes it harder to reduce. Furthermore, the charge transfer complex formed between naphthalene and the viologen inside the **CB[8]** makes it also harder to reduce. Electrochemical studies also show that, because of the inclusion, the electron transfer from the excited state of $Ru(bpy)_3$ to the viologen part of a molecule is also slightly harder to reduce after the molecule is included inside the cavity.

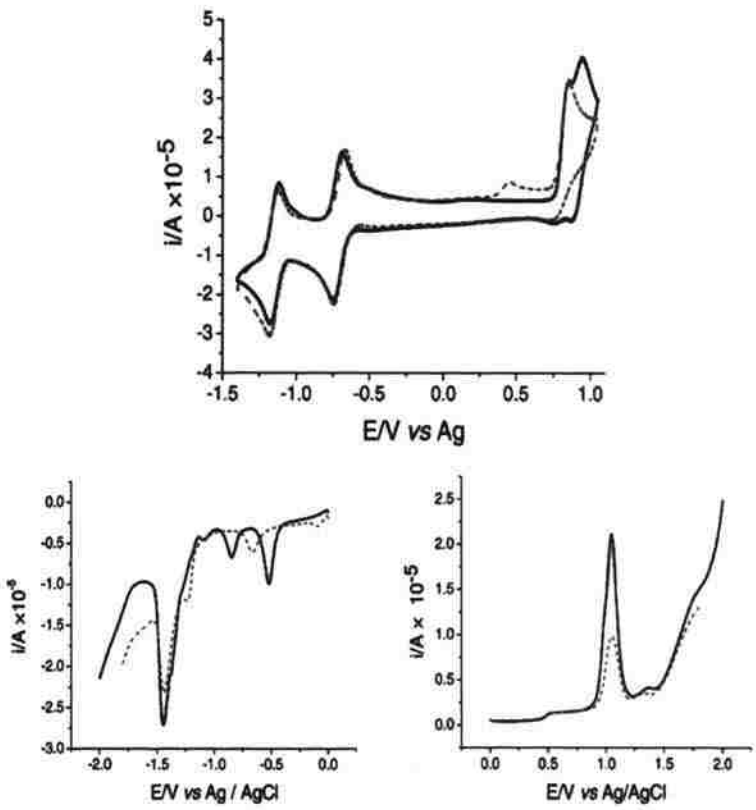

Figure 1.22. Electrochemical study of a molecule (Ru^{2+}-MV^{2+}-$Np(OH)_2$) with **CB[8]**. (Top) Cyclic voltammograms of triad (Ru^{2+}-MV^{2+}-$Np(OH)_2$) (1×10^{-3} M) (solid line) and ligand (MV^{2+}-$Np(OH)_2$) (1×10^{-3} M) (dashed line) in acetonitrile, with Bu_4NPF_6 (0.1 M) as supporting electrolyte, glassy carbon disk as working electrode, and $Ag/AgNO_3$ as reference electrode. (Bottom) Differential pulse voltammograms of triad Ru^{2+}-MV^{2+}-$Np(OH)_2$ (1×10^{-3} M) in the absence (solid line) and in the presence (dashed line) of 1 equiv of **CB[8]** in 0.1 M phosphate buffered (pH 7.0) water solution at room temperature, glassy carbon as working electrode, Ag/AgCl as reference electrode; scan rate: v = 0.1 V s^{-1}.

Steinke et al.,[51] used **CB[6]** as a reaction vessel for 1,3-dipolar cycloaddition that leads to the formation of self-threading polyrotaxane. The **CB[6]** catalysis of the 1,3-dipolar cycloaddition (Figure 1.23) facilitates simultaneous polymerization and rotaxane formation. The author used ammonium azido and ammonium alkyne as the reactant for 1,3-dipolar addition, which may have formed a 1:2 inclusion complex with **CB[6]**. As the reaction proceeded, the stoichiometry changed to 1:1 and formed self-threading polyrotaxane (Figure 1.24). The use of **CB[6]** as a catalyst has the advantage of not only catalyzing the reaction, but also assisting the self-threading of the monomers.

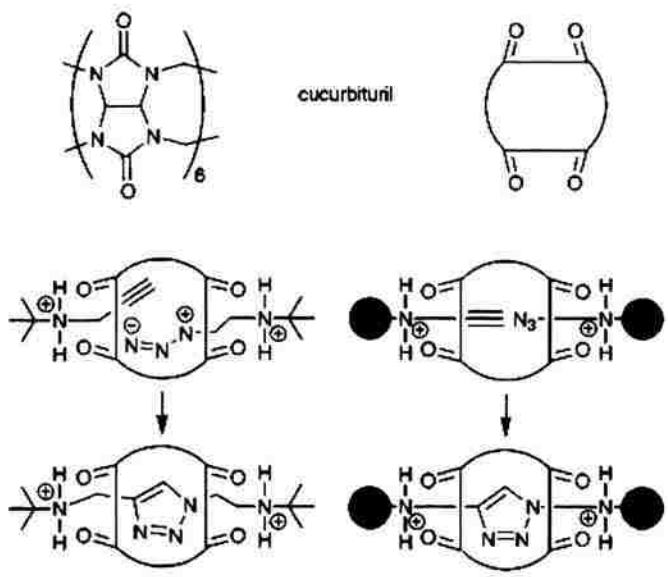

Figure 1.23. 1,3-Dipolar cycloaddition catalyzed by **CB[6]**.

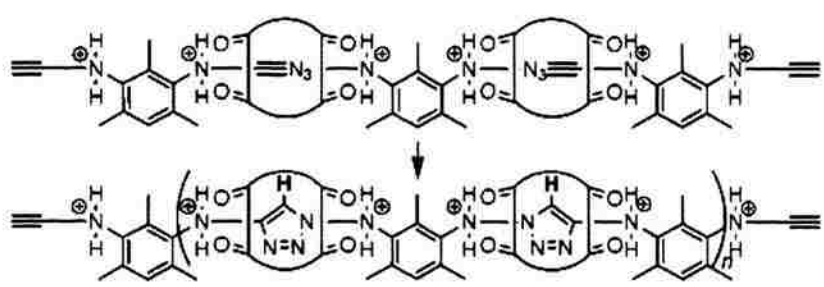

Figure 1.24. Formation of polyrotaxane catalysed by **CB[6]**.

Under normal aqueous conditions, the photo excitation of diazastilbene produces mainly hydration, isomerization, and cyclization; [52,53] it does not result in the dimerization of the reactant because the three former reactions are significantly faster than dimerization. To revert the reaction, i.e., to get dimerization as the main reaction product, Kim et al., showed that **CB[8]** can be used as templating agent that forms a 1:2 inclusion complex with diazastilbene.

Kim et al.,[52] reported that **CB[8]** mediates the photo dimerization of aminostilbene in water (Figure 1.25). The protonated aminostilbene under aqueous conditions forms a 2:1 inclusion complex with **CB[8].** The two aminostilbenes can preorient either syn- or anti- inside the **CB[8]**. Because of the geometrical restriction of **CB[8]**, the two aminostilbenes form the most stable conformation of a syn adduct. Upon photoirradiation for 30 min, the syn–adduct undergoes a [2+2] photocycloaddition, and subsequent base treatment produces the tetrakis (4-aminophenyl)cyclobutane.

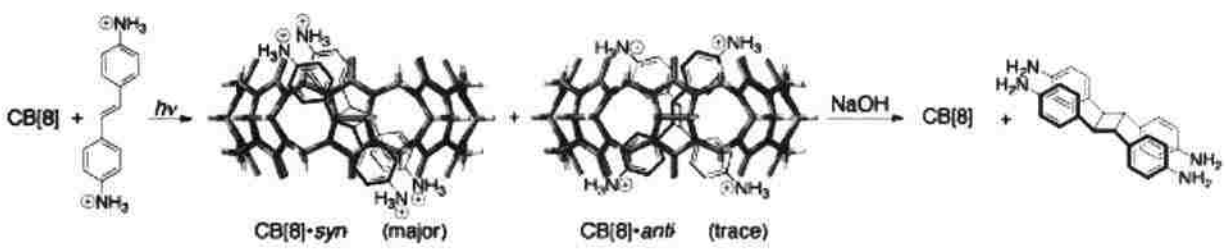

Figure 1. 25. CB[8] mediated dimerization of diaminostilbene in water.

By following Kim's work, Maddipatla et al.,[53] showed that diazastilbene also behaves exactly like aminostilbene. It forms a 2:1 complex with **CB[8]**, which upon photoirradiation undergoes [2+2] cycloaddition and forms *syn* as a major and *anti* as a minor product (Figure 1.26). Because of the templating effect of **CB[8]**, there was no hydration, isomerization or cyclization.

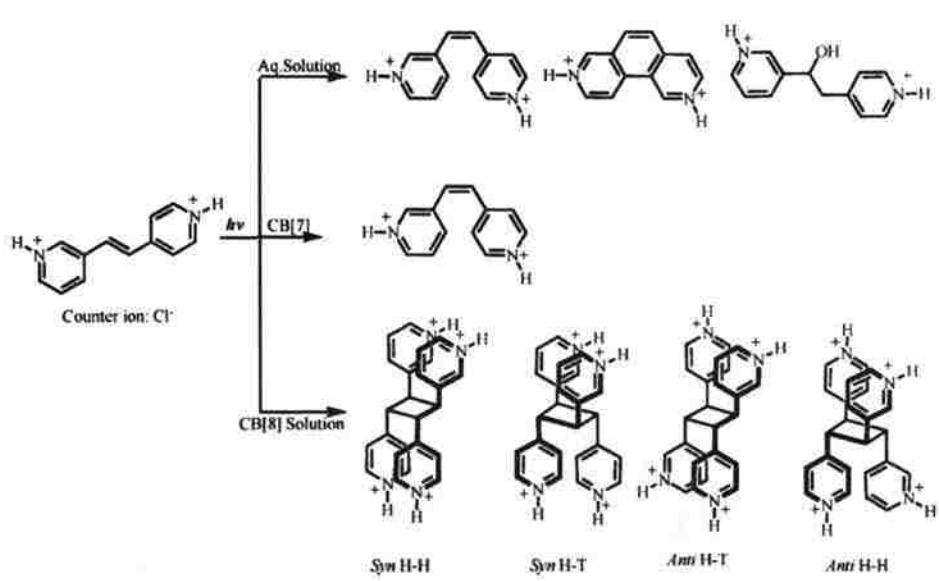

Figure 1.26. CB[8] mediated dimerization of diazastilbene in water.

This dissertation examines the interactions of cucurbiturils as barrel-shaped hosts, having a hydrophobic cavity, with substituted benzoylpyrydinium (papers 1&2), diazaanthraquinonediium (paper 3), and phenypyrylium (paper 4) cations as guests.

Paper 1 focuses on the use of **CB[7]** to control the keto to *gem*-diol equilibrium. In water, *N*-methyl-4-(*p*-substituted benzoyl)pyridinium cations exist in equilibrium with their hydrated forms (*gem*-diols). In the presence of **CB[7]**, the keto form is favored by **CB[7]** over the *gem*-diol as the former is more hydrophobic in nature. This selective inclusion causes the shift of keto to *gem*-diol equilibrium toward the keto form, meaning that the stabilization through hydrophobic interactions of the benzoyl group in the **CB[7]** cavity exceeds the hydrogen bonding stabilization of the *gem*-diol in the aqueous environment.

In Paper 2, since substituted benzoylpyrydinium cations have two redox centers that show chemically reversible electron transfer in aprotic solvents such as DMSO, it became possible to measure rates of heterogeneous e-transfer by simple cyclic voltammetry. It was found that 4-benzoylpyrydinium cations undergo heterogeneous electron transfer simultaneously from both their free state as well as their complexes with **CB[7]**.

Paper 3 is in the same line of work as paper I. The quinone to *gem*-diol equilibrium was studied using *N,N'*-dimethyl-2,6-diaza-9,10-anthraquinonediium dication as a guest and **CB[7]** as a host. In neutral aqueous media, quinone exists as an aggregate in equilibrium with its *gem*-diol. In acidic media (pH<1), the aggregate breaks up and also the quinone to *gem*-diol equilibrium is shifted exclusively towards the keto form. Under both neutral and acidic conditions, the quinone form undergoes inclusion with **CB[7]** by slow exchange in which both free and **CB[7]**-intercalated forms were observed by ^{1}H NMR.

In paper 4, in order to understand the role of guest's size, shape and size of cavity during the inclusion process, 2,6-disubsituted-4-phenylpyrylium cations **(Pylm)** were chosen as guests with **CB[7]** and **CB[8]** as hosts. The size and shape of the guest was modified by changing the nature of the substituents at 2 and 6 positions (**Me, *i*Pr, Ph, *t*-Bu**). These pyryliums exist as dimers in water and as such they enter the **CB[8]** cavity (2:1 complexes) whereas with **CB[7]**, the dimers break up forming 1:1 complexes. All

PAPER

1. CONTROL OF THE KETONE TO *GEM*-DIOL EQUILIBRIUM BY HOST-GUEST INTERACTIONS

Abdel Monem M. Rawashdeh,[1,†] Arumugam Thangavel,[2] Chariklia Sotiriou-Leventis[*,2] and Nicholas Leventis[*,2]

1. Department of Chemistry, Yarmouk University, Irbid, 211-63, Jordan.

2. Department of Chemistry, Missouri University of Science and Technology[‡], Rolla, MO 65409, U.S.A.

leventis@mst.edu; cslevent@mst.edu

1.1. ABSTRACT

In water, *N*-methyl-4-(*p*-substituted benzoyl)pyridinium cations, **BP-X**, exist in equilibrium with their hydrated forms (*gem*-diols), whose concentrations depend on the para-substituent (-X). In the presence of cucurbit[7]uril (**CB[7]**), the benzoyl group shows a preference for the **CB[7]** cavity (Figure 1.1), and the ketone to *gem*-diol equilibrium is shifted towards the keto form, meaning that the stabilization realized through hydrophobic interactions of the benzoyl group in the **CB[7]** cavity exceeds the hydrogen-bonding stabilization of the *gem*-diols in the aqueous environment.

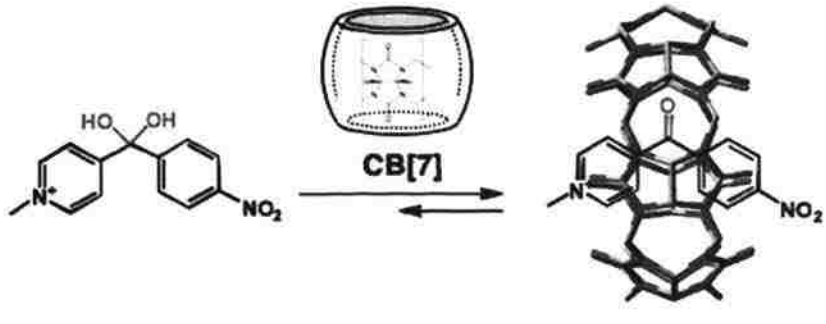

Figure 1.1. Schematic representation of controlling ketone to *gem*-diol equilibrium.

---

† Visiting faculty at the University of Missouri-Rolla, Summer 2007.

‡ Formerly, University of Missouri-Rolla.

1.2. INTRODUCTION

Host-guest complexes are vehicles for understanding and using supramolecular interactions for purposeful function in sensors, molecular machines and switches.[1] Cucurbiturils (CB[x], $5 \leq x \leq 10$), the result of a condensation reaction between glucouril and formaldehyde, are barrel-shaped hosts (Figure 1.2) with a hydrophobic cavity whose mean internal diameter ranges from 4.4 Å (**CB[5]**) to >10 Å (**CB[10]**).[2,3]

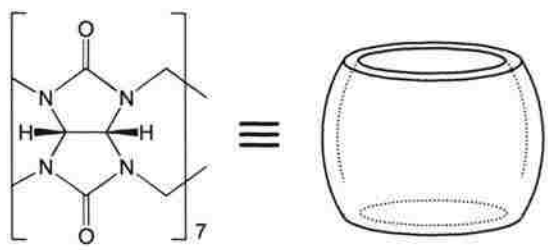

CB[7]

Figure 1.2. Pictorial representation of cucurbit[7]uril.

Since the rims are formed by the negative ends of the carbonyl dipoles, they can develop hydrogen bonding and ion-dipole interactions with their environment. Consequently, some members of the CB[x] family are water soluble, and the cavity can bind one or more cationic guests, depending on their size. This property has been explored recently in conjunction with photoisomerization and photodimerization. For instance, only one trans-diaminostilbene dihydrochloride dication (DAS) can be accommodated in **CB[7]**; irradiation leads to the cis-isomer, which is not thermally converted back to trans- at room temperature owing to stabilization by interaction of both terminal protonated amines with the two negative rims of **CB[7]**.[4] **CB[8]**, however, can accommodate two molecules of DAS leading to stereoselective photodimerization.[5] Similar results have been obtained more recently with 2:1 complexes between trans-1,2-bis-(4-pyridyl)ethylene and **CB[8]**,[6] while **CB[7]** can accommodate two of the smaller 2-aminopyridine hydrochloride cations whose irradiation leads to stereoselective [4+4] photodimerization.[7] Modulation of thermal equilibria of the quests are also known, e.g., shifting the 4,4′-bis-(dimethylamino) diphenyl carbinol/carbocation equilibrium towards the carbocation with **CB[7]**.[8] Here we demonstrate host-guest interactions between **CB[7]** and a family of guests based on the *N*-methyl-4-(*p*-substituted benzoyl) pyridinium cation (**BP-X,** where X = $-OCH_3$, $-CH_3$, -H, -Br, -CHO, $-NO_2$, $-S^+(CH_3)_2$), and we report that the

ketone to *gem*-diol equilibrium in water (eq 1) is controlled by the preference of the keto form for the **CB[7]** cavity.

Scheme 1.1. Ketone to *gem*-diol equilibrium of **BP-X**.

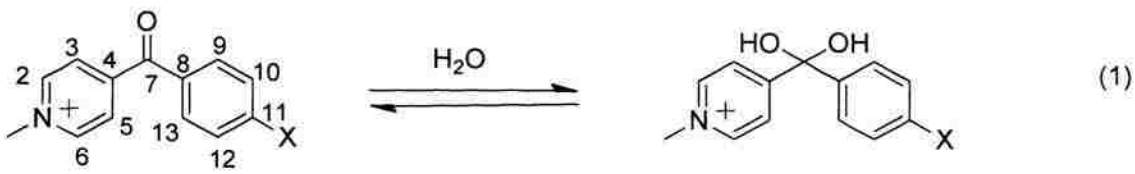

(1)

1.3. RESULTS AND DISCUSSION

In aqueous solution, carbonyl compounds exist in equilibrium with their hydrated forms (*gem*-diols). The concentration of the latter is usually very low, but it can increase if substitution renders the carbonyl group more susceptible to nucleophilic addition.[9] The position of this equilibrium can be of vital importance in biological systems where reactivity may be either associated with or stereoelectronically controlled by only one of the two forms.[10-13] Ideally, the carbonyl/*gem*-diol equilibrium would be controlled with supramolecular additives rather than by modifying the substrate or the environment (e.g., by changing the pH).

All **BP-X**s of this study were available from previous work,[14] and were chosen as model ketones because of their water solubility, their relation to the NAD^+/NADH coenzyme of dehydrogenases, their expected adjustable aptitude for hydration by para-substitution, and their structural similarity to methyl viologen (*N,N′*-dimethyl-4,4′-bipyridinium dication, MV^{2+}),[15,16] which warrants interaction with **CB[7]**. In this regard it is noted that MV^{2+} fits well in **CB[7]** and the two positive charges are stabilized by ion-dipole interactions with the carbonyl groups of the rims.[2,15,16] By the same token, however, since **BP-X**s have only one pyridinium ring, their orientation relative to the cavity of **CB[7]** was not obvious a *priori*: they could assume either an *exo*- or an *endo*-stereochemistry as illustrated below:

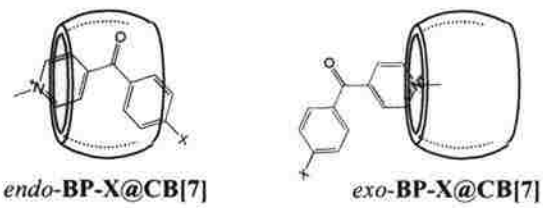

endo-**BP-X@CB[7]** *exo*-**BP-X@CB[7]**

Figure 1.3. Possible orientations of **BP-X** in **CB[7]**.

The *exo*- versus *endo*-orientation was elucidated by ^{1}H NMR. As shown in Figure 1.4 for the aromatic region, in the presence of **CB[7]** (purchased from Aldrich), the ^{1}H NMR of **BP-H** (X = H) in D_2O shows an upfield shift for all protons, consistent with the *endo*-**BP-H@CB[7]**. Identical results were observed for all **BP-X** of this study. The *exo*-orientation is in fact observed with the corresponding *N*-hexyl-4-(*p*-substituted benzoyl) pyridinium cations, by analogy to that reported for hexyl viologen (*N*,*N*′-dihexyl-4,4′-bipyridinium dication; refer to the Supporting Information).[16]

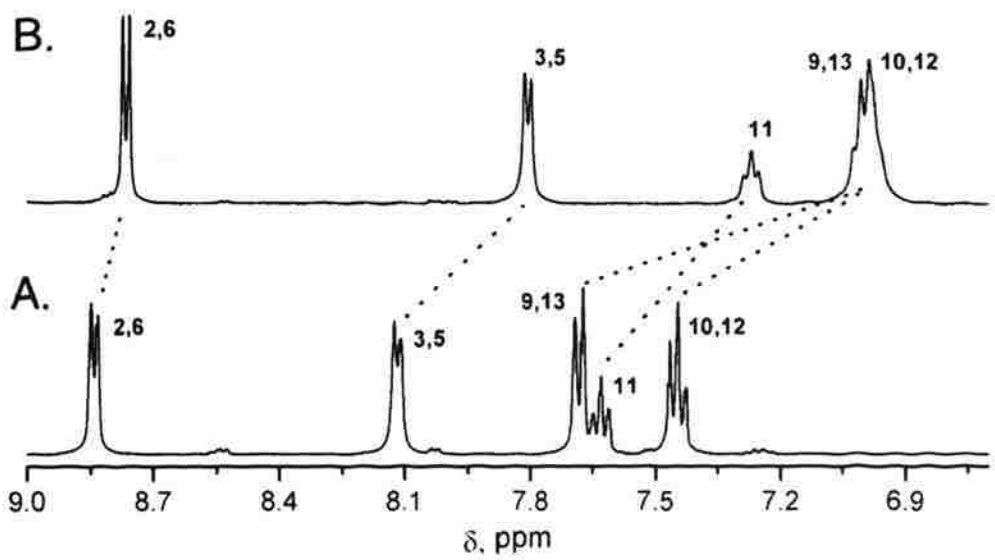

Figure 1.4. Room temperature (23 °C) ^{1}H NMR of the aromatic region of **BP-H** (X = H; 16.1 mM) in D_2O/0.1 M KCl before (A) and after (B) addition of 1.25 mol equivalents of **CB[7]**. The upfield shift of all protons supports the *endo*-orientation. The small "impurities" in the baseline is the *gem*-diol form of **BP-H** in equilibrium with the dominant keto form.

Clearly, the benzoyl group, despite possible H-bonding interactions with the solvent through the carbonyl oxygen, prefers to retreat into the hydrophobic cavity where it must enjoy greater stabilization through hydrophobic interactions. As shown in Figure 1.5, upon intercalation in **CB[7]** the longest wavelength electronic absorption of **BP-X** decreases in analogy to what has been reported for MV^{2+}.[17] The 1:1 stoichiometry of the resulting **BP-X@CB[7]** complexes is supported by the presence of stable isosbestic points in the UV-titration of **BP-X** with **CB[7]** and in the case of **BP-H** it was confirmed by a peak at m/z = 1361.58 (expected at m/z = 1361.20) in the ESI mass spectrum of the **BP-H/CB[7]** aqueous solution (see Supporting Information). The strong binding aptitude of **BP-H** with **CB[7]** is reflected in the equilibrium constant for complex formation (K_{eq} = (6.2 ± 2.1) × 10^3 M^{-1}, by analysis of the UV titration data of Figure 1.5: Supporting Information).[18]

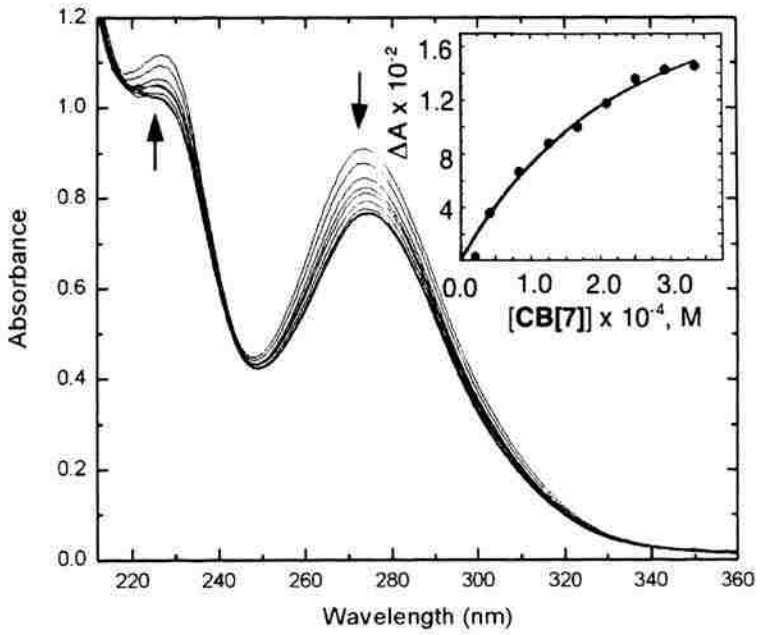

Figure 1.5. Room temperature (23 °C) titration of **BP-H** (9.88 × 10^{-5} M) in H_2O/0.1 M KCl with **CB[7]**. (Initial pH~6.0; after addition of **CB[7]**, pH~4.0. Results identical in phosphate buffer at pH = 7.0.) Inset curve: by non-linear regression (see Supporting Information).

Similarly, all the other **BP-X**s examined showed strong binding aptitudes towards **CB[7]**. Equilibrium constants, K_{eq}, increase with electron withdrawing substitution (Figure 1.6, $\rho = 0.58 \pm 0.06$) reflecting that as the benzoyl group becomes more electron deficient, its ability to form H-bonding with the aqueous environment decreases, thus increasing its preference for the hydrophobic interior of **CB[7]**. The extreme case of **BP-S$^+$(CH$_3$)$_2$** is noteworthy because it shows an abnormally high affinity for **CB[7]** (K_{eq} = $(3.6 \pm 1.0) \times 10^5$ M^{-1}), most probably because that complex is stabilized by two cation-dipole interactions, much like **MV^{2+}** whose $K_{eq} \sim 2 \times 10^5$ M^{-1}.[15-1]

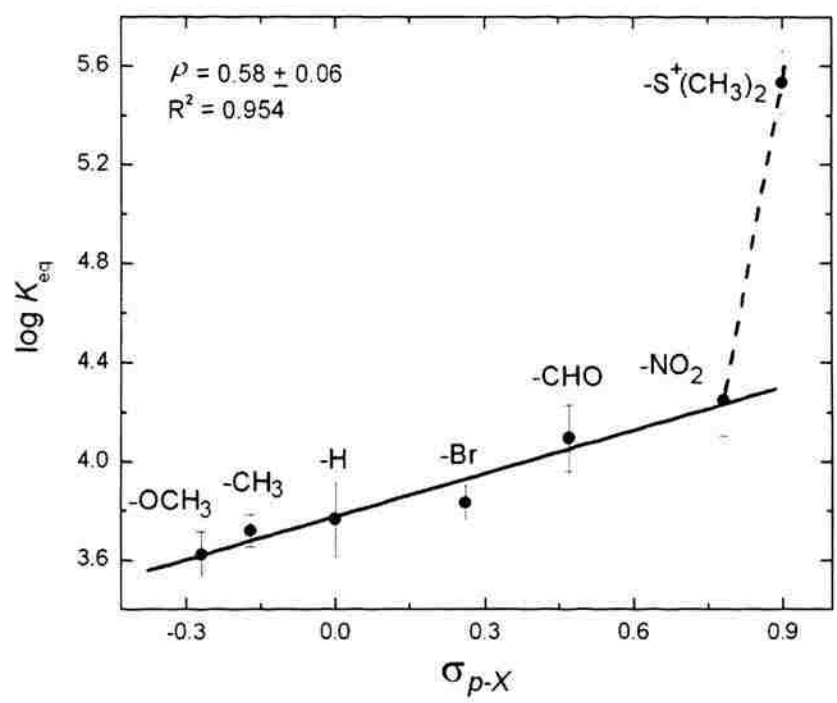

Figure 1.6. Substitution effects for the **BP-X** + **CB[7]** $\rightleftharpoons$ **BP-X@CB[7]** equilibrium in D_2O/0.1 M KCl showing that as **BP-X** becomes more electron deficient, its compatibility with the hydrophobic cavity of **CB[7]** increases.

If the effect of substitution is also followed by ^{1}H NMR (no **CB[7]** present) we are able to see that as X- becomes more electron withdrawing (e.g., going from -H to -NO_2), in aqueous solutions **BP-X** exist in equilibrium with progressively increasing amounts of their *gem*-diol forms, whose identity was confirmed by the ^{13}C NMR signature resonance of the $C(OH)_2$ carbon at ~94.5 ppm. The relative ratio of the two

forms, and therefore the value of each ketone $\rightleftharpoons$ *gem*-diol equilibrium constant (K_{diol}) is extracted directly from the ^{1}H NMR spectra. K_{diol} data show a good Hammett correlation (Figure 1.7) with a reaction constant $\rho = 1.31 \pm 0.02$, that is similar to values reported for substituted benzaldehydes (1.71-1.75).[19]

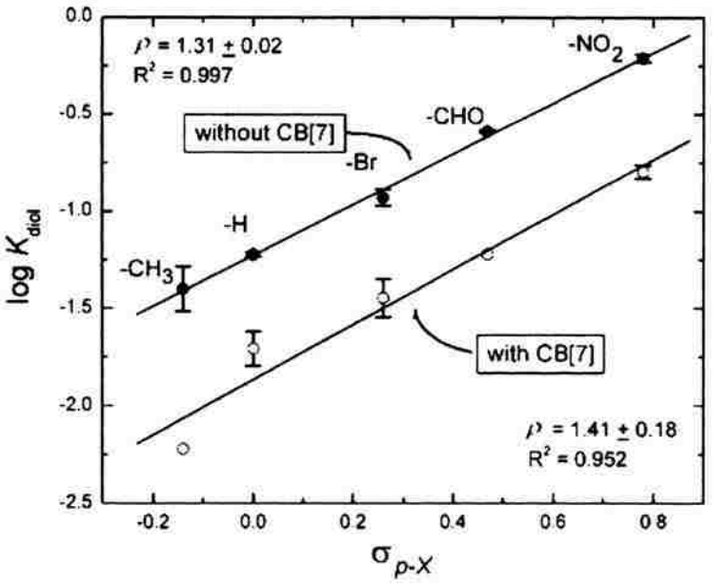

Figure 1.7. Substitution effect for the keto/*gem*-diol equilibrium in D_2O/0.1 M KCl with and without 1.0 mol equivalent of **CB[7]**. ([**BP-X**] = 16.0 ± 0.6 mM.) Equilibrium constants, K_{diol}, directly from ^{1}H NMR data: spectra recorded 15 min and 24 h after dissolving **BP-X** in D_2O/0.1 M KCl were practically identical. Data for **BP-S$^+$(CH$_3$)$_2$** are not included because the $t_{1/2}$ of the ketone to *gem*-diol equilibrium was a few hours.

The effect of **CB[7]** upon the keto/*gem*-diol equilibrium is best illustrated with the *N*-methyl-4-(*p*-formylbenzoyl)pyridinium cation (**BP-CHO**), which in CH_3CN appears as a pure compound (Figure 1.8A), while in D_2O consists of a mixture of three forms (Figure 1.8B).[20] Upon addition of increasing amounts of **CB[7]** (Figures 1.8C and 1.8D) the fate of the individual forms in equilibrium can be followed separately: the dicarbonyl form, **BP-CHO**, shows an evolution-pattern similar to that of **BP-H** in Figure 1.4, underscoring the preference of the benzoyl group for the **CB[7]** cavity. A similar case is made for the hydrated aldehyde: **BP-CH(OH)$_2$**. However, when the *gem*-diol is on the benzoyl group only small chemical shift changes are observed with increasing the concentration of **CB[7]** indicating that this form is oriented mostly outside the cavity. Starting with similar geometries (the carbonyl or the *gem*-diol groups inside the cavity),

PM3-optimized structures of **BP-NO$_2$@CB[7]** and of the corresponding *gem*-diol support that the *gem*-diol of the benzoyl group prefers to stay outside the cavity, where presumably it can be further stabilized by hydrogen bonding with the aqueous environment.[21]

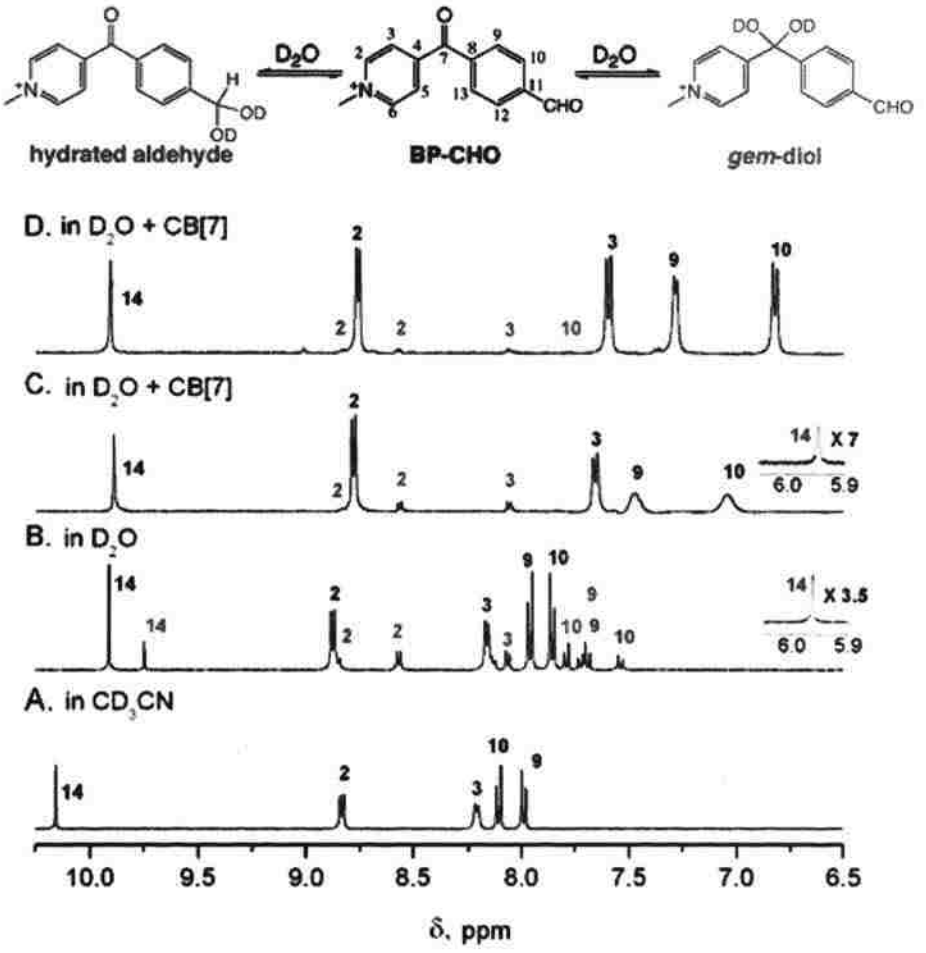

Figure 1.8. ^{1}H NMR data of **BP-CHO** in CD_3CN (A) and in D_2O/0.1 M KCl without **CB[7]** (B), with 0.75 mol equivalents (C), and 1.25 mol equivalents of **CB[7]** (D).

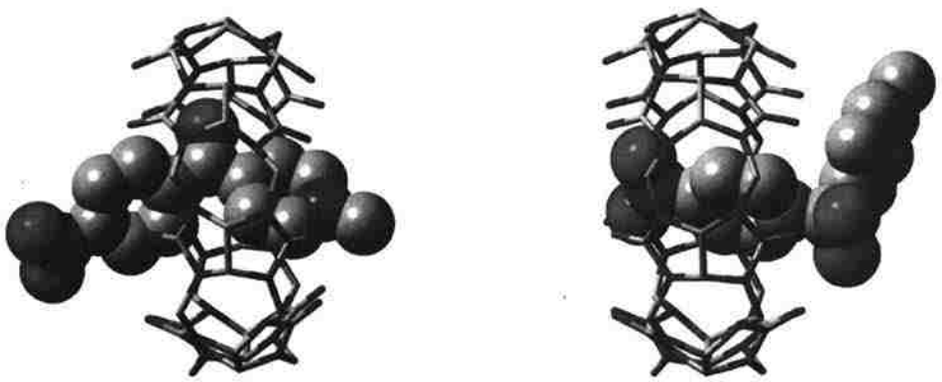

BP-NO_2@CB[7] ***gem*-diol_of_BP-NO_2@CB[7]**

Figure 1.9. PM3-optimized structures of **BP-NO_2@CB[7]** and of the corresponding *gem*-diol.

The most significant observation in Figure 1.8, however, is that upon addition of increasing amounts of **CB[7]**, the relative amount of **BP-CHO** increases at the expense of both hydrated forms. After addition of 1.25 mol equivalent of **CB[7]** into the aqueous solution of **BP-CHO**, the ^{1}H NMR spectrum (Figure 1.8D) looks similar to that in CD_3CN (Figure 1.8A), while the relative ratios of the three forms **BP-CHO**:*gem*-diol:hydrated aldehyde change from 1.0:0.26:0.20 to 1.0:0.06:<0.01 after addition of one equivalent of **CB[7]**.[22] The new keto $\rightleftharpoons$ *gem*-diol equilibrium constants after addition of **CB[7]**, still show a good Hammett correlation (Figure 1.7). The new line runs almost parallel to (ρ = 1.41 ± 0.18), but below the one representing the keto/*gem*-diol equilibrium before the addition of **CB[7]** reflecting similar stereoelectronic factors but much lower equilibrium concentrations of *gem*-diols. Clearly, the stabilization realized by H-bonding of the *gem*-diols in water is still less than the stabilization realized through hydrophobic interactions of the benzoyl groups in the interior of the cavity.[23] It is noteworthy that in systems where the benzoylpyridinium group assumes the exo-configuration (the case of *N*-hexyl-4-benzoylpyridinium cations), the keto to *gem*-diol equilibrium is affected less by the presence of **CB[7]** (see Supporting Information).

1.4. CONCLUSIONS

The results described herewith have been possible because all **BP-X@CB[7]** complexes seem to include strong hydrophobic interactions with the **CB[7]** cavity and are oriented *endo-* in water. Our results viewed together with those reported in recent and current literature suggest that the broader scope of exerting control on potentially useful homogeneous reactions of the guest via host-guest interactions should be explored further.[2,4-7] Finally, **BP-X@CB[7]** having one redox center, the benzoyl group, inside the cavity invites further studies of the electron transfer through the cage wall.

1.5. ACKNOWLEDGMENT

The authors thank the University of Missouri Research Board for financial support.

1.6. REFERENCES

1. (a) Kaifer, A. E.; Gomez-Kaifer, M. *Supramolecular Electrochemistry* Wiley-VCH Verlag GmbH: Weinheim, Germany, 1999. (b) Balzani, V.; Credi, A.; Raymo, F. M.; Stoddart, J. F. *Angew. Chem., Int. Ed.,* **2000**, *39*, 3348-3391.
2. (a) Lagona, J.; Mukhopadhyay, P.; Chakrabarti, S.; Isaacs, L. *Angew. Chem. Int. Ed.* **2005**, *44*, 4844-4870. (b) Lee, J. W.; Samal, S.; Selvapalam, N.; Kim, H.-J.; Kim, K. *Acc. Chem. Res.* **2003**, *36*, 621-630. (c) Kim, K. *Chem. Soc. Rev.* **2002**, *31*, 96-107.
3. Liu, S. L.; Zavalij, P. Y.; Isaacs, L. *J. Am. Chem. Soc.* **2005**, *127*, 16798-16799.
4. Choi, S.; Park, S. H.; Ziganshina, A. Y.; Ko, Y. H.; Lee, J. W.; K. K. *Chem. Commun.* **2003**, 2176-2177.
5. Jon, S. Y.; Ko, Y. H.; Park, S.-H.; Kim, H.-J.; Kim, K. *Chem. Commun.* **2001**, 1938-1939.
6. Maddipatla, M. V. S. N.; Kaanumalle, L. S.; Natarajan, A.; Pattabiraman, M.; Ramamurthy, V. *Langmuir* **2007**, *23*, 7545-7554.
7. Wang, R.; Yuan, L.; Macartney, D. H. *J. Org. Chem.* **2006**, *71*, 1237-1239.
8. Wang, R.; Macartney, D. H. *Tetrahedron Lett.* **2008**, *49*, 311-314.
9. See for example: Greenzaid, P.; Luz, Z.; Samuel, D. *J. Am. Chem. Soc.* **1967**, *89*, 749-756.
10. Silva, A. M.; Cachau, R. E.; Sham, H. L.; Erickson, J. W. *J. Mol. Biol.* **1996**, *255*, 321-346.
11. Eisses, K. Th. *Bioorganic Chemistry* **1989**, *17*, 268-274.
12. Likar, M. D.; Taylor, R. J.; Fagerness, P. E.; Hiyama, Y.; Robins, R. H. *Pharmaceutical Research* **1993**, *10*, 75-79.

13. Hanessian, S.; Roy, R. *Tetrahedron Lett.* **1981**, *22*, 1005-1008.

14. Leventis, N.; Rawashdeh, A.-M. M.; Zhang, G.; Elder, I. A.; Sotiriou-Leventis, C. *J. Org. Chem.* **2002**, *67*, 7501-7510.

15. Kim, H-J.; Jeon, W. S.; Ko, Y. H.; Kim, K. *PNAS* **2002**, *99*, 5007-5011.

16. Moon, K.; Kaifer, A. E. *Org. Lett.* **2004**, *6*, 185-188.

17. Ong, W.; Gómez-Kaifer, M.; Kaifer, A. E. *Org. Lett.* **2002**, *4*, 1791-1794.

18. Connors, K. A. *Binding Constants. The Measurement of Molecular Complex Stability*, John Wiley and Sons, Inc.: New York, N.Y., 1987, Chapter 4, p 141.

19. Baymak, M. S.; Vercoe, K. L.; Zuman, P. *J. Phys. Chem. B* **2005**, *109*, 21928-21929.

20. The bis *gem*-diol of **BP-CHO** is not detectable, reflecting the change in the electronic properties of carbonyls converted to *gem*-diols.

21. DFT-optimized structures (by the B3LYP/6-31G* method) were used as inputs of the PM3 optimizations for all three: **CB[7]**, **BP-NO_2** and the *gem*-diol of the latter.

22. It is emphasized that in the presence of **CB[7]** the concentration of **BP-$CH(OH)_2$** is extremely small, hence the point for **BP-CHO** in the Hammett plot of Figure 1.7 falls in line with the rest of the substituents.

23. Apparently, **CB[7]** can intercalate even neutral aromatic ketones.[24] Equilibrium constant data in the presence of K^+ are about one order of magnitude less than the values plotted in Figure 1.6, probably reflecting the lack of positive charge.

24. Mezzina, E.; Cruciani, F.; Pedulli, G. F.; Lucarini, M. *Chem. Eur. J.* **2007**, *13*, 7223-7233.

APPENDIX – A

SUPPORTING INFORMATION

Appendix S.1.1, Equilibrium Constant Calculations and Data.; Appendix S.1.2, Room temperature ^{1}H NMR of *N*-hexyl-4-benzoylpyridinum tetrafluoroborate in D_2O/0.1 M KCl, with and without 1.25 mol excess of **CB[7]**; Appendix S.1.3, Room temperature ^{1}H NMR of *N*-methyl-4-(*p*-nitrobenzoyl)pyridinum tetrafluoroborate in D_2O/0.1 M KCl, with and without 1.25 mol excess of **CB[7]**; Appendix S.1.4, Full ^{1}H NMR titration of *N*-methyl-4-(*p*-nitrobenzoyl)pyridinum tetrafluoroborate in D_2O/0.1 M KCl at room temperature; Appendix S.1.5, Room temperature ^{1}H NMR of *N*-hexyl-4-(*p*-nitrobenzoyl)pyridinum tetrafluoroborate in D_2O/0.1 M KCl, with and without 1.25 mol excess of **CB[7]**; Appendix S.1.6, Selected ESI mass spectral data.

Appendix S.1.1: Equilibrium Constant Calculations and data.

UV absorption data were analyzed in order to find equilibrium constants of the host + guest $\rightleftharpoons$ complex reaction using eq 4.5 in "Binding Constants The Measurement of Molecular Complex Stability" by K. A. Connors, John Wiley &Sons, New York, 1987, Chapter 4, p 148.

$$\frac{\Delta A}{b} = \frac{S_t K_{11} \Delta\varepsilon_{11}[L]}{1 + K_{11}[L]} \qquad (4.5)$$

ΔA is the difference in absorbance at a certain wavelength of the substrate and the complex, b is the optical path (1 cm), S_t is the total substrate concentration (free and complexed) where substrate here is the *N*-methyl-4-(*p*-substituted benzoyl) pyridinium cation (**BP-X**), K_{11} is the equilibrium constant for 1:1 complex formation (which is our case), $\Delta\varepsilon_{11}$ is the difference in extinction coefficients between **BP-X** and its complex with **CB[7]**, and **[L]** is the equilibrium concentration of <u>free</u> titrant, namely **CB[7]**. If [L]>>S_t, then we can consider [L]~L_t. Then we can invert eq. 4.5, obtain eq. 4.10 (the Benesi-Hildebrand equation), plot $1/\Delta A$ versus $1/L_t$ and obtain K_{11} by dividing intercept over slope of the expected straight line. (L_t is the total concentration of **CB[7]**, free and complexed.)

$$\frac{b}{\Delta A} = \frac{1}{S_t K_{11} \Delta\varepsilon_{11} L_t} + \frac{1}{S_t \Delta\varepsilon_{11}} \qquad (4.10)$$

If the condition [L]>>L_t is not met, then we need to calculate [L] as a function of L_t via eq 2.39 of Connors book, p 44:

$$L_t = [\mathrm{L}] + \frac{K_{11} S_t [L]}{1 + K_{11}[L]} \qquad (2.39)$$

Thus, by rearranging 4.5 and substituting into 2.39 one can obtain:

$$[\mathrm{L}] = L_t - \frac{\Delta A}{b\Delta\varepsilon_{11}}$$

Substituting now the last equation back into 4.5 we obtain a quadratic equation that can be solved into:

$$\Delta A = \frac{b\Delta\varepsilon_{11}\left[L_t + S_t + \frac{1}{K_{11}} \pm \sqrt{(L_t + S_t + \frac{1}{K_{11}})^2 - 4 S_t L_t} \right]}{2}$$

The experimental data consist of measured absorption difference ΔA ($A-A_o$) versus added (total) concentration of **CB[7]** (L_t). S_t is a known constant for each titration, while $b\Delta\varepsilon_{11}$ and K_{11} are treated as adjustable parameters that are obtained by non-linear least square fitting of the ΔA versus L_t data. Table S1 provides the values obtained for K_{11} (which for the purposes of this paper is referred to as K_{eq}) and for $b\Delta\varepsilon_{11}$ for the **BP-X** compounds studied. The log (K_{eq}) values are shown in the Hammett plot of Figure 1.7 in the paper.

Table S.1.1. Equilibrium constant data obtained via spectrophotometric titrations and non-linear data fitting for the host-guest complex formation of the various **BP-X**s of this study with **CB[7]**.

Compound	K_{eq} ($\times 10^3$, M^{-1})	$b\Delta\varepsilon_{11}$ ($\times 10^3$, M^{-1})
BP-OCH$_3$	4.3 ± 0.9	3.0 ± 0.3
BP-CH$_3$	5.3 ± 0.8	2.3 ± 0.2
BP-H	6.2 ± 2.1	2.4 ± 0.4
BP-Br	6.9 ± 1.1	3.0 ± 0.2
BP-CHO	13.1 ± 4.0	4.9 ± 0.5
BP-NO$_2$	18.7 ± 6.0	3.3 ± 0.3
BP-S$^+$(CH$_3$)$_2$	357 ± 104	3.4 ± 0.1

Table S.1.2. Absorbance data for **BP-OCH$_3$** [a]

[**CB[7]**], (M)	Absorbance	A_o-A
0.0	1.097	
1.591E-04	0.975	0.122
1.909E-04	0.958	0.139
2.545E-04	0.921	0.176
2.863E-04	0.920	0.177
3.818E-04	0.888	0.209
3.672E-04	0.889	0.208

a. $S_t = 1.22 \times 10^{-4}$ M

Table S.1.3. Absorbance data for **BP-CH$_3$**[a]

[CB[7]], (M)	Absorbance	A_o-A
0.00	1.036	
5.54E-05	0.994	0.042
8.31E-05	0.981	0.055
9.69E-05	0.975	0.061
1.11E-04	0.966	0.070
1.38E-04	0.953	0.083
1.66E-04	0.943	0.093
1.94E-04	0.936	0.100
2.22E-04	0.922	0.114
2.77E-04	0.910	0.126

a. $S_t = 1.00 \times 10^{-4}$ M

Table S.1.4. Absorbance data for **BP-H**[a]

[CB[7]], (M)	Absorbance	A_o-A
0.0	0.912	0
2.10E-05	0.910	0.002
4.20E-05	0.876	0.036
8.39E-05	0.845	0.067
1.259E-04	0.824	0.088
1.68E-04	0.812	0.100
2.098E-04	0.794	0.118
2.518E-04	0.776	0.136
2.937E-04	0.769	0.143
3.357E-04	0.766	0.146

a. $S_t = 9.88 \times 10^{-5}$ M

Table S.1.5. Absorbance data for **BP-Br**[a]

[**CB[7]**], (M)	Absorbance	A_o-A
0	1.137	
5.64E-05	1.081	0.056
8.46E-05	1.060	0.077
9.87E-05	1.045	0.092
1.128E-04	1.037	0.100
1.410E-04	1.014	0.123
1.692E-04	1.004	0.133
1.974E-04	0.992	0.145
2.256E-04	0.976	0.161
2.820E-04	0.966	0.171

a. $S_t = 9.57 \times 10^{-5}$ M

Table S.1.6. Absorbance data for **BP-CHO**[a]

[**CB[7]**], (M)	Absorbance	A_o-A
0	1.875	0
5.28E-05	1.745	0.130
7.92E-05	1.680	0.195
9.24E-05	1.685	0.190
1.056E-04	1.640	0.235
1.320E-04	1.599	0.276
1.584E-04	1.549	0.326
1.848E-04	1.545	0.330
2.112E-04	1.529	0.346
2.640E-04	1.493	0.382

a. $S_t = 1.11 \times 10^{-4}$ M

Table S.1.7. Absorbance data for **BP-NO_2**[a]

[**CB[7]**], (M)	Absorbance	A_o-A
0	1.649	0
4.92E-05	1.547	0.102
8.61E-05	1.515	0.134
8.61E-05	1.496	0.153
9.84E-05	1.494	0.155
1.230E-04	1.453	0.196
1.476E-04	1.439	0.210
1.721E-04	1.431	0.218
1.967E-04	1.403	0.246
2.459E-04	1.397	0.252

a. $S_t = 1.02 \times 10^{-4}$ M

Table S.1.8. Absorbance data for **BP-$S^+(CH_3)_2$**[a]

[**CB[7]**], (M)	Absorbance	A_o-A
0	0.319	
2.67E-05	0.222	0.097
5.33E-05	0.147	0.172
8.00E-05	0.100	0.219
1.066E-04	0.081	0.238
1.333E-04	0.076	0.243
1.599E-04	0.070	0.249
1.866E-04	0.068	0.251
2.132E-04	0.067	0.252
2.666E-04	0.070	0.249

a. $S_t = 7.48 \times 10^{-5}$ M

Calculation of the equilibrium constants for the ketone to *gem*-diol reaction

K_{diol} was calculated as the ratio of the peak integrals for the *gem*-diol and ketone protons. About 3 mg of each **BP-X** was dissolved in 0.5 ml of D_2O with KCl (0.1 M) and was titrated with **CB[7]**. Data obtained by ^1H NMR using relaxation time = 250 s. The concentration ratio of *gem*-diol to ketone reaches its limiting value after addition of one mol equivalent of **CB[7]** (see Figure 4.2 S-B below), and therefore K_{diol} in the presence of **CB[7]** were calculated in the presence of one equivalent of **CB[7]**.

$$K_{diol} = K'_{diol}[D_2O] = \frac{[gem-\text{diol}]}{[\text{ketone}]}$$

Table S.1.9. Equilibrium constant data for the *gem*-diol formation reaction in D_2O at room temperature without **CB[7]**.

Compound	K_{diol}
BP-CH_3	0.041 ± 0.010
BP-H	0.060 ± 0.002
BP-Br	0.118 ± 0.013
BP-CHO	0.258 ± 0.002
BP-NO_2	0.615 ± 0.025

Table S.1.10. Equilibrium constant data for the *gem*-diol formation reaction in D_2O at room temperature with one mol equivalent of **CB[7].**

Compound	K_{diol}
BP-CH_3	0.006 ± 0.001
BP-H	0.020 ± 0.004
BP-Br	0.038 ± 0.015
BP-CHO	0.060 ± 0.001
BP-NO_2	0.160 ± 0.021

Appendix S.1.2: Room temperature ^{1}H NMR of *N*-hexyl-4-benzoylpyridinum tetrafluoroborate.

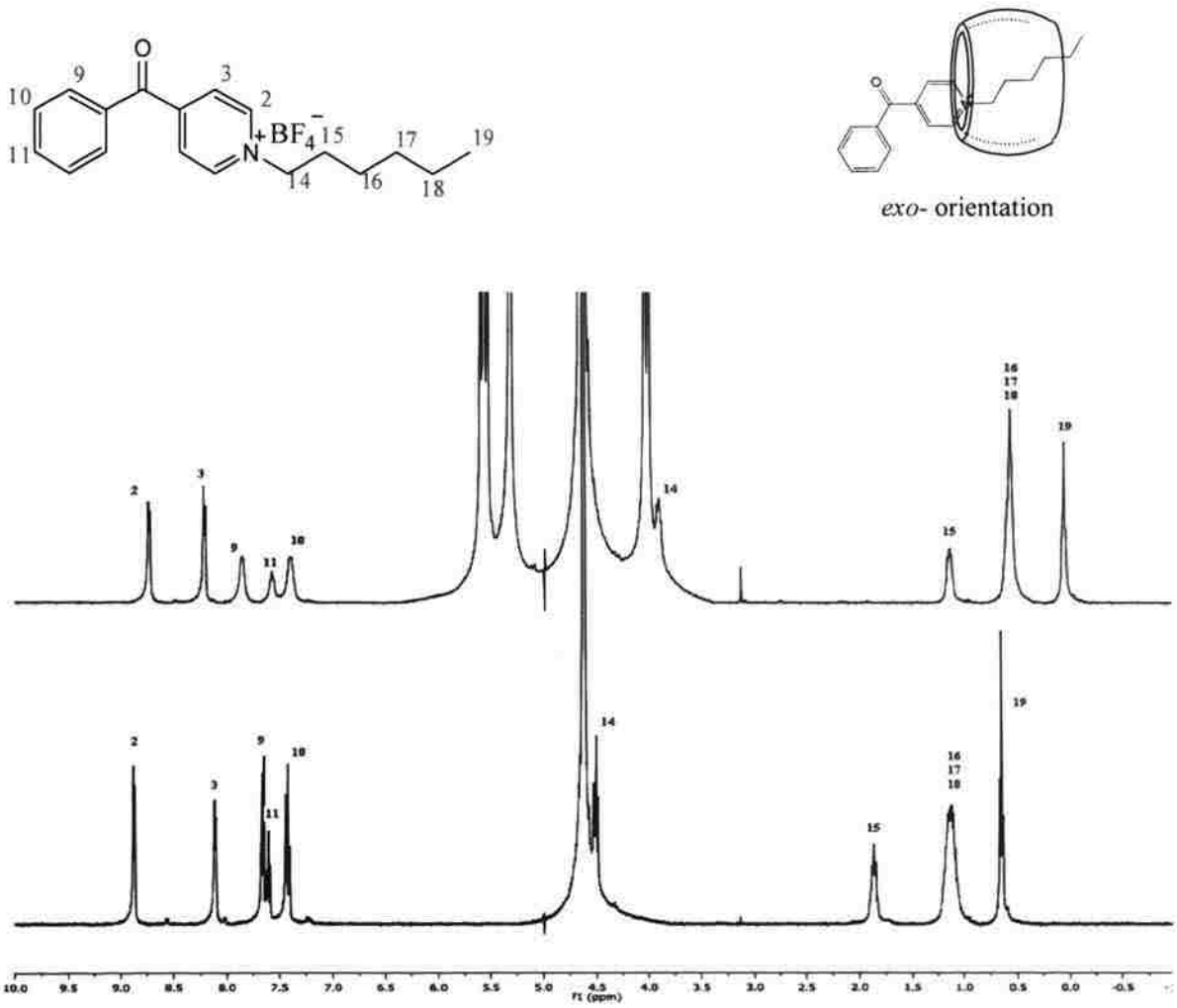

Figure S.1.1. Room temperature (23 °C) ^{1}H NMR of *N*-hexyl-4-benzoylpyridinum tetrafluoroborate in D_2O/0.1 M KCl before (bottom) and after (top) addition of 1.25 mol equivalent of **CB[7]**. The strong upfield shift of the hexyl protons supports the *exo*-orientation in analogy to results reported for hexyl viologen.[S1] The small "impurities" in the baseline is the *gem*-diol form of *N*-hexyl-4-benzoylpyridinum cation in equilibrium with the dominant keto form.

S1. Moon, K.; Kaifer, A. E. *Org. Lett.* **2004**, *6*, 185-188.

Appendix S.1.3: Room temperature (23 °C) ^{1}H NMR of *N*-methyl-4-(*p*-nitrobenzoyl)pyridinium tetrafluoroborate.

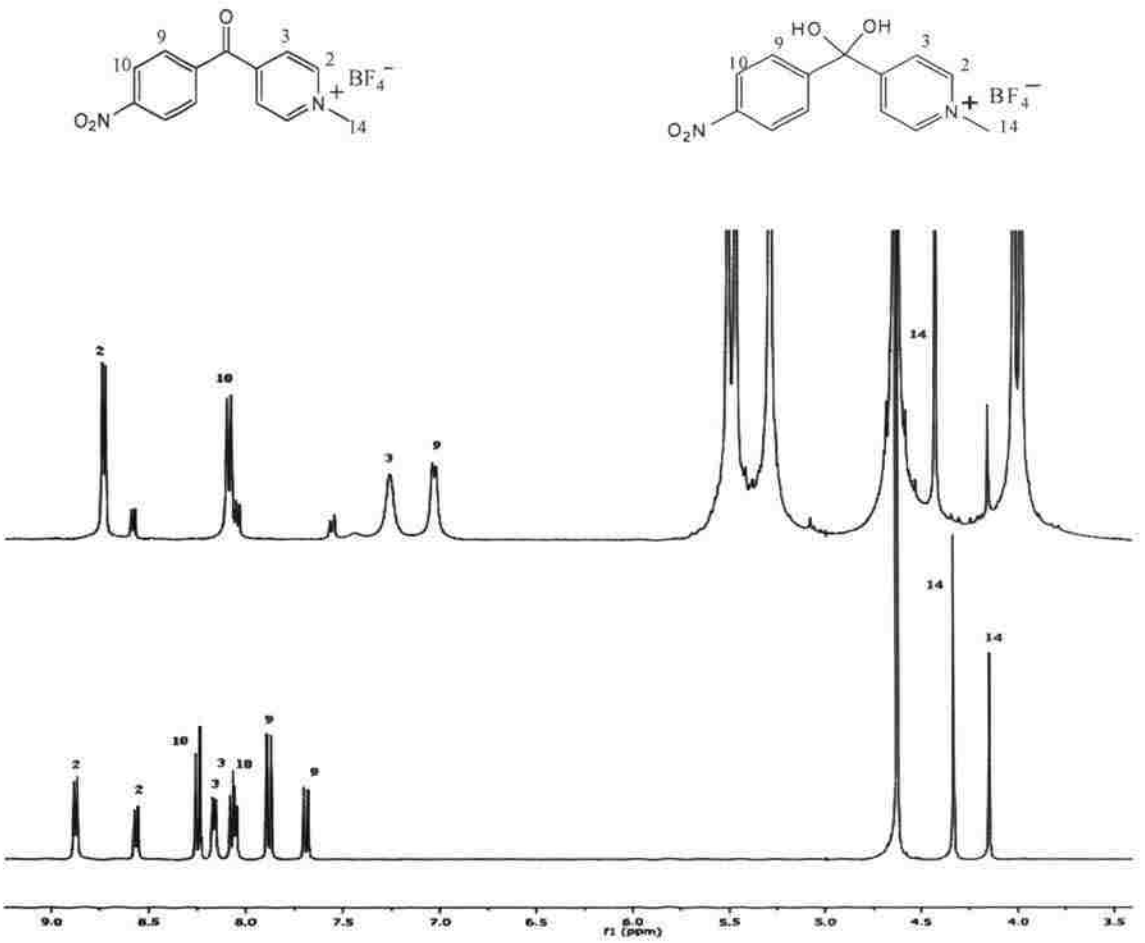

Figure S.1.2. Room temperature (23 °C) ^{1}H NMR of *N*-methyl-4-(*p*-nitrobenzoyl)pyridinium tetrafluoroborate in D_2O/0.1 M KCl before (bottom) and after (top) addition of 1.25 mol equivalent of **CB[7]**. The K_{diol} equilibrium constant is calculated from the ^{1}H NMR integral of H2,6 before and after addition of **CB[7]**. Before **CB[7]** addition, K_{diol}=0.615. After **CB[7]** addition, K_{diol}=0.160.

Appendix S.1.4: Room temperature ^{1}H NMR of *N*-methyl-4-(*p*-nitrobenzoyl)pyridinum tetrafluoroborate.

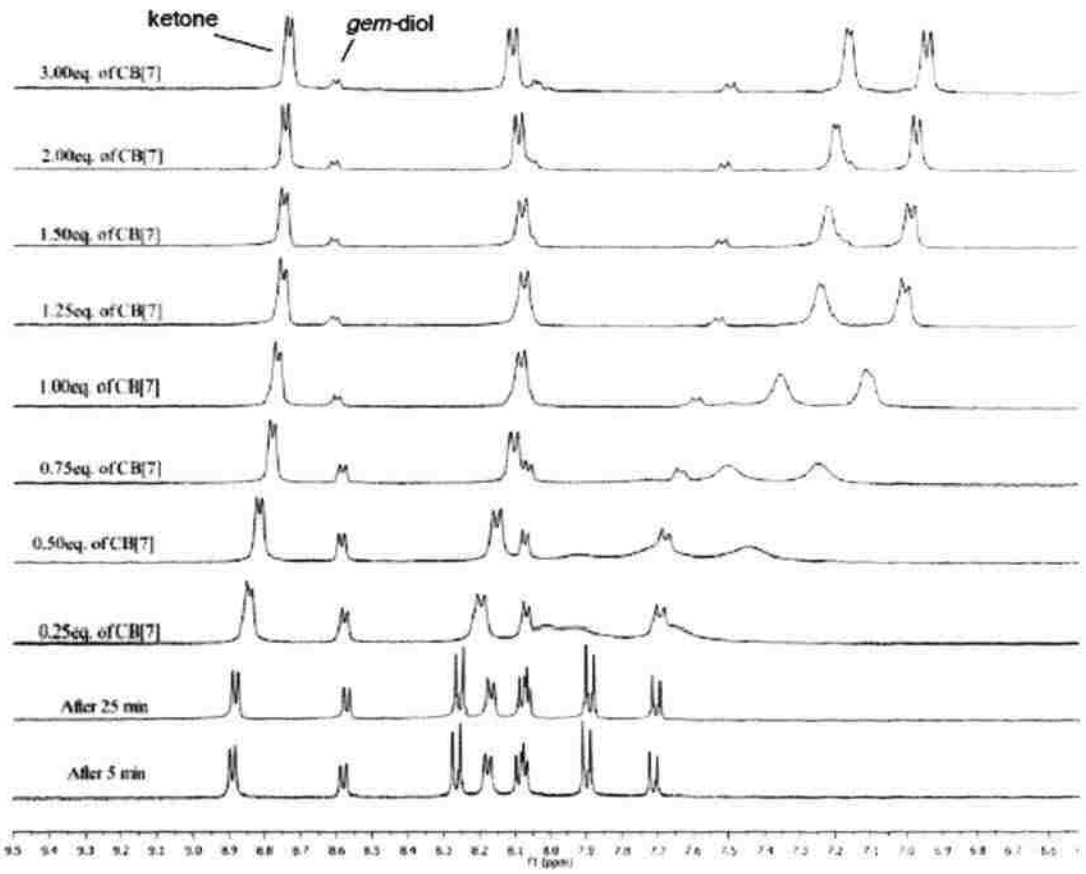

Figure S.1.3. Full ^{1}H NMR titration of *N*-methyl-4-(*p*-nitrobenzoyl)pyridinium (**BP-NO_2**) tetrafluoroborate (16 mM) with **CB[7]** in D_2O/0.1 M KCl at room temperature (23 °C).

Appendix S.1.5: Full ^{1}H NMR titration of *N*-methyl-4-(*p*-nitrobenzoyl)pyridinum tetrafluoroborate.

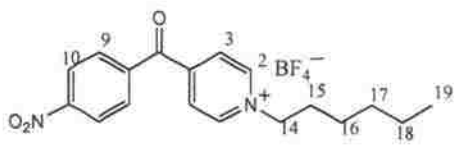

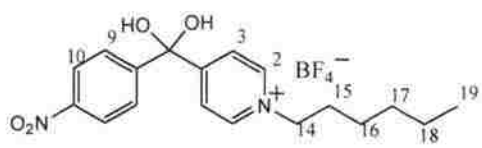

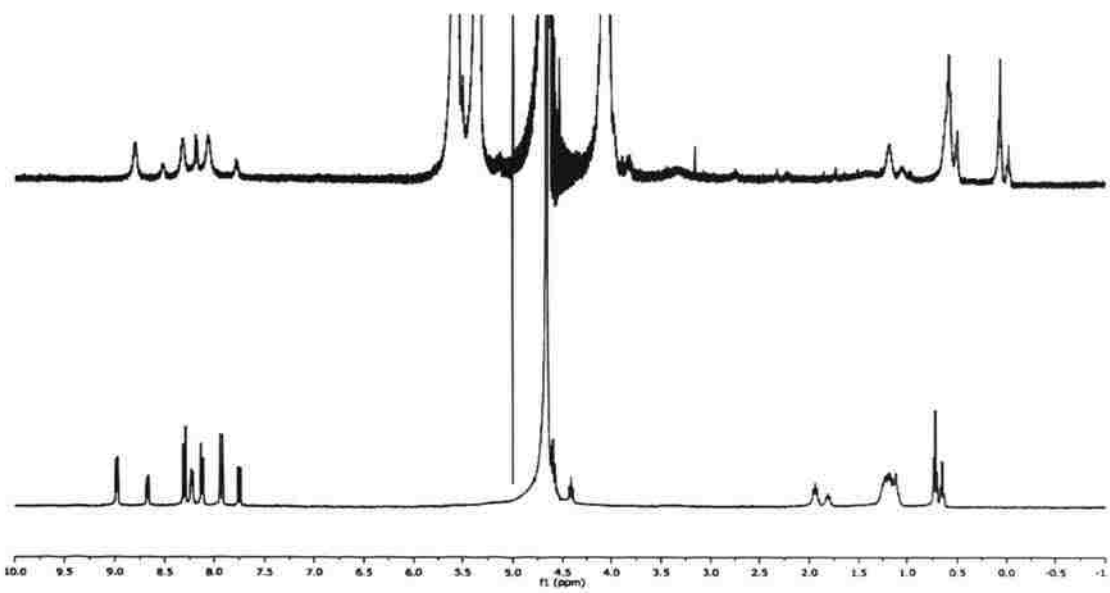

Figure S.1.4. Room temperature (23 °C) ^{1}H NMR of *N*-hexyl-4-(*p*-nitrobenzoyl)pyridinum tetrafluoroborate in D_2O/0.1 M KCl before (bottom) and after (top) addition of 1.25 mol equivalent of **CB[7]**. The upfield shift of the hexyl protons again supports the *exo*-orientation. The ratio *gem*-diol:keto form of *N*-hexyl-4-benzoylpyridinum cation before addition of **CB[7]** gives K_{diol}=0.637, which is about equal to K_{diol} in the case of the *N*-methyl derivative (K_{diol}=0.615, see Figure S.1.2). After addition of **CB[7]** K_{diol}=0.372, versus K_{diol}=0.160 for the *N*-methyl-4-benzoylpyridinum cation (see Figure S.1.2). The higher amount of the *gem*-diol form in the case of the *N*-hexyl derivative is attributed to the *exo*-orientation (see Figure S.1.1) and therefore the less efficient "protection" of the carbonyl against hydration.

Appendix S.1.6: Selected ESI mass spectral data.

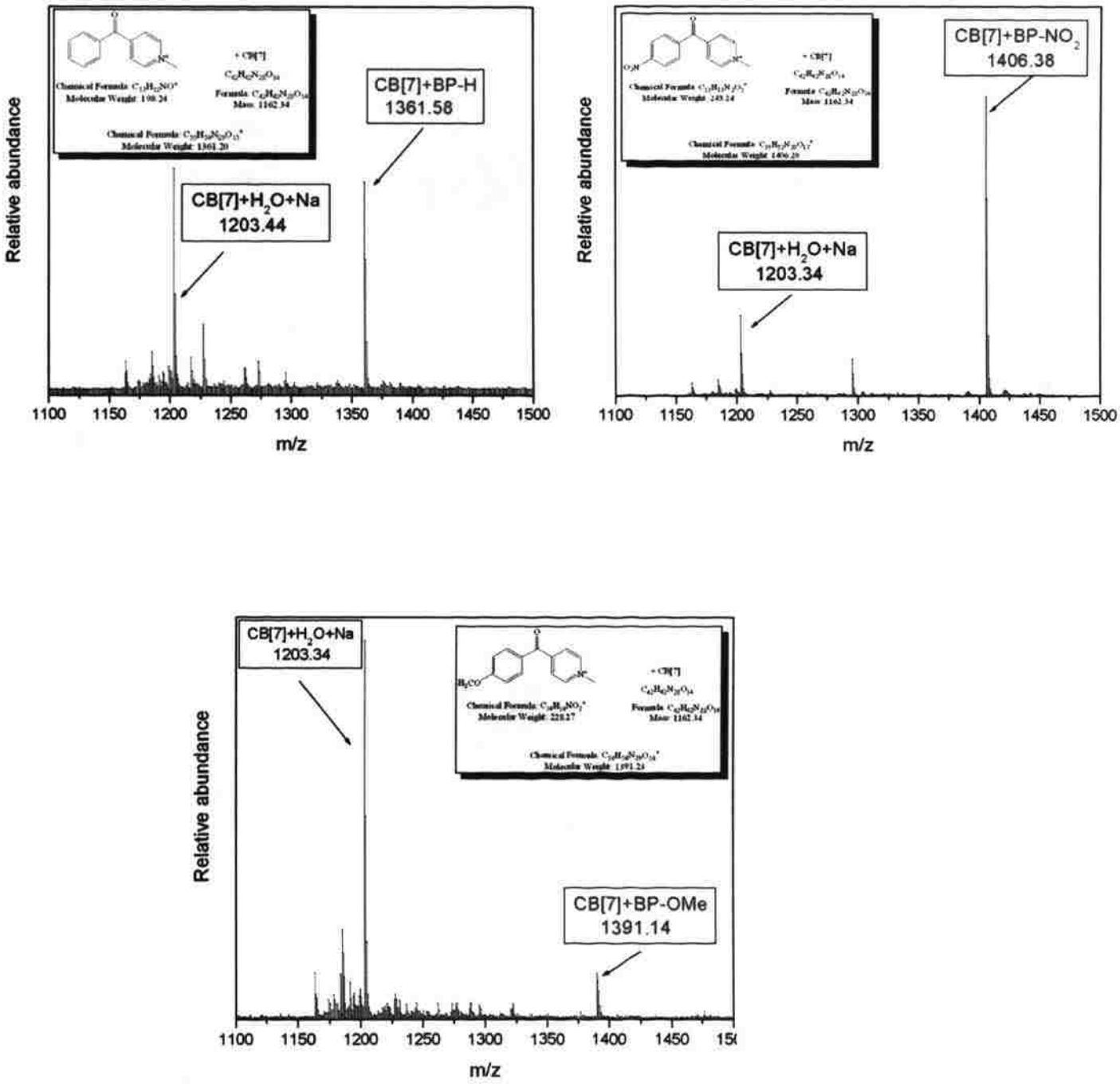

Figure S.1.5. Selected ESI mass spectral data.

Appendix S.1.7: Selected 2D NMR spectra.

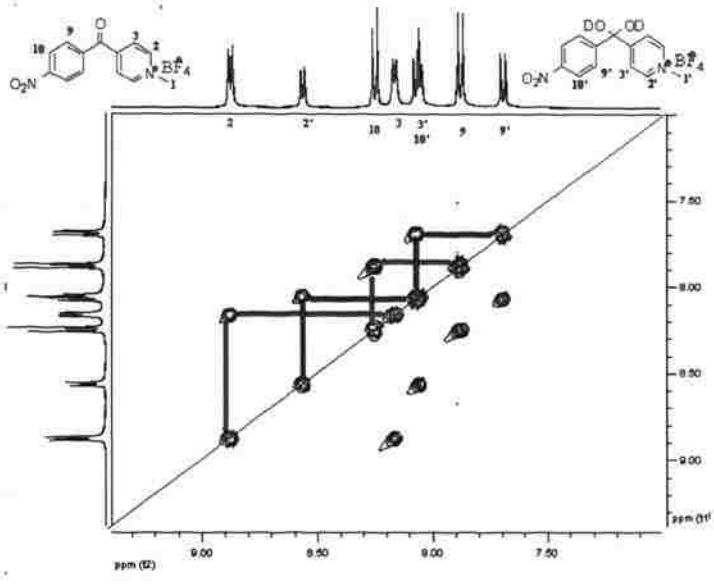

Figure S.1.6. ^{1}H-^{1}H COSY NMR of **BP-NO$_2$** in D_2O.

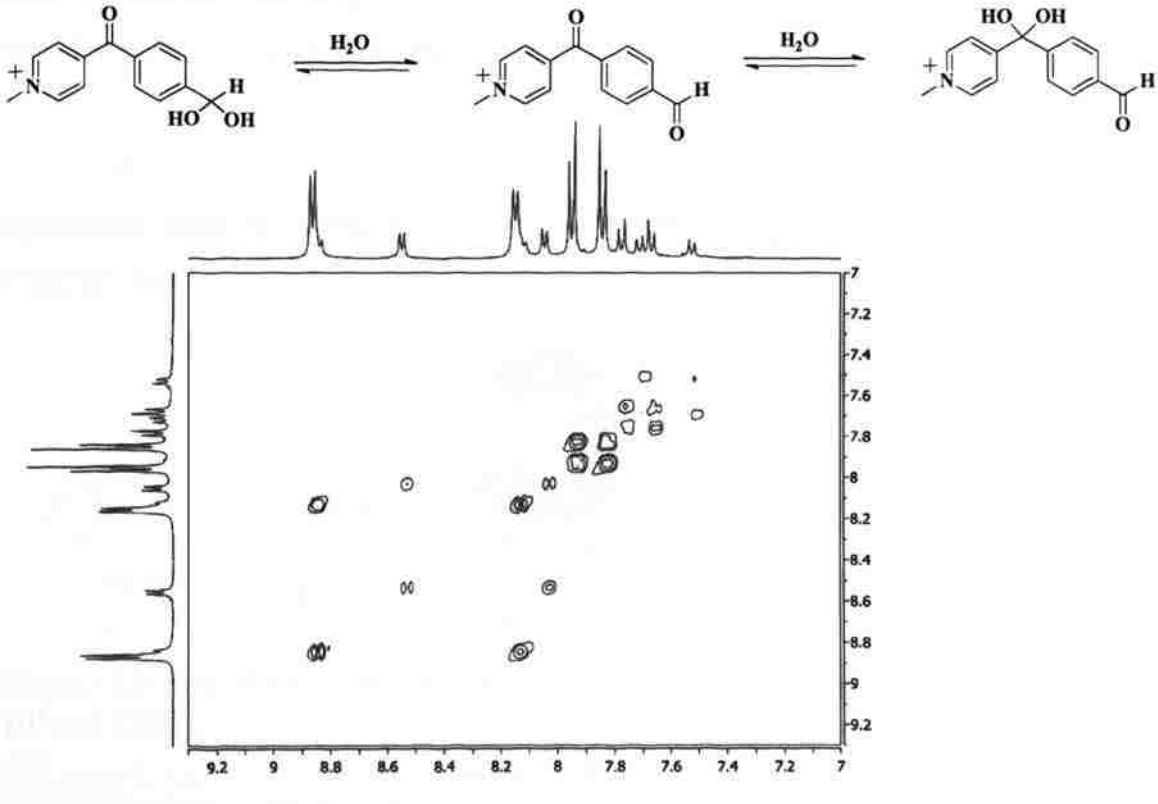

Figure S.1.7. ^{1}H-^{1}H COSY NMR of **BP-CHO** in D_2O.

2. SIMULTANEOUS ELECTRON TRANSFER FROM FREE AND INTERCALATED 4-BENZOYLPYRIDINIUM CATIONS IN CUCURBIT[7]URIL

Arumugam Thangavel,[1] Abdel Monem M. Rawashdeh,[2,†] Chariklia Sotiriou-Leventis[*,1] and Nicholas Leventis[*,1]

1. Department of Chemistry, Missouri University of Science and Technology[‡], Rolla, MO 65409, U.S.A.
2. Department of Chemistry, Yarmouk University, Irbid, 211-63, Jordan

leventis@mst.edu; cslevent@mst.edu

2.1. ABSTRACT

N-Methyl-, *N*-benzyl- and *N*-hexyl-4-benzoylpyridinium monocations (**Me-BP**, **Bz-BP** and **Hex-BP**, respectively) form stable host-guest complexes with cucurbit[7]uril (**CB[7]**) (*Keq* ≈ 0.6–1.9 × 10^3 M^{-1}). Irrespective of the orientation of the guest) (*endo*- or *exo*-) e-transfer in all three systems is controlled by the host-guest equilibrium, showing simultaneous reversible e-transfer from the free guests and quasi-reversible processes from the complexes. For **Me-BP@CB[7]** (Figure 2.1) the standard rate constant is k*s*=1.0 × 10^{-4} $cm{\cdot}s^{-1}$ corresponding to a distance of 5.7 Å between **Me-BP** and the electrode, in agreement with the distance of the intercalated guest from the outer perimeter of **CB[7]**(5.3Å).

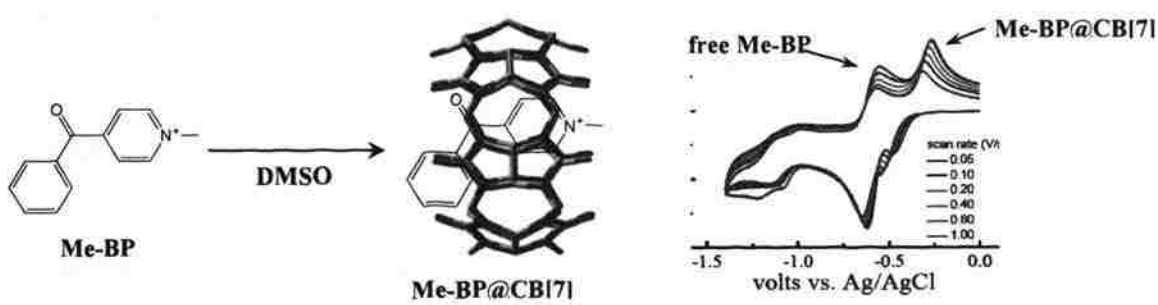

Figure 2.1. Schematic representation of intercalation and electron transfer between **Me-BP** and **CB[7]**.

---

† Visiting faculty at the University of Missouri-Rolla, Summer 2007.
‡ Formerly, University of Missouri-Rolla.

2.2 INTRODUCTION

The redox chemistry of host-guest complexes is studied for its relevance to biological electron transfer (e.g., in redox proteins) and also to applications based on molecular recognition (e.g., sensors).[1] The overwhelming majority of those studies report e-transfer exclusively from the free guests. Very few aberrations from this trend have been reported, e.g., when the guest is locked inside the host (case of hemicacerand/ferrocene),[2] or in the case of dicationic methylviologen (**MV**) in cucurbit[x]uril (CB[x], x=7, 8) where heterogeneous e-transfer takes place exclusively from the complex.[1,3] Simultaneous homogeneous e-transfer has been reported from free and **CB[7]**-intercalated (trimethylammonio)methylferrocene,[4] while here we provide evidence whereas a new class of guests, the *N*-substituted-4-benzoyl-pyridinium cations, undergoes e-transfer simultaneously from both their free state as well as their complexes with **CB[7]**.

CB[7], a water-soluble barrel-shaped host, consists of 7 glycoluril groups and 14 methylene bridges at both ends. The two rims are formed by the glycoluril carbonyl oxygens, thereby are negatively charged and they develop ion-dipole interactions with cationic guests.[5] Since the portal diameter of **CB[7]** (5.4 Å) is wide enough for **MV** to enter the cavity easily, and also the length of the two species are comparable (9.1 Å and 7.3 Å, respectively), **MV@CB[7]** maximizes both the hydrophobic and the ion-dipole interactions between the two species resulting in a high complex formation constant (K_{eq}=2×10^5 M^{-1}).[1]

2.3 RESULTS AND DISCUSSION

Monocationic *N*-methyl-4-benzoylpyridinium (**Me-BP**) is similar in length (7.7 Å) to **MV** and intercalates in **CB[7]** from water assuming an *endo*-orientation that places the benzoyl group inside the cavity.[6] Furthermore, in analogy to **MV**, **Me-BP** undergoes two sequential e-transfers.[7] However, unlike viologen, electrochemical studies with **Me-BP** cannot be conducted in water, because its 2e reduced form develops hydrogen bonding with the solvent, shifting and merging the second reduction wave with the first, leading directly to the benzyl alcohol via a chemically irreversible 2e reduction process.[7d] Thus, e-transfer studies of the **Me-BP/CB[7]** system had to be conducted in organic

aprotic media. **CB[7]** is not soluble in organic solvents; however, these studies became possible because the complexation itself increases the solubility of **CB[7]** in DMSO to the ten-millimolar range, in analogy to what has been observed with heptyl viologen.[8] Nevertheless, the orientation of the **Me-BP@CB[7]** complex in DMSO (*exo-* or *endo-*) is not obvious *a priory* and it may have important implications in the electrochemical reduction of the guest; hence, the latter should be considered together with the former. For this, the relative orientation and electrochemistry of **Me-BP@CB[7]** were considered comparatively with two other control systems (Figure 2.2), **Bz-BP@CB[7]** and **Hex-BP@CB[7]** which, in analogy to corresponding viologens,[8,9] assume *exo*-orientations placing their most hydrophobic groups (benzyl and hexyl) inside the **CB[7]** cavity, leaving their benzoyl groups outside.

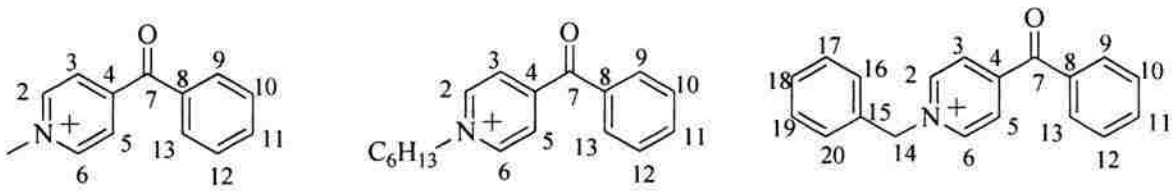

Figure 2.2. Structure of the compounds used in the study.

Synthesis of the three guests has been described before.[7b-c] **CB[7]** was prepared by modification of a literature procedure (see Supporting Information).[10] The stoichiometry of the three **CB[7]** complexes is 1:1 (by ESI mass spectrometry in water and by Job's plots in DMSO; see Supporting Information).[11] The possible orientations of the complexes was investigated with PM3 semiempirical calculations[12] using DFT-optimized structures (6-31G(d) basis set) for all three guests and **CB[7]**. All results (Figure 2.3) show two local minima very close in energy (e.g. -0.3501 vs. -0.3647 a.u. for **Me-BP@CB[7]** and -0.306 vs. -0.315 a.u. for **Bz-BP@CB[7]**) corresponding to the *endo-* and *exo-* orientations, respectively).

The actual orientation in DMSO was investigated by ^{1}H-NMR in comparison to water. All chemical shifts have been color-coded and are summarized in Scheme 2.1.

Scheme 2.1. Color-coded ^{1}H-NMR data for **Me-BP** and **Bz-BP** in the presence of 1 mol equivalent of **CB[7]**.

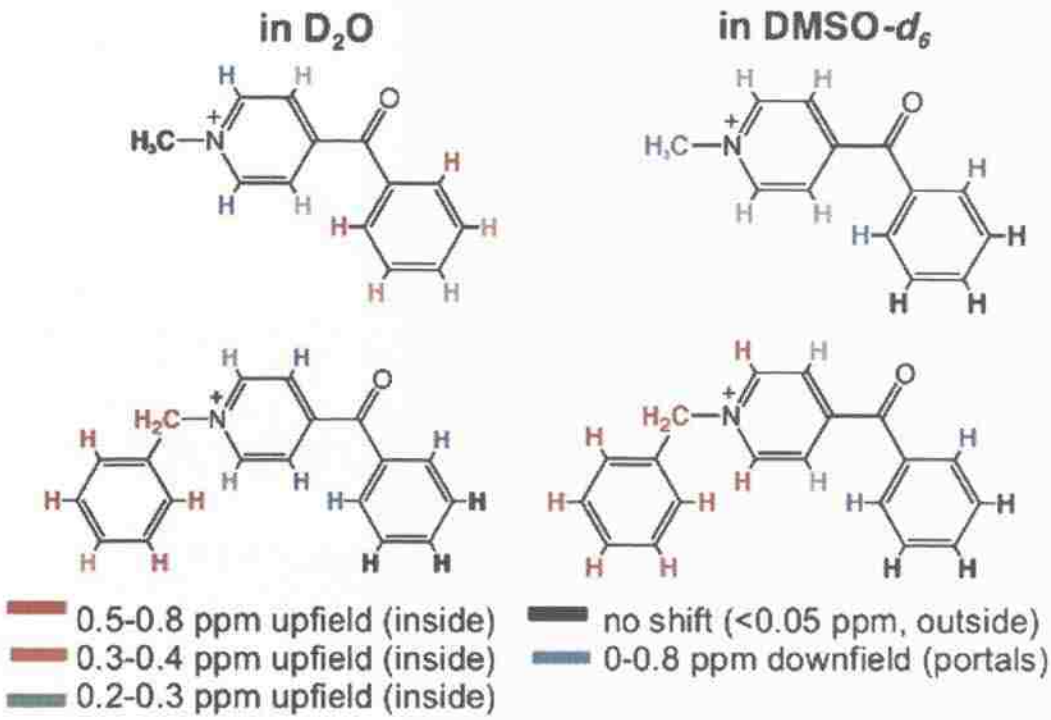

In D_2O *all* aromatic protons move upfield in the presence of **CB[7]** (compare Figures 2.4A-3.4D), consistent with the *endo*-orientation where the entire benzoylpyridinium system is inside the cavity (Figure 2.3A).[13] In DMSO-d_6 some protons move upfield, some downfield, while others hardly move (Scheme 2.1), consistent with an intermediate state between *endo*- and *exo*- (compare Scheme 2.1 with Figures 2.3A and 2.3B). In both solvents, the evolution of the chemical shifts from zero to 1.25 mol equivalents of **CB[7]** is consistent with fast exchange of **Me-BP** between its free and complexed states. The line-broadening observed in DMSO-d_6, taken together with the position of **Me-BP** in the cavity might originate from the equilibrium between the *endo*- and *exo*- forms. The more effective retreat of **Me-BP** inside **CB[7]** in water is attributed exclusively to the solvent polarity.[8]

By ^{1}H-NMR again, the mode of intercalation of **Hex-BP** and **Bz-BP** with **CB[7]** is the same in both water and DMSO, and analogous to the interaction of **Me-BP** with **CB[7]** in DMSO in the sense that some protons move strongly upfield, some downfield and some protons hardly move at all. Figure 2.5 demonstrates those patterns for **Bz-BP** and the results have been color-coded in Scheme 2.1. (Results for **Hex-BP** are given in Supporting Information). Clearly **Bz-BP@CB[7]** assumes the *exo*-orientation (compare Figures 2.3C, 2.3D and Scheme 2.1), signifying the importance of placing the most hydrophobic group inside the cavity.

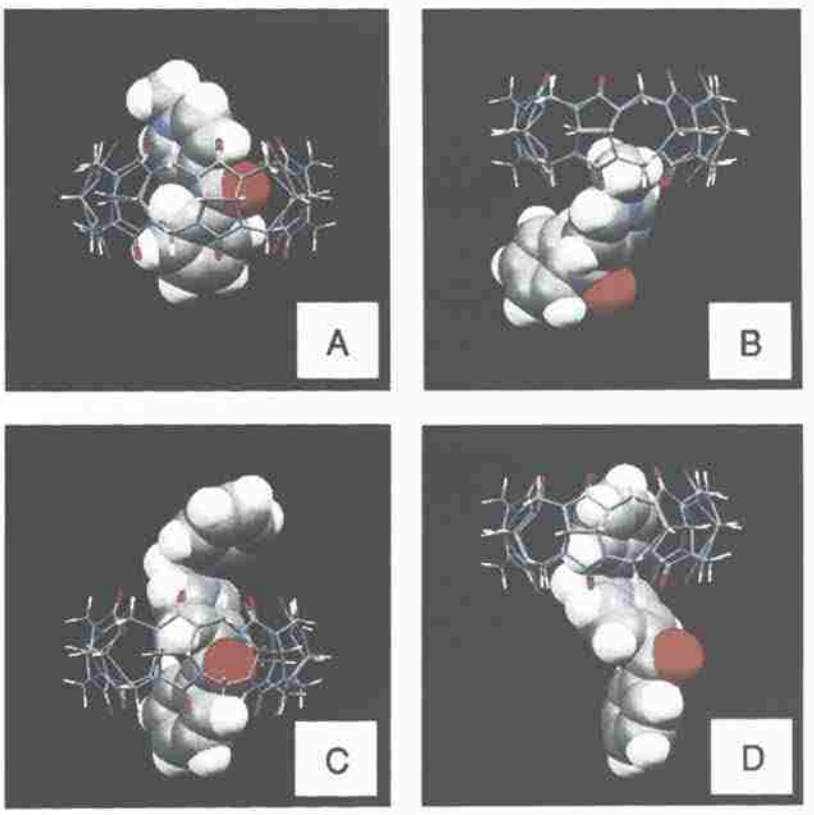

Figure 2.3. PM3 optimized structures for **Me-BP@CB[7]** (A, B) and **Bz-BP@CB[7]** (C, D) showing two minima: an *endo*- (A, C) and an *exo*- (B, D).

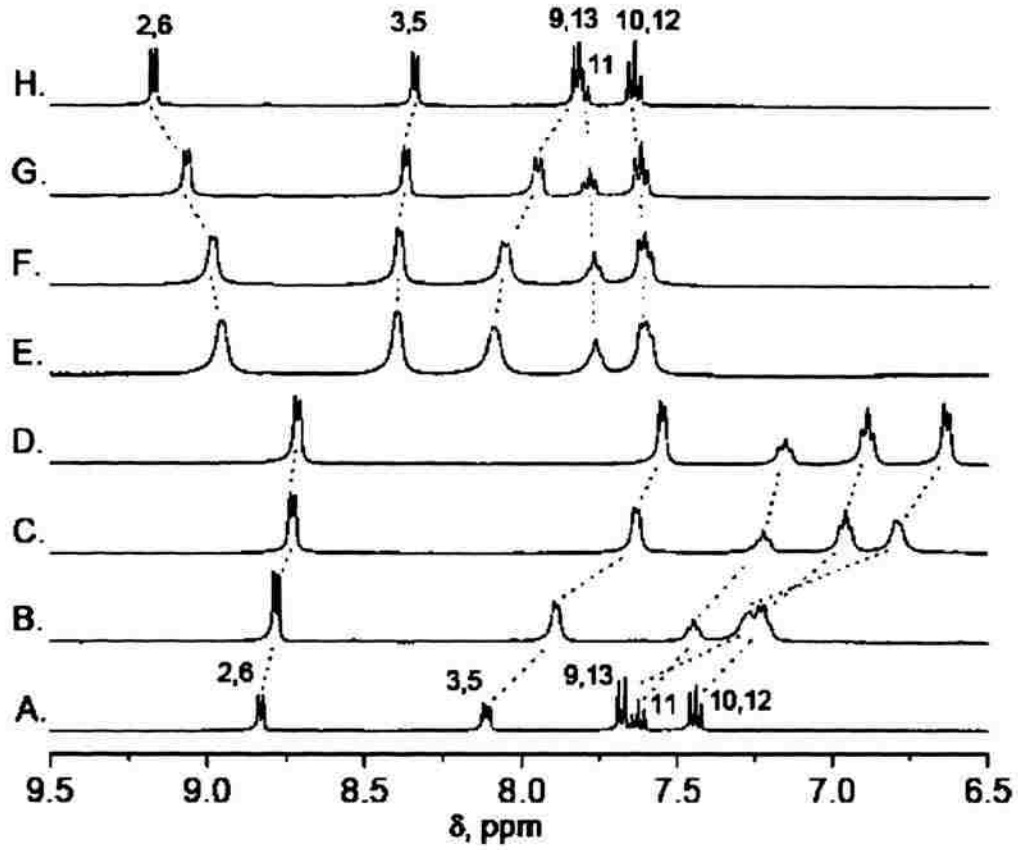

Figure 2.4. ^{1}H NMR at 23 °C of the aromatic protons of **Me-BP** in D_2O (A-D; 21.1 mM) and DMSO-d_6 (E-H; 9.1 mM). A,H: no **CB[7]**. B,G: 0.5 mol equiv of **CB[7]**. C,F: 1.0 mol eq. of **CB[7]**. D,E: 1.25 mol equiv of **CB[7]**.

All equilibrium constants, *Keq*, of the guest-host complex formation reactions were determined from spectrophotometric titration data (e.g., Figure 2.6 for **Me-BP**) using the Benesi-Hildebrand double reciprocal method (see Inset in Figure 2.6; K_{eq}=slope/intercept) and the results are summarized in Table 2.1.[14] Qualitatively, the evolution of the absorption spectra by adding **CB[7]** supports the modes of inclusion identified by ^{1}H-NMR.

Table 2.1. Equilibrium constants (K_{eq}) of the host-guest complex formation in water and DMSO at 23 °C.[a]

	K_{eq} (M^{-1})	
guest	in water	in DMSO
Me-BP	$(3.1 \pm 0.3) \times 10^{3}$.[b]	$(0.59 \pm 0.13) \times 10^{3}$
Hex-BP	$(9.1 \pm 0.1) \times 10^{3}$	$(1.3 \pm 0.5) \times 10^{3}$
Bz-BP	$(3.4 \pm 0.1) \times 10^{3}$	$(1.9 \pm 0.0_4) \times 10^{3}$

a. Experiments conducted twice, errors are spreads. b. Value reported before ($6.2 \pm 2.1 \times 10^{3}$ M^{-1}) was obtained through non-linear fit of titration results at low **CB[7]** concentrations.[5]

For **Me-BP**, for example, the different mode of inclusion in the two solvents causes an absorbance increase in water (Figure 2.6A) and a decrease in DMSO (Figure 2.6B), matching the relative polarity of the environment around the benzoyl chromophore: in water (*endo*-orientation) the chromophore is inside the hydrophobic cavity, while in DMSO it also interacts with the portal carbonyl dipoles. Since in both solvents **Bz-BP@CB[7]** and **Hex-BP@CB[7]** are *exo*-oriented, the benzoyl groups are near the portal dipoles and the absorbance increases by adding **CB[7]** (see Supporting Information). Overall, K_{eq} values are higher in water than in DMSO. **Hex-BP**, with the longest hydrophobic group, has the highest tendency to avoid water, while in less polar DMSO, its K_{eq} is similar to that of **Bz-BP**.

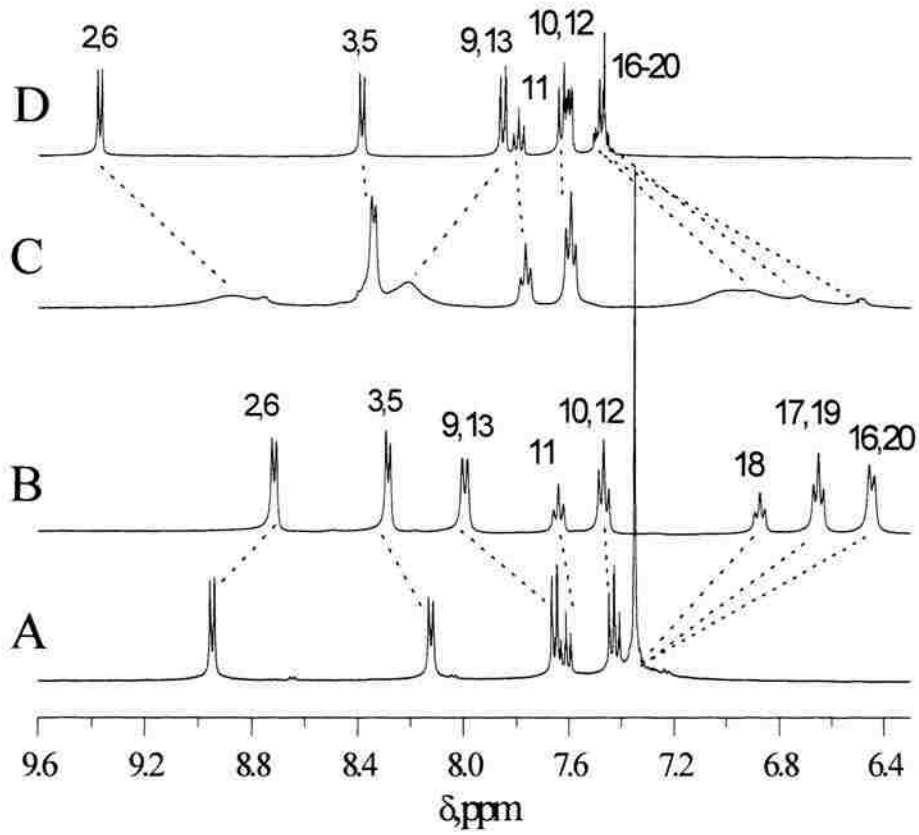

Figure 2.5. ^{1}H NMR at 23 °C of the aromatic region of **Bz-BP**. A, D: no **CB[7]**, in D_2O (9.4 mM) and DMSO-d_6 (18.8 mM), respectively. B, C: plus 1.0 mol equiv of **CB[7]** in D_2O and DMSO-d_6, respectively.

The redox chemistry of the three host-guest complexes was studied by cyclic voltammetry in DMSO/0.1 M $NaClO_4$. All free guests show two chemically reversible 1e reductions ($i_{p,c} \approx i_{p,a}$) of the pyridinium and the benzoyl group, respectively.[7] Data for **Me-BP** are shown in Figure 2.7, for **Bz-BP** and **Hex-BP** see Supporting Information.

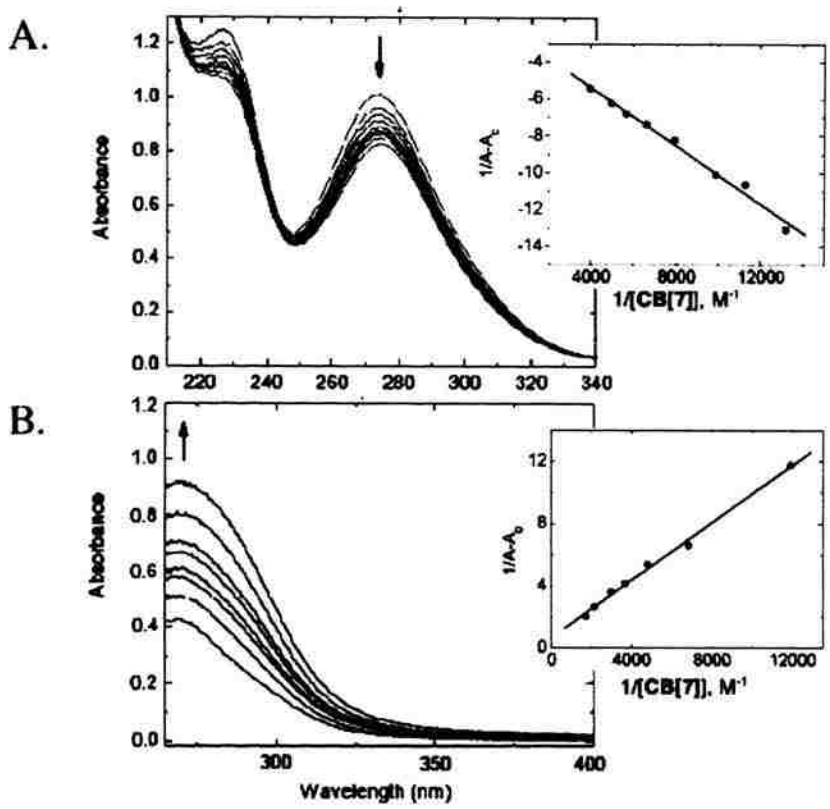

Figure 2.6. Titration at 23 °C of **Me-BP** with **CB[7]** in H_2O/0.1 M KCl (A, [**Me-BP**]=1.01 × 10^{-4} M, λ_{max}=274 nm) and in DMSO/0.1 M $NaClO_4$ (B, [**Me-BP**]=2.03 × 10^{-4} M, λ_{max}=270 nm).

In the absence of **CB[7]**, voltammograms normalized by dividing the faradaic current by the square root of the sweep rate coincide (Figure 2.7A), showing fast interfacial e-transfer kinetics (electrochemical reversibility). Upon addition of **CB[7]** we note two new waves (in addition to the old ones) at more positive potentials relative to those of free **Me-BP** (Figure 2.7B).

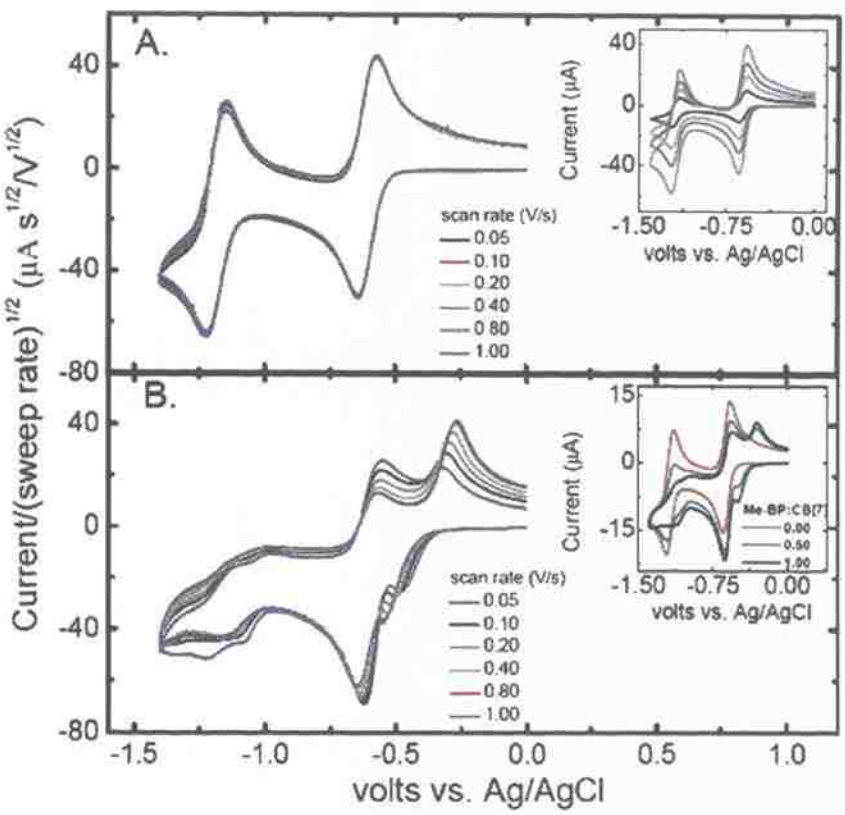

Figure 2.7. Normalized voltammetry of **Me-BP** (3.2 mM) in Ar-degassed DMSO/0.1 M $NaClO_4$ using a Au-disk (0.0201 cm^2) working electrode. A. No **CB[7]**; Inset: raw data. B. After addition of 1 mol equiv of **CB[7]**; Inset: voltammetry by adding **CB[7]** (raw data).

Normalized voltammograms no longer coincide implying quasi-reversible (slow) interfacial e-transfer. The positive shift of the first new wave is consistent with complexation that stabilizes the LUMO of the free guest;[15] based on $nF\Delta E^o=RT\ln K_{eq}$ and $\Delta E_{1/2}\approx\Delta E^o$, the wave of **Me-BP@CB[7]** should be 0.162 V more positive than the wave of free **Me-BP**, in agreement with the experiment (0.201 V). Based on K_{eq}=590 M^{-1} (Table 2.1), an equimolar solution (3.2 mM) of Me-BP and **CB[7]** contains 1.6 mM of each free guest and **Me-BP@CB[7]**, in agreement with the relative sizes of the voltammetric waves (taking into consideration the significantly lower diffusion coefficient expected for **Me-BP@CB[7]**). The peak-to-peak separation ($\Delta E_{p\text{-}p}$) of the wave assigned to **Me-BP@CB[7]** increases with the sweep rate, (as expected from a quasi-reversible e-transfer). **Bz-BP@CB[7]** and **Hex-BP@CB[7]** behave similarly (see Supporting information.) supporting that irrespective of the guest position in the cavity

the rate of e-transfer is low. $\Delta E_{p\text{-}p}$ in the case of **Me-BP@CB[7]** is measured easily and it was analyzed according to Kochi's method (see Supporting information),[16] yielding a standard rate constant k_s = 1.0 × 10^{-4} $cm{\cdot}s^{-1}$ (comparable to the one reported for MV).[1] With a reversibility limit for *ks* at about 0.03 $cm{\cdot}s^{-1}$ (this value yields $\Delta E_{p\text{-}p}$=65 mV at 0.1 Vs^{-1} for D=10^{-5} cm^2s^{-1}), and a distance attenuation factor for long-range electron transfer of 10 nm^{-1},[17] it is calculated that in **Me-BP@CB[7]** e-transfer takes place from a distance of 5.7 Å, which is about equal to the vertical distance (5.3 Å) between the edge of the rim and the outer perimeter of **CB[7]**. Spectroelectrochemically (see Supporting information), the neutral 1e reduced form of **Me-BP** (**Me-BP**$^{\cdot}$) remains intercalated in **CB[7]** and from the positive shift (~0.12 V) of its reduction wave from the 2nd wave of free **Me-BP** it is calculated that its formation equilibrium constant from free **Me-BP**$^{\cdot}$ and **CB[7]** is ≈110 M^{-1}.

2.4. CONCLUSIONS

Clearly, the ability to observe electrochemically both of the free and the complexed guest in the **Me-BP/CB[7]** systems is determined by the pre e-transfer K_{eq}.[18] In the **MV/CB[7]** system, where K_{eq}=2×10^5 M^{-1}, the equilibrium concentration of free **MV** is very small and consequently it is not observed electrochemically.[1] These results have definite implications in the design of molecular devices, while the aptitude of the most hydrophobic groups for the cavity is further explored for supramolecular protection in fundamental organic reactions such as the Hoffmann elimination and the Sandmeyer reaction.

2.5. ACKNOWLEDGMENTS

We thank the University of Missouri Research Board for financial support.

2.6. REFERENCES

1. Kim, H.-J.; Jeon, W. S.; Ko, Y. H.; Kim, K. *Proc. Nat. Acad. Sci. 2002*, **99**, 5007-5011.
2. Mendoza, S.; Davidov, P. D.; Kaifer, A. E. *Chem. Eur. J.* **1988**, *4*, 864-870.
3. Jeon, W. S.; Kim, H.-J.; Lee, C.; Kim, K. *Chem. Commun.* **2002**, 1828-1829.
4. Yuan, L.; Macartney, D. H. *J. Phys. Chem. B* **2007**, *111*, 6949-6954.
5. Lee, J. W.; Samal, S.; Selvapalam, N.; Kim, H.-J.; Kim, K. *Acc. Chem. Res.* **2003**, *36*, 621-630.
6. Rawashdeh, A.-M. M.; Thangavel, A.; Sotiriou-Leventis, C.; Leventis, N. *Org. Lett.* **2008**, *10*, 1131-1134.
7. (a) Leventis, N.; Meador, M. A. B.; Zhang, G.; Dass, A.; Sotiriou-Leventis, C. *J. Phys. Chem. B.* **2004**, *108*, 11228-11235. (b) Leventis, N.; Rawaswdeh, A.-M. M.; Zhang, G.; Elder, I. A.; Sotiriou-Leventis, C. *J. Org. Chem.* **2002**, *67*, 7501-7510. (c) Leventis, N.; Elder, I. A.; Gao, X.; Bohannan, E. W.; Sotiriou-Leventis, C.; Rawashdeh, A.-M. M.; Overschmidt, T. J.; Gaston, K. R. *J. Phys. Chem. B* **2001**, *105*, 3663-3674. (d) Leventis, N.; Gao, X. *J. Electroanal. Chem.* **2001**, *500*, 78-94.
8. Moon, K.; Kaifer, A. E. *Org. Lett.* **2004**, *6*, 185-188.
9. Sindelar, V.; Moon, K.; Kaifer, A. E. *Org. Lett.* **2004**, *6*, 2665-2668.
10. Halterman, R. L.; Moore, J. L.; Mannel, L. M. *J. Org. Chem.* **2008**, *73 (8)*, 3266 - 3269.
11. Cartwright, H. M. *Microchem. J.* **1986**, *34*, 313-318.
12. (a) Marques, C.; Hudgins, R. R.; Nau, M. W. *J. Am. Chem. Soc.* **2004**, *126*, 5806-5816. (b) Buschmann, H.-J.; Wego, A.; Zielesny, A.; Schollmeyer, E. *Journal of Inclusion Phenomena and Macrocyclic Chem.*, **2006**, *54*, 85-88.
13. Choi, S.; Park, H. S.; Ziganishina, A. Y.; Ko, Y. H.; Lee, J. W.; Kim, K. *Chem.Commun.* **2003**, 2176-2177.
14. Connors, K. A. Binding Constants, The Measurement of Molecular Complex *Stability*, John Wiley and Sons, Inc.: New York, N.Y., 1987.
15. It is noted that since the absorbance l_{max} does not change, both the HOMO and the LUMO of **Me-BP** are stabilized by the same energy.
16. Klingler, R. J.; Kochi, J. K. *J. Phys. Chem.* **1981**, *85*, 1731-1541.
17. Amatore, C.; Bouret, Y.; Maisinhaute, E.; Abruña, H. D.; Goldsmith, J. I. *C. R. Chimie* **2003**, *6*, 99-115.
18. Bard, A. J.; Faulkner, L. J. *Electrochemical Methods, Fundamentals and Applications*, 2nd ed.; Wiley: New York, 2000.

Appendix S.2.1, Preparation of **CB[7]**; Appendix S.2.2, Stoichiometry determination for **Me-BP@CB[7]**, **Hex-BP@CB[7]** and **Bz-BP@CB[7]** in water (ESI mass spectroscopy) and in DMSO (via Job Plots); Appendix S.2.3, Additional ^{1}H-NMR information for the **Me-BP/CB[7]** and **Bz-BP/CB[7]** systems; Appendix S.2.4, ^{1}H-NMR data of **Hex-BP** in D_2O and DMSO-d_6; Appendix S.2.5, Optical absorption data for **Bz-BP** and **Hex-BP** in water and DMSO; Appendix S.2.6, Electrochemical data for **Bz-BP** and **Hex-BP** in DMSO/0.1 M $NaClO_4$; Appendix S.2.7, Spectroelectrochemical data for **Me-BP** in DMSO/0.1 M $NaClO_4$; Appendix S.2.8, Kinetic analysis of the electrochemical data for the **Me-BP/CB[7]** system.

Appendix S.2.1: Preparation of CB[7].

CB[7] was prepared by modification of a literature procedure.[1] Glycoluril (20.0 g, 141 mmol) was mixed with finely powdered paraformaldehyde (8.45 g, 202 mmol) in a 500 mL beaker. HCl (5M, 250 mL) was ice-cooled and it was added slowly to the beaker under magnetic stirring. After the addition was complete, the beaker was covered with a watch glass and it was heated to ~90 °C. Heating of the reaction mixture under stirring was continued for five days while the volume was maintained at ~250 mL by addition of HCl.

On the fifth day, the reaction mixture was cooled to room temperature and methanol (400 mL) was added causing immediate formation of a white precipitate. The precipitate was filtered and it was air-dried at room temperature. The dry white solid was suspended in 400 mL of 20% aqueous glycerol in a 500 mL beaker and the solution was heated to ~80 °C under vigorous stirring for about 3 h. The heterogeneous mixture was filtered and the colorless aqueous glycerol solution was transferred to a 1L beaker and CH_3OH (400 mL) was added. A white precipitate was formed immediately, and the suspension was allowed to stand at room temperature for 24 h. Subsequently, the mixture was suction-filtered and the solid was rinsed on the filter with plenty of methanol till all glycerol was removed (monitored by ^{1}H NMR with samples taken from the precipitate and dried in a vacuum heating oven). At the end the precipitate was dried in the open air

---

1. Halterman, R. L.; Moore, J. L.; Mannel, L. M. *J. Org. Chem.* **2008**, *73 (8)*, 3266 -3269.

for about three days. The purity of the product was checked by ^{1}H NMR and was more than 95%.

The crude product was purified further by first dissolving it in the minimum amount of water. (To facilitate dissolution, one may need to add a few drops of HCl.) Subsequently, enough methanol was added to the homogeneous clear solution to induce cloudiness and the mixture was placed in the refrigerator for about 6 h. The precipitate that was formed was filtered and dried. Recrystallization was repeated twice. Yield of pure **CB[7]**: 4 g (3.44 mmol, 17.1 %).

Appendix S.2.2: Stoichiometry determination for **Me-BP@CB[7]**, **Hex-BP@CB[7]** and **Bz-BP@CB[7]** in water (ESI mass spectrometry) and in DMSO (via Job plots).

ESI mass spectra

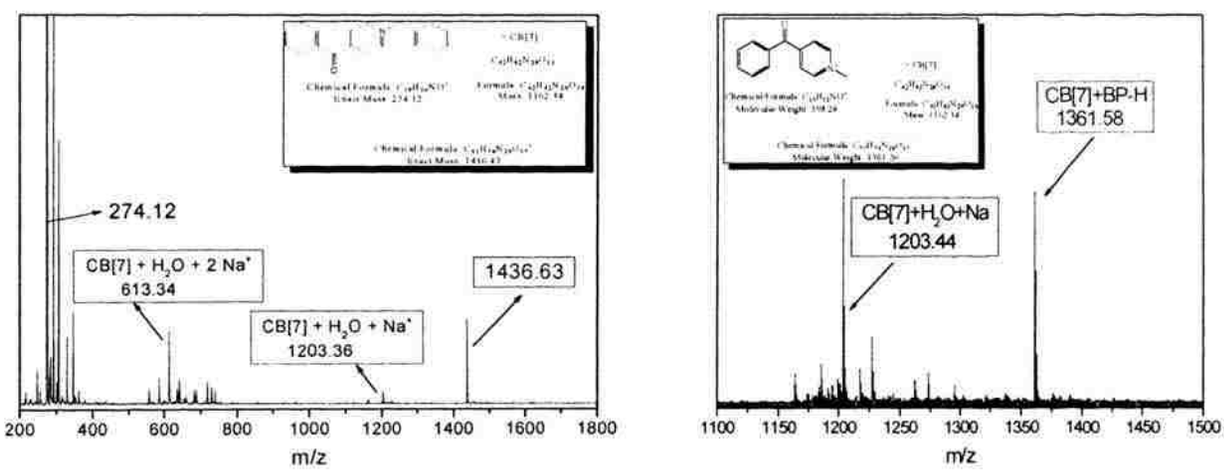

Figure S.2.1. ESI/MS of **Me-BP@CB[7]** and **Bz-BP@CB[7]** in H_2O.

Job Plots[2]

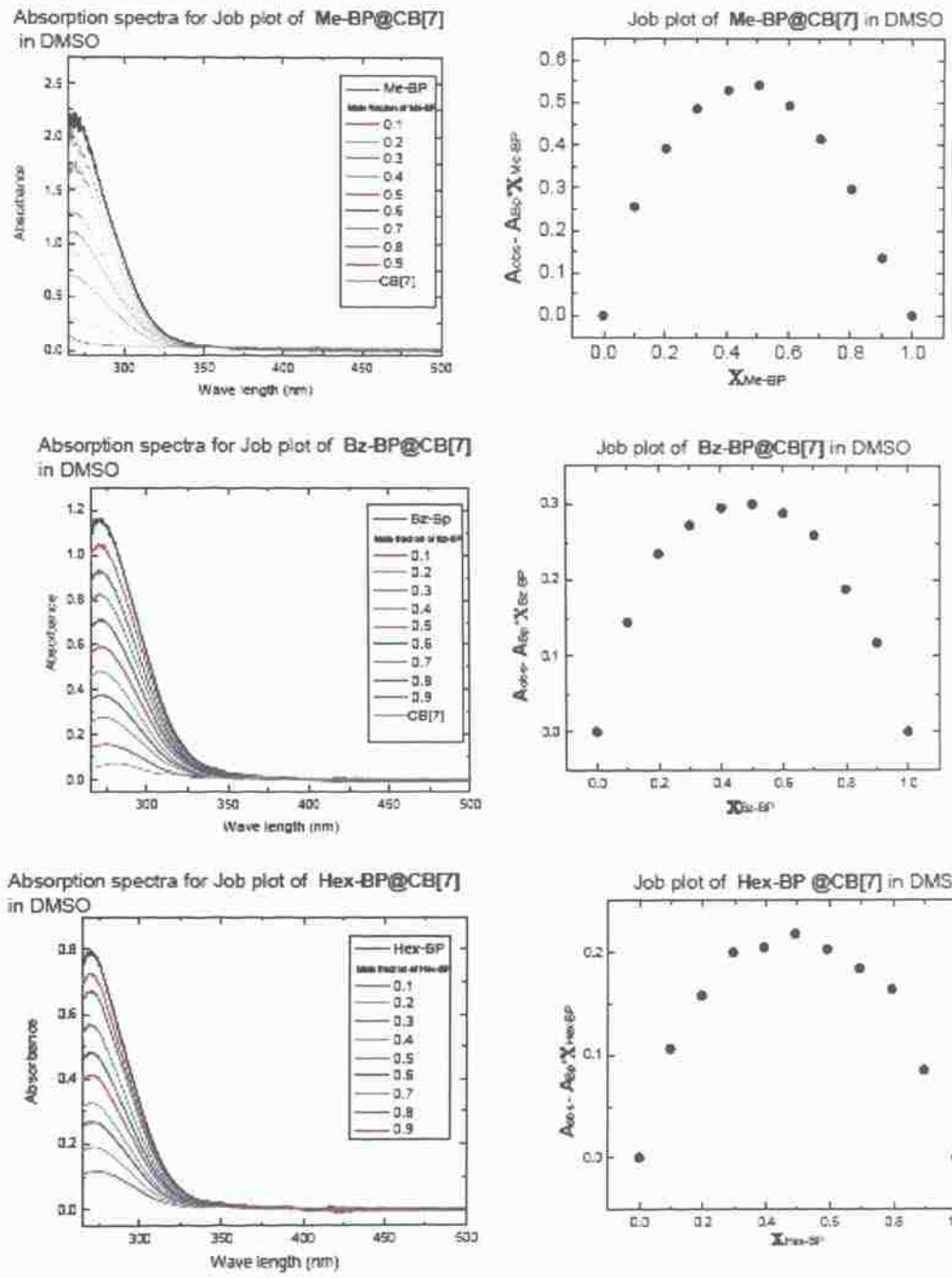

X = mole ratio of benzoylpyridinium: (BP) = mol BP / (mol BP + mol **CB[7]**). The maximum of the Job plot is always at **X**=0.5, therefore the complex stoichiometry is 1:1.

Figure S.2.2. Job plot of **Me-BP@CB[7]**, **Bz-BP@CB[7]** and **Hex-BP@CB[7]** in DMSO.

---

2. (a) Job, P. *Annali di Chimica Applicata* **1928**, *9*, 113-203. (b) Krunz, M. M.; Pfendt, L. B. *Microchem. J.* **1983**, *28*, 162-167. (c) Cartwright, H. M. *Microchem. J.* **1986**, *34*, 313-318.

Appendix S.2.3: Additional ^{1}H-NMR information for the **Me-BP/CB[7]** and **Bz-BP/CB[7]** systems.

Data for **Me-BP/CB[7]** in D_2O and DMSO-d_6 (no salts added)

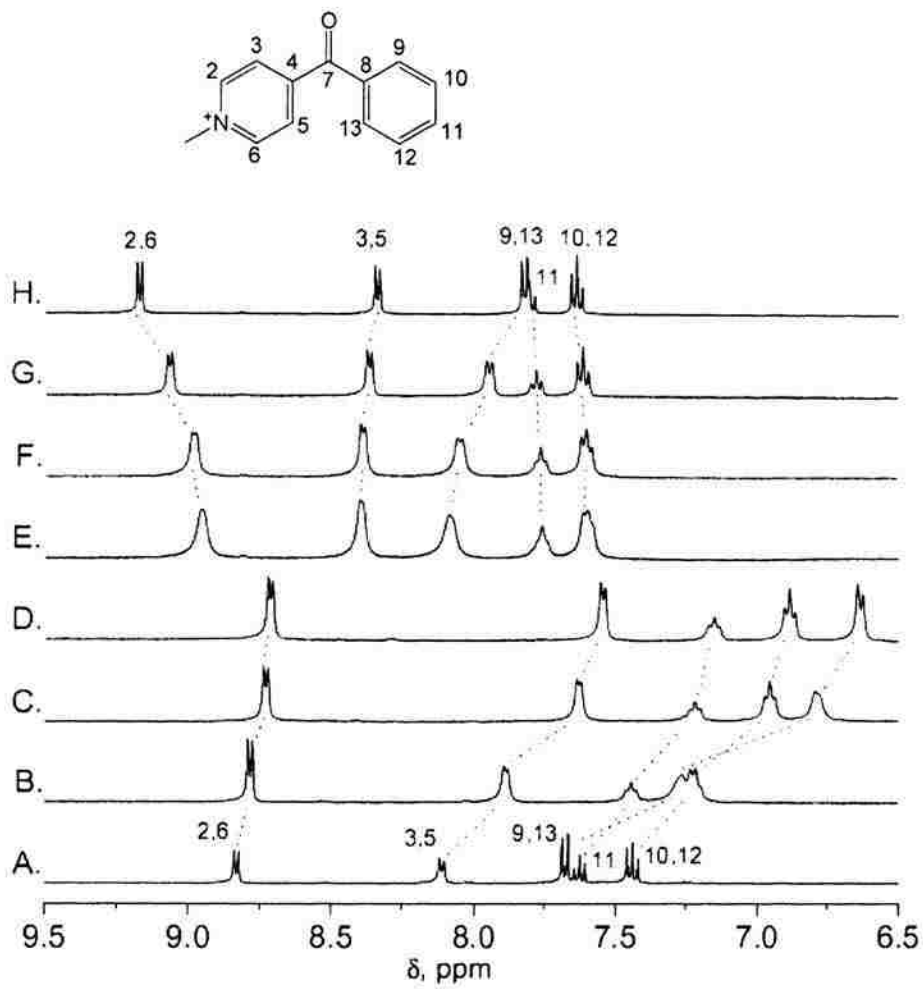

Figure S.2.3. ^{1}H-NMR at 23 °C of the aromatic protons of **Me-BP** in D_2O (A-D; 21.1 mM)[3] and DMSO-d_6 (E-H; 9.1 mM). A,H: no **CB[7]**. B,G: 0.5 mol eq. of **CB[7]**. C,F: 1.0 mol eq. of **CB[7]**. D,E: 1.25 mol eq. of **CB[7]**.

---

3. ^{1}H-NMR of **Me-BP** in D_2O in our previous studies was conducted in the presence of 0.1 M KCl.[3] In this study, in order to correlate the ^{1}H-NMR data with the structures obtained via semi-empirical calculations, ^{1}H-NMR was conducted in the absence of salts. We observe that the mode of inclusion does not change in the presence or absence of KCl: all protons move upfield in both cases, but to a lesser extent with KCl.

The largest shifts are observed for H3,5 (0.24 ppm), H9,13 (0.58 ppm), H10,12 (0.34 ppm) and H11 (0.28 ppm). Protons H2,6 move upfield by only 0.06 ppm indicating that they are near the carbonyls (i.e, the transition zone between the interior-shielding and exterior-deshielding), while the *N*-CH_3 protons are almost insensitive to the presence of **CB[7]**, moving *downfield* by 0.03 ppm indicating that they are outside but not very near the portals. On the contrary, in DMSO-d_6 some aromatic protons move upfield and some downfield. Protons H2,6 and H3,5 move upfield by 0.25 ppm, while protons H10,12 and H11 at the other end of **Me-BP** are practically insensitive to the presence of **CB[7]**. Protons H9,13 and the *N*-CH_3 protons both move *downfield* by 0.57 ppm and 0.73 ppm, respectively. From these data, in DMSO-d_6 H2,6 and H3,5 are inside the cavity, H9,13 and the *N*-methyl protons are just outside and interact strongly with the carbonyls at the two portals, leaving H10,12 and H11 outside and far from the cavity.

Data for **Bz-BP/CB[7]**

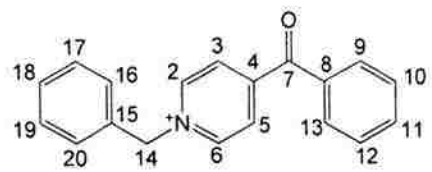

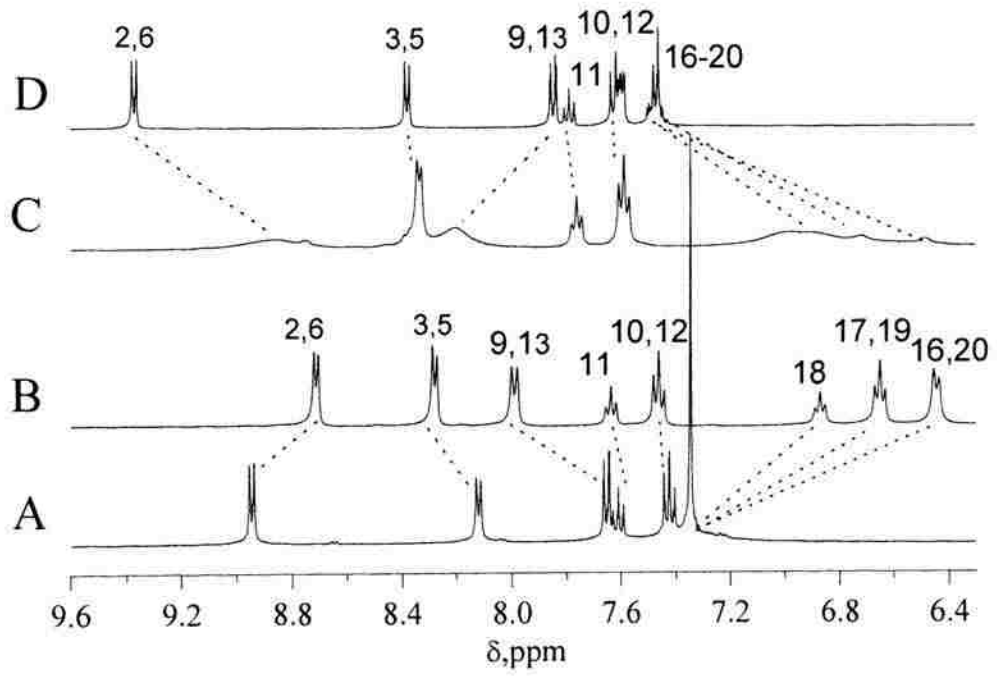

Figure S.2.4. Room temperature (23 °C) ^{1}H-NMR of the aromatic region of **Bz-BP**. A, D: no **CB[7]**, in D_2O (9.4 mM) and DMSO-d_6 (18.8 mM), respectively. B, C: plus 1.0 mol equivalent of **CB[7]** in D_2O and DMSO-d_6, respectively.

In both D_2O and DMSO-d_6 benzyl protons move upfield (0.5-0.9 ppm) indicating that the benzyl group is inside the cavity. Similarly, H2,6 move upfield (by 0.23 ppm in D_2O and by 0.50 ppm in DMSO-d_6) indicating that they are also inside the cavity. H3,5 move 0.16 ppm *downfield* in D_2O and only 0.04 ppm upfiled in DMSO-d_6, indicating that they are in the transition carbonyl region. H9,13 move downfield in both solvents (0.34 ppm in D_2O and 0.35 ppm in DMSO-d_6) indicating that they are outside and near the portal oxygens. H10,12 and H11 are practically insensitive to **CB[7]**, moving downfield by only 0.02-0.04 ppm indicating that they are outside and far from the portals.

Appendix S.2.4: ^{1}H-NMR data of **Hex-BP** in D_2O and DMSO-d_6

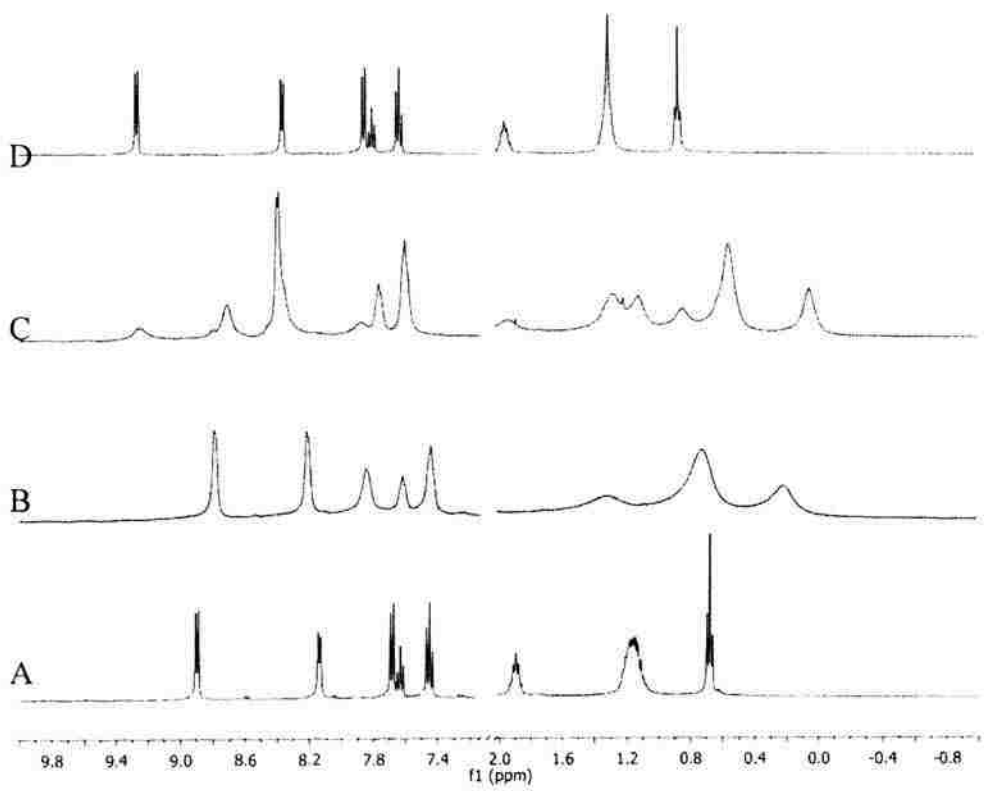

Figure S.2.5. Room temperature (23 °C) ^{1}H-NMR of the aromatic region of **Hex-BP**. A, D: no **CB[7]**, in D_2O (12.8 mM) and DMSO-d_6 (13.5 mM), respectively. B, C: plus 1.0 mol equivalent of **CB[7]** in D_2O and DMSO-d_6, respectively.

Appendix S.2.5: Optical absorption data for **Bz-BP** and **Hex-BP** in water and DMSO.

Bz-BP in water

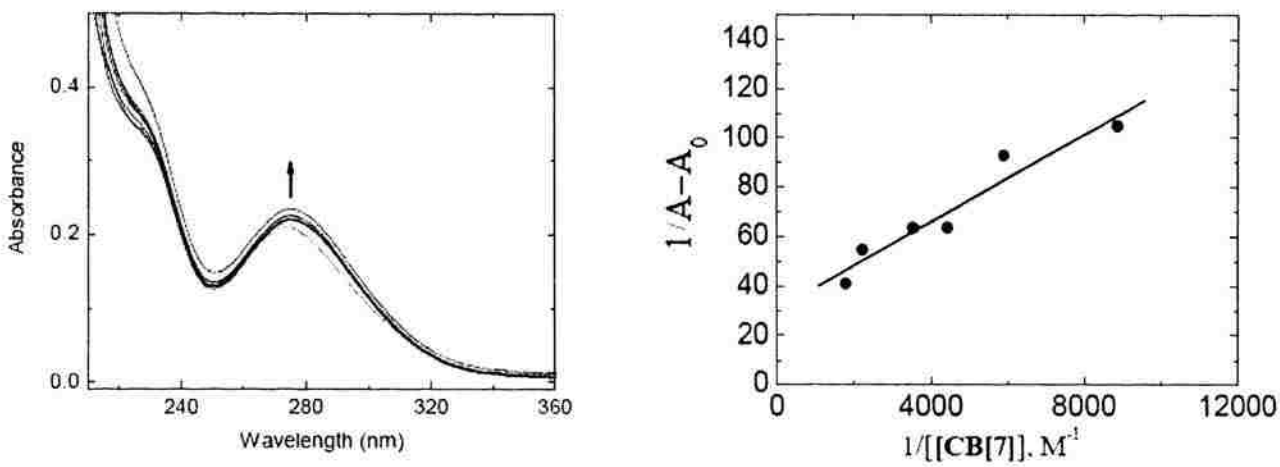

Figure S.2.6. Left: Room temperature (23 °C) titration of **Bz-BP** (2.05×10^{-5} M) with **CB[7]** in H_2O/0.1 M KCl; λ_{max}=274 nm. Right: Benesi-Hildebrand plot.

Bz-BP in DMSO

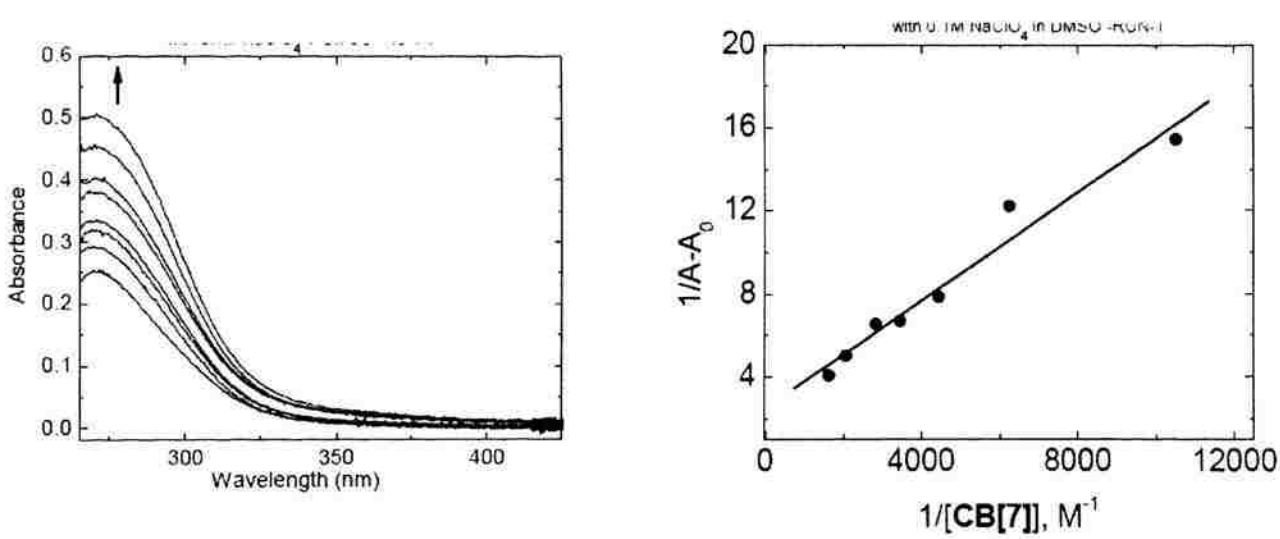

Figure S.2.7. Top: Room temperature (23 °C) titration of **Bz-BP** (1.72×10^{-4} M) with **CB[7]** in DMSO/0.1 M $NaClO_4$; λ_{max}=274 nm. Bottom: Benesi-Hildebrand plot.

Appendix S.2.6: Electrochemical data for **Me-BP**, **Bz-BP** and **Hex-BP** in DMSO/0.1 M $NaClO_4$.

Me-BP

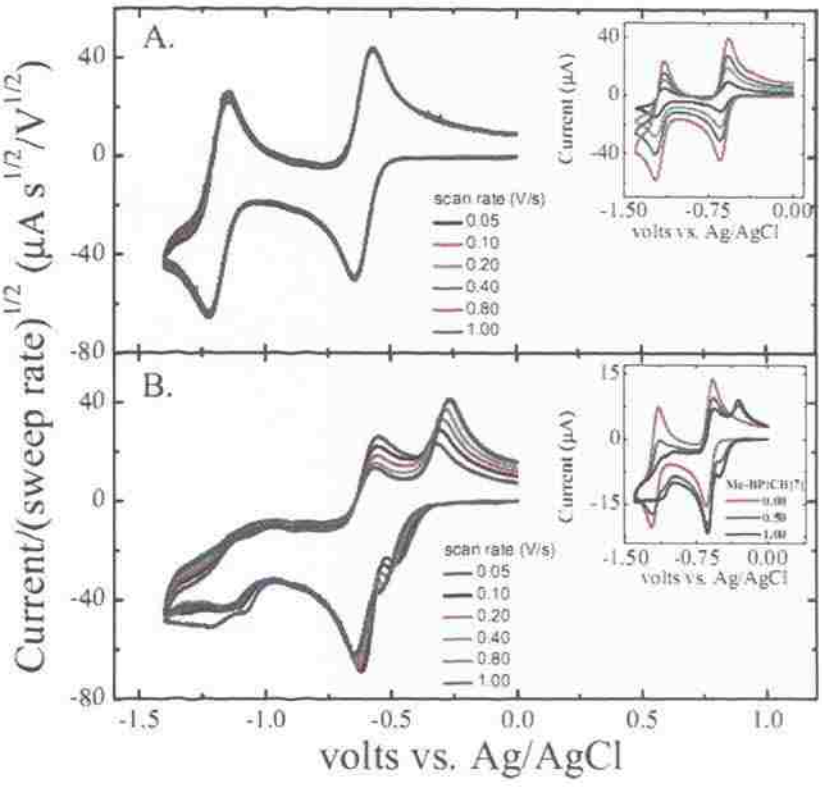

Figure S.2.10. Normalized voltammetry (by dividing faradaic current by the square root of the sweep rate) of **Me-BP** (3.2 mM) in Ar-degassed DMSO/0.1 M $NaClO_4$ using a Au-disk (0.0201 cm^2) working electrode. A. No **CB[7]**; Inset: raw data. B. After addition of 1 mol equivalent of **CB[7]**; Inset: Successive voltammograms by adding **CB[7]** (raw data).

Me-BP

$E_{1/2}$(1st wave): -0.606 V vs. Ag/AgCl ($\Delta E_{p\text{-}p}$ = 0.060 V)

$E_{1/2}$(2nd wave): -1.185 V vs. Ag/AgCl ($\Delta E_{p\text{-}p}$ = 0.070 V)

Me-BP@CB[7]

$E_{1/2}$(1st wave): -0.405 V vs. Ag/AgCl ($\Delta E_{p\text{-}p}$ varies, see Appendix 8)

$E_{1/2}$(2nd wave): -1.070 V vs. Ag/AgCl ($\Delta E_{p\text{-}p}$ varies)

For the exact peak positions at the various sweep rates see the kinetic analysis in Appendix 8, below.

Bz-BP

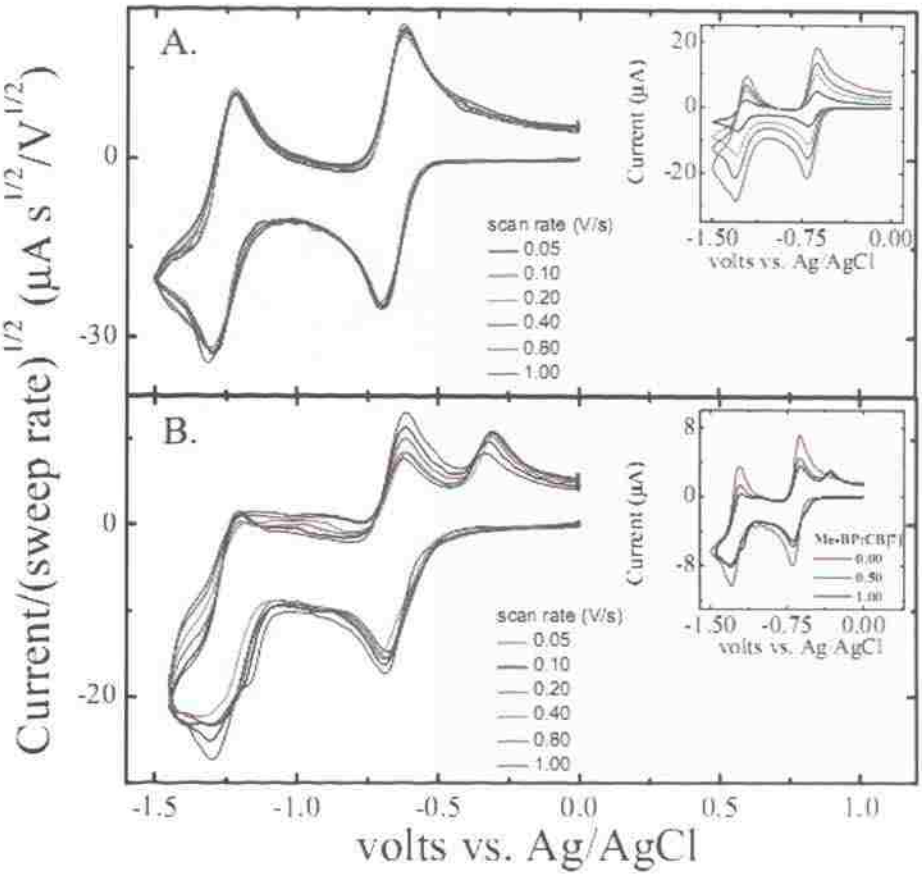

Figure S.2.11. Normalized voltammetry (by dividing faradaic current by the square root of the sweep rate) of **Bz-BP** (3.0 mM) in Ar-degassed DMSO/0.1 M $NaClO_4$ using a Au-disk (0.0201 cm^2) working electrode. A. No **CB[7]**: Inset: raw data. B. After addition of 1 mol equivalent of **CB[7]**; Inset: Successive voltammograms by adding **CB[7]** (raw data).

Although the re-oxidation wave owing to the first-electron reduction of **Bz-BP@CB[7]** is clearly visible and its peak potential shifts in the positive direction by increasing the sweep rate (indicating quasi-reversibility and slow interfacial e-transfer kinetics), analysis according to Kochi's method was not attempted because the reduction wave is merged with the reduction wave of free **Bz-BP** and determination of the peak-to-peak separation is not possible.

Hex-BP

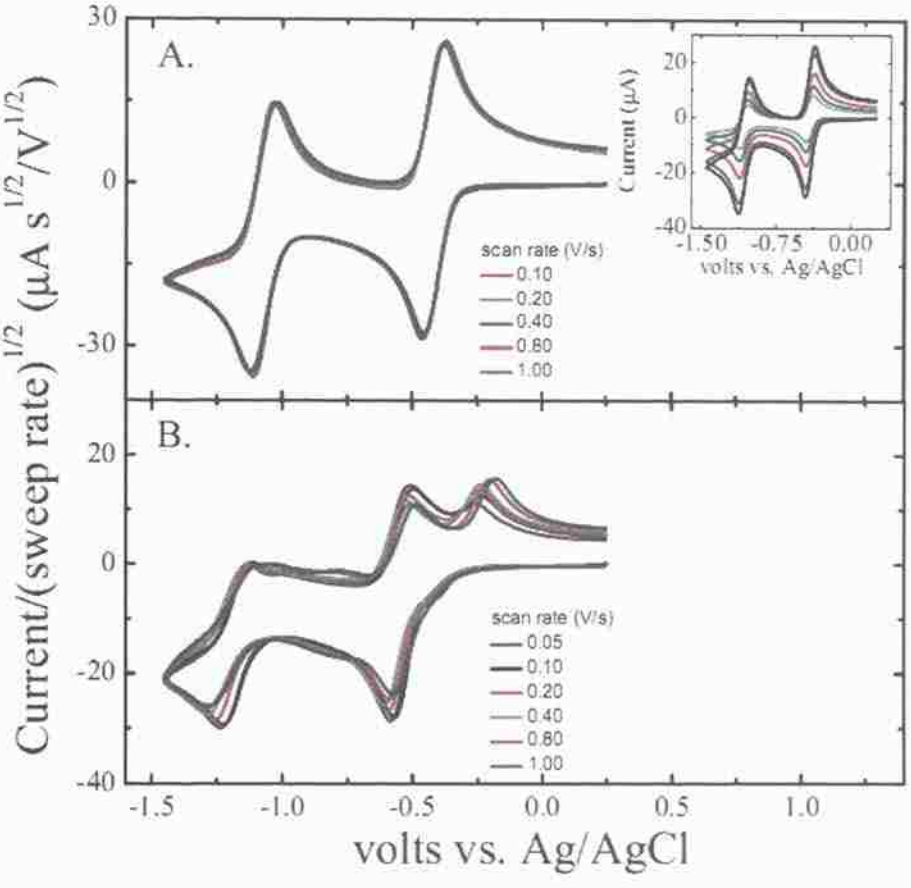

Figure S.2.12. Normalized voltammetry (by dividing faradaic current by the square root of the sweep rate) of **Hex-BP** (3.3 mM) in Ar-degassed DMSO/0.1 M $NaClO_4$ using a Au-disk (0.0201 cm^2) working electrode. A. No **CB[7]**; Inset: raw data. B. After addition of 1 mol equivalent of **CB[7]**.

Again, although the re-oxidation wave owing to the first-electron reduction of **Hex-BP@CB[7]** is clearly visible and its peak potential shifts in the positive direction by increasing the sweep rate (indicating quasi-reversibility and slow interfacial e-transfer kinetics), analysis according to Kochi's method was not attempted because the reduction wave is merged with the reduction wave of free **Hex-BP** and determination of the peak-to-peak separation is not possible.

Appendix S.2.7: Spectroelectrochemical data for **Me-BP** in DMSO/0.1 M $NaClO_4$

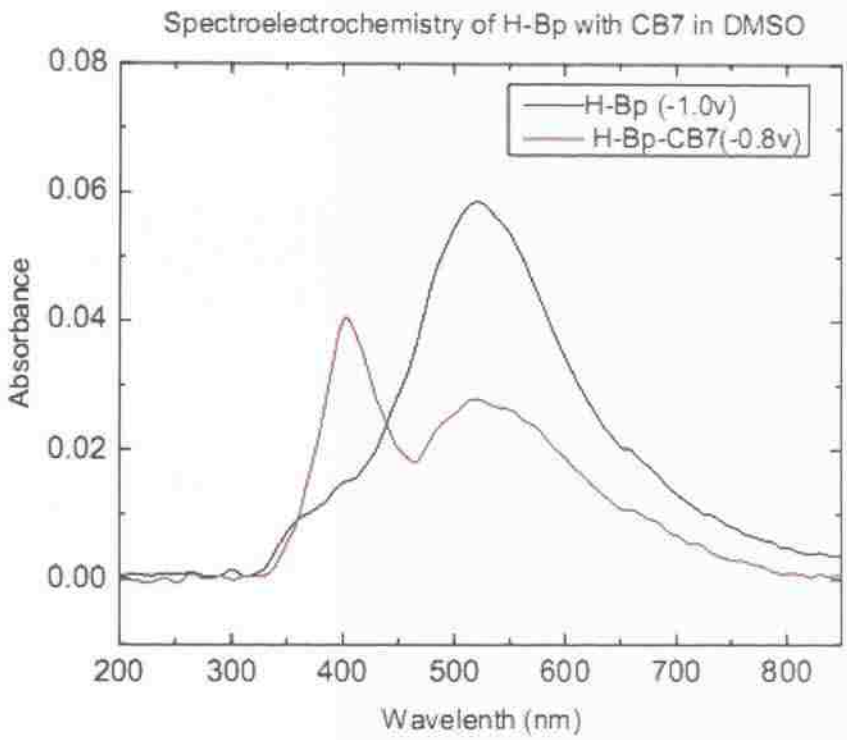

Figure S.2.13. Spectroelectrochemistry of the one-electron reduced form **Me-BP** and of **Me-BP@CB[7]** using a thin layer cell (~0.15 mm thick) made of two ITO glasses in a solution containing **Me-BP** (3.0 mM) without (black line) and with (red line) 1 mol equivalent of **CB[7]**.

The presence of **CB[7]** causes a change in the vibrational resolution of the absorpion spectrum of the 1e-reduced form of **Me-BP**, signifying that the neutral radical does form a complex with **CB[7]**.

Appendix S.2.8: Kinetic analysis of the electrochemical data for the **Me-BP/CB[7]** system.

The peak-to-peak separation can be introduced in eq. S1,[4] for the calculation of the standard rate constant k_s of a quasi-reversible e-transfer process:

$$k_s = 2.18\left(\frac{D\beta_w nF\upsilon}{RT}\right)^{1/2} \exp\left[-\frac{\beta_w{}^2 nF}{RT}(E_p^{anodic} - E_p^{cathodic}\right] \qquad \text{(S1)}$$

where D is the diffusion coefficient of the redox active species (approximated here at 8×10^{-6} cm^2s^{-1}), n is the number of electrons exchanged with the electrode per molecule, F the Faraday constant, R the gas constant, T the absolute temperature, υ the potential sweep rate (in Vs^{-1}), E_p^{anodic} and $E_p^{cathodic}$ (in volt) are the anodic and cathodic peak-current potentials, and the transfer coefficient β_w is given by eq S2,[5]

$$\beta_w = \left[\frac{1.857RT}{nF}\right]\left[E_p^{cathodic} - E_{p/2}^{cathodic}\right]^{-1} \qquad \text{(S2)}$$

where $E_{p/2}^{cathodic}$ is the potential (in volt) where the cathodic current is equal to half the cathodic peak current ($i_{pc}/2$) that is recorded at $E_p^{cathodic}$.

The k_s value may vary as the potential sweep rate, υ, increases. The k_s value reported for the quasi-reversible 1e reduction of **Me-BP@CB[7]** (1.0×10^{-4} $cm\,s^{-1}$) is the one reached asymptotically at high $\Delta E_{p\text{-}p}$ separations (high potential scan rates).

---

4. Eq. 26 in: Klingler, R. J.; Kochi, J. K. *J. Phys. Chem.* **1981**, *85*, 1731-1541.

5. Eq. 24 in the reference of footnote 4.

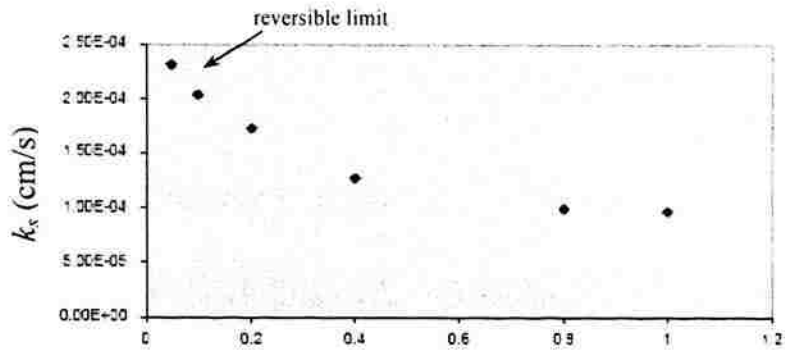

Figure S.2.14. Standard rate constants, k_s, calculated via equations S1 and S2 from the data of Figure S.2.8 at various potential scan rates.

Table S.2.1. Data extracted from Figure S.2.8 for the derivation of the standard rate constant, *ks*, of the first-electron reduction of **Me-BP@CB[7]** according to eq.s S1 and S2.

Scan rate (V/s)	$E_{p\text{-}c}(1)$ (mV)	$E_{p\text{-}a}(1)$ (mV)	$\Delta E_{p\text{-}p}(1)$ (mV)	$E_{p\text{-}c}(2)$ (mV)	$E_{p\text{-}a}(2)$ (mV)	$\Delta E_{p\text{-}p}(2)$ (mV)	i_{pc}* (μA)	$i_{pc}/2$ (μA)	$E_{p\text{-}c/2}(1)$ (mV)	$E_{p\text{-}c}(1)$- $E_{p\text{-}c/2}(1)$ (V)	β_w**	k_s (cm/s)
0.05	-487.50	-311.80	175.7	-636.74	-570.18	66.56	-27.28	-13.68	-420.53	0.0669	0.712	2.31E-04
0.1	-504.04	-305.19	198.85	-633.44	-573.49	59.95	-30.46	-15.23	-438.30	0.0657	0.725	2.04E-04
0.2	-520.57	-295.26	225.31	-636.74	-570.18	66.56	-32.79	-16.39	-453.19	0.0674	0.708	1.73E-04
0.4	-533.80	-275.42	258.38	-649.97	-570.18	79.79	-35.91	-17.95	-469.72	0.0641	0.744	1.27E-04
0.8	-550.34	-262.19	288.15	-646.66	-573.49	73.17	-38.68	-19.34	-479.23	0.0711	0.671	9.98E-05
1.0	-553.65	-258.88	294.77	-646.66	-566.88	79.78	-38.3	-19.15	-486.26	0.0674	0.708	9.72E-05

* $i_{pc} = i_{p\text{-}c}(1)$-$i_{@0.2V}$

** $\beta_w = [1.857\,RT / nF][E_p\text{-}E_{p/2}]^{-1}$

3. CONTROL OF QUINONE TO *GEM*-DIOL EQUILIBRIUM BY INTERACTION WITH CUCURBIT[7]URIL

Arumugam Thangavel, Chariklia Sotiriou-Leventis,* and Nicholas Leventis*

Department of Chemistry, Missouri University of Science and Technology‡,

Rolla, MO 65409, U.S.A.

leventis@mst.edu; cslevent@mst.edu

3.1. ABSTRACT

N,N'-dimethyl-2,6-diaza-9,10-anthraquinonediium dication (**DAAQ**) in water not only exists in equilibrium with its *gem*-diol but also forms aggregates which cause line-broadening in ^{1}H NMR. At low pH (<1), the aggregates break up and the equilibrium is shifted exclusively toward the quinone form. In the presence of **CB[7]**, the quinone form undergoes inclusion with **CB[7]** by slow exchange in both water and aqueous acid. Both free and **CB[7]**-intercalated quinone forms are observed by ^{1}H NMR.

3.2. INTRODUCTION

Aza and diazaanthraquinones represent an important class of antitumor[1,2] and antimicrobial agents.[3] Moreover, anthraquinone derivatives show two successive electron reduction steps that make them ideal molecules for sensors in electroanalytical applications. Because of their unique photophysical properties, they are used as chemosensors for metal ions[4] and anions.[5,6] They are also being used in photoinduced electron transfer as electron acceptors linked to a plethora of different molecules ranging from conjugated polymers,[7] to porphyrin-containing polyamide dendrimers.[8]

Several studies regarding the intercalation of anthraquinone derivatives with DNA[9] and synthetic hosts such as cucurbit[7]uril (**CB[7]**)[10] and cyclodextrin[11] have been published. Recently, we have reported that monocationic *N*-substituted-4-benzoylpyridiniums can be oriented either *exo*- or *endo*-, placing the most hydrophobic group inside the hydrophobic **CB[7]** cavity.[12,13] The driving force is so strong that those guests shift their keto to *gem*-diol equilibrium towards the keto form in order to place the keto form inside the cavity, despite the solvent (H_2O) stabilization of the *gem*-diol via H-

---

‡ Formerly, University of Missouri-Rolla.

bonding. As an extension to this work, and in order to test the generality of these results, we set out to study the effect of keto to *gem*-diol equilibrium on dicationic guests such as *N,N'*-dimethyl-2,6-diaza-9,10-anthraquinonediium (**DAAQ**) in the presence of **CB[7]**.

3.3. RESULTS AND DISCUSSION

3.3.1. ^{1}H NMR Study. According to Figure 3.1, **DAAQ** in DCl-D_2O (4.67 Molar, pH<1) shows only three signals in the aromatic region corresponding to $H_{1,6}$(s), $H_{3,8}$(d) and $H_{4,9}$(d) of the quinone form. In D_2O, **DAAQ** shows extra peaks in addition to the peak broadening. Careful examination reveals that these extra peaks: H_1 (s), H_6 (s), H_3 (d), H_8 (d), $H_{4,9}$ (partially overlapping d) come from the *gem*-diol, a product of hydration of **DAAQ** (Scheme 3.1). Hydration of carbonyl compounds has been investigated in recent years,[12] including an analysis in terms of multidimentional Marcus theory.[14] On the other hand, **DAAQ** in anhydrous DMSO-d_6, shows three broad singlets suggesting aggregate formation **(DAAQ)n**. This is supported by X-ray crystallography, as the BF_4^- counter ions promote electrostatic aggregate formation by holding together **DAAQ** dications which would have had otherwise electrostatic repulsions via their positively charged nitrogens (see Supporting Information). Upon titration of a solution of **DAAQ** in D_2O with varied mol equivalents of aq. DCl, disappearance of the gem-diol peaks and progressively conversion of the broad aggregate **(DAAQ)n**, peaks into sharper quinone peaks was observed (Figure 3.2). Thus in the presence of an acid (pH<1), the equilibrium of Scheme 3.1 is shifted towards the quinone form **DAAQ** via protonation of one of the hydroxyl groups of the *gem*-diol, followed by dehydration.

Scheme 3.1. Hydration of **DAAQ**

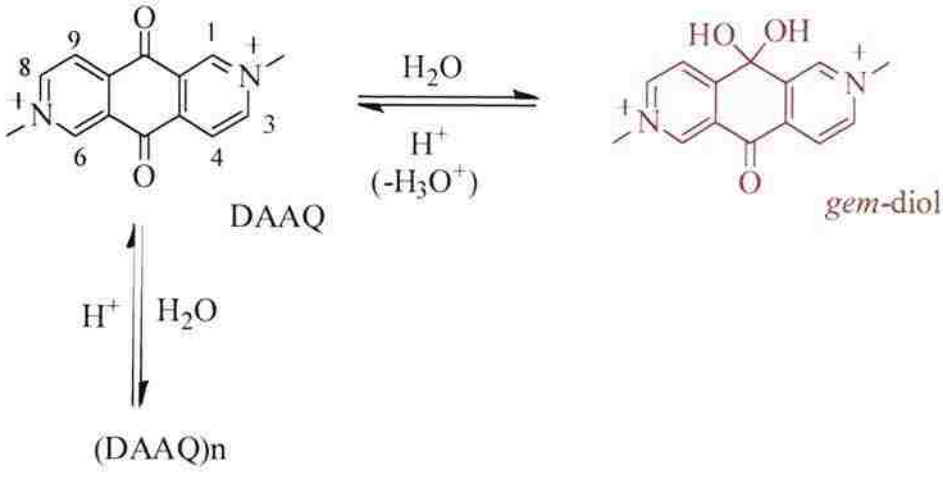

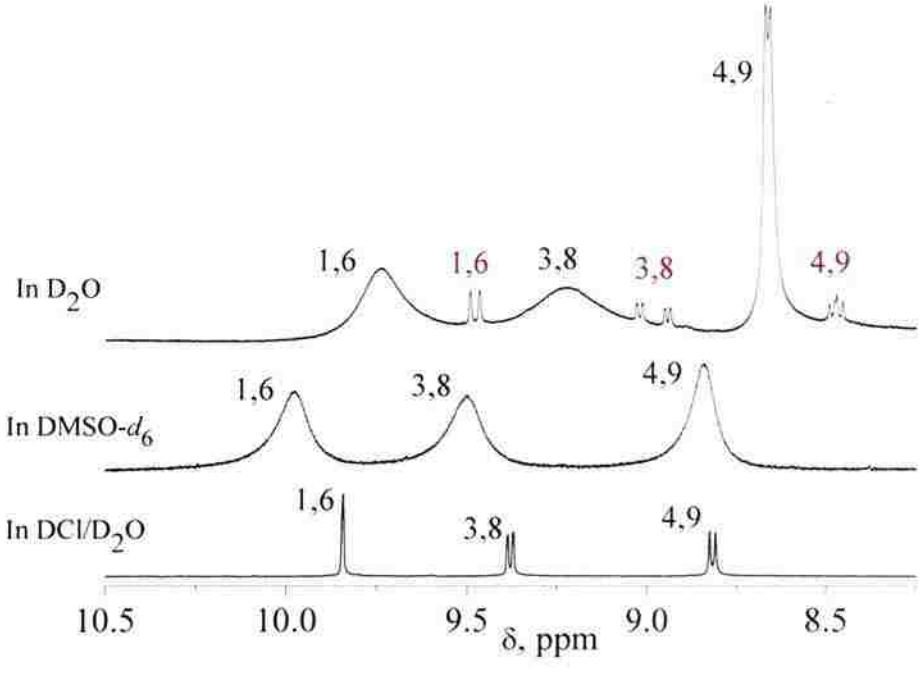

Figure 3.1. ^{1}H NMR spectra of the aromatic region of **DAAQ** in D_2O, DMSO-d_6 and DCl/D_2O.

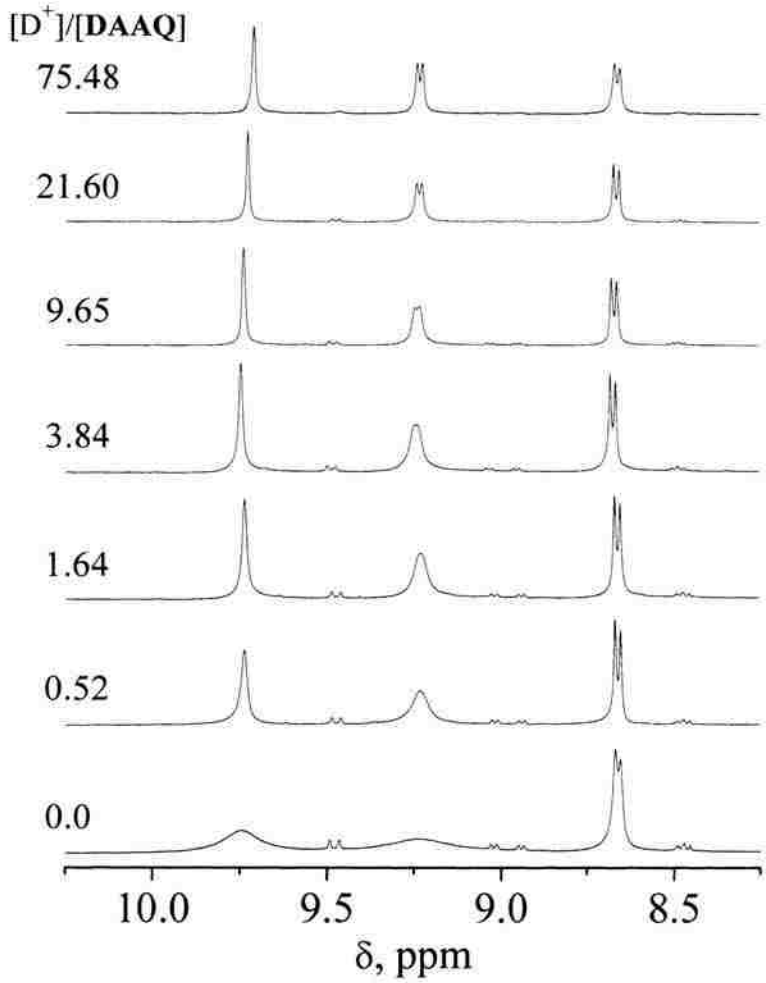

Figure 3.2. Titration of a solution of **DAAQ** in D_2O (20 mM) with different mol equivalents of DCl.

^1H NMR is a reliable tool for structural elucidation of host-guest complexes. Figure 3.3 shows the evolution of the spectra of **DAAQ** in DCl/D_2O upon progressive addition of **CB[7]**. When 0.25 mol equivalents of **CB[7]** were added, quinone forms an inclusion complex with **CB[7]** with such a slow rate so that both intercalated: **DAAQ@CB[7]** and free **DAAQ** can be observed within the time scale of ^1H NMR. As the addition of **CB[7]** progresses, the amount of **DAAQ@CB[7]** increases at the expense of **DAAQ**. At saturation (addition of 1.25 mol equivalents of **CB[7]**), only the **DAAQ@CB[7]** peaks are visible. $H_{1,6}$ and $H_{4,8}$ are being shielded upfield by 0.376 ppm and 0.106 ppm, respectively, indicating that are inside the **CB[7]** host. On the other hand, $H_{3,8}$ and the -Me groups are deshielded by 0.075 ppm and 0.144 ppm, respectively,

meaning that they are located in the vicinity of the rim oxygens, just outside the **CB[7]** cavity.

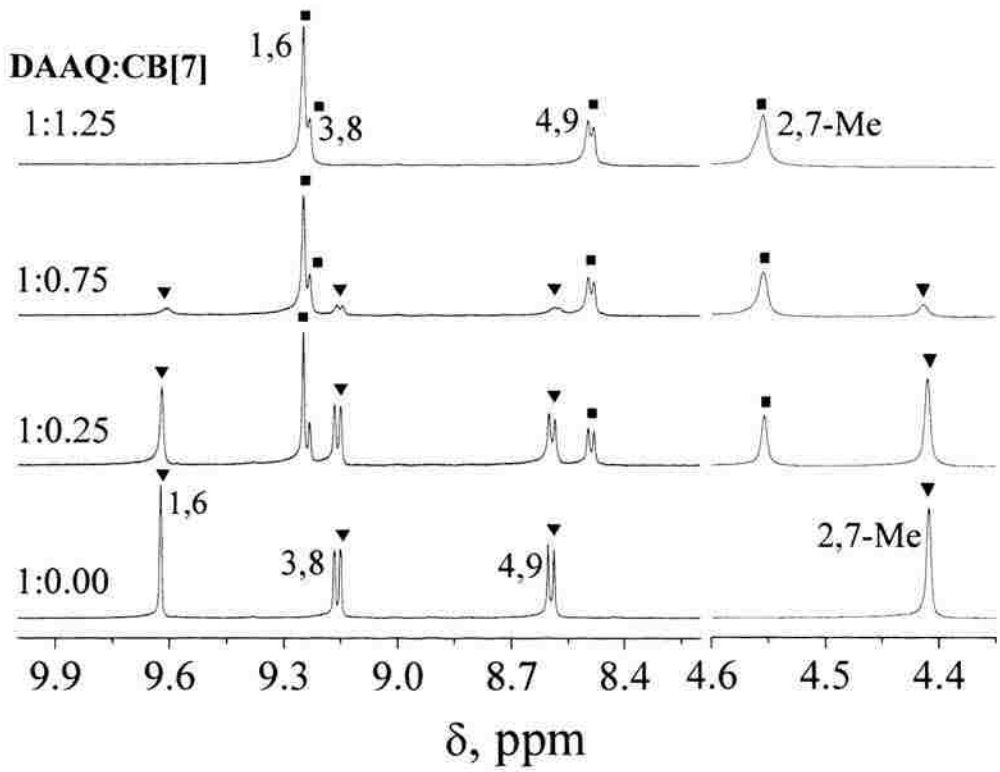

Figure 3.3. ^{1}H NMR spectra of **DAAQ** in DCl/D_2O with different mol equivalents of **CB[7]**; ■: **DAAQ@CB[7]**, ▲: Free **DAAQ**.

Figure 3.4 shows the ^{1}H NMR of **DAAQ** in D_2O followed by progressive addition of **CB[7]**. As the addition of **CB[7]** progresses, intercalated and free **DAAQ** are noted. After adding 1.25 mole equivalents of **CB[7]**, $H_{1,6}$ and $H_{4,9}$ are shielded by 0.365 ppm and 0.056 ppm, respectively (inside the cavity). While protons $H_{3,8}$ are deshielded by 0.159 ppm (outside the cavity). Clearly, both carbonyl groups of the quinone are inside the **CB[7]** cavity. In addition, the peaks corresponding to *gem*-diol have disappeared, meaning that when the **DAAQ** is inside the cavity of **CB[7]**, hydration is prohibited because the cavity is hydrophobic in nature. Also, **$(DAAQ)_n$** aggregates break up as **DAAQ** enters the **CB[7]** cavity resulting in sharper peaks corresponding to **DAAQ@CB[7]**.

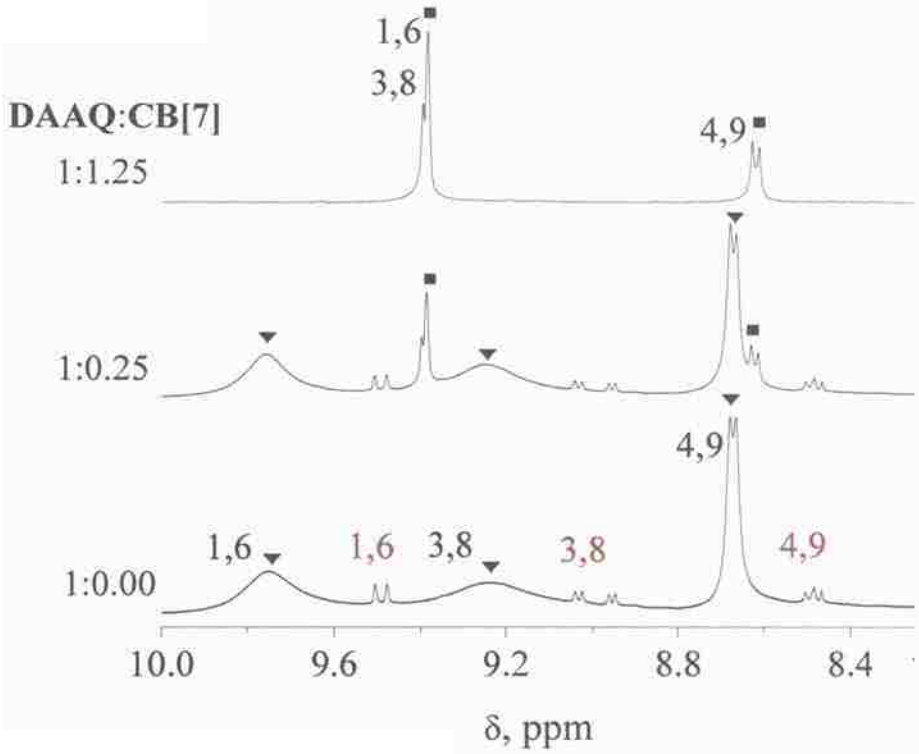

Figure 3.4. ^{1}H NMR spectra of **DAAQ** in D_2O with different mol equivalents of **CB[7]**; ■: **DAAQ@CB[7]**, ▲: Free **DAAQ**.

3.3.2. Mass Spectroscopy. The presence of *gem*-diol (*m/z* = 601.2) is confirmed by ESI/MS of an aqueous solution of **DAAQ** (Figure 3.5). Moreover, ESI/MS shows the formation of aggregates $[(DAAQ)_n.(BF_4^-)_{2(n-1)}]^{2+}$ where n=2-8. On the other hand, ESI/MS of an aqueous solution of **DAAQ@CB[7]** (Figure 3.6) reveals the formation of a 1:1 complex of **DAAQ** with **CB[7]** (m/z = 701.5).

3.3.3. PM3 Calculation. The B3LYP/6-31G* basis was used to optimize the **CB[7]** and **DAAQ** structures. These optimized structures were used as an input for PM3 calculation. Figure 3.7 shows the PM3 optimized structure of **DAAQ@CB[7],** which reveals that the protons $H_{1,6}$ and $H_{4,9}$ are inside the cavity, whereas the protons $H_{3,8}$ are outside of the cavity.

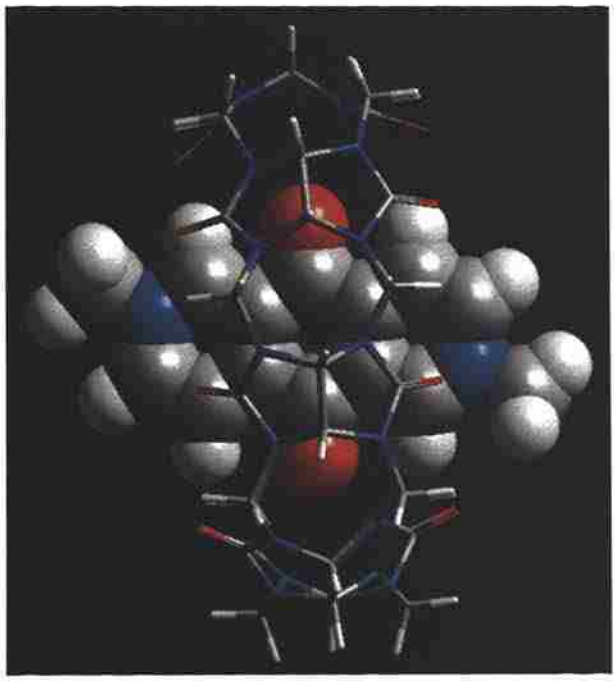

Figure 3.7. PM3 optimized structure of **DAAQ@CB[7]**.

PM3 calculation adds support to the NMR study of **DAAQ@CB[7]**. This shows that the carbonyl group is inside the cavity where it experiences hydrophobic interactions. Because of these interactions, the *gem*-diol of **DAAQ**, which is hydrophilic in nature, does not intercalate in **CB[7]**.

3.3.4. UV-Vis Study. The binding constant of **DAAQ** with **CB[7]** was calculated via spectrophotometric titrations at 225 nm (Figure 3.8). Nonlinear regression analysis of the data (see Supporting Information)[15] gave a very strong binding constant K_{eq} = (3.61±1.63) × 10^6 M^{-1} which is ~3 orders of magnitude greater than the binding constant of monocationic benzoylpyrydinium guests[12] but closer to dicationic methylviologens whose Keq ~ 2 × 10^5 M^{-1} with **CB[7].**[16-18] The recorded UV-Vis spectra reveal the presence of an isosbestic point at 320 nm implying that two different chromophores are present in the system and as the concentration of **CB[7]** increases, the absorbance of one chromophore is increased at the expense of the other. This shows that equilibrium of quinone to gem-diol is affected by the **CB[7]** and it favors the quinone form.

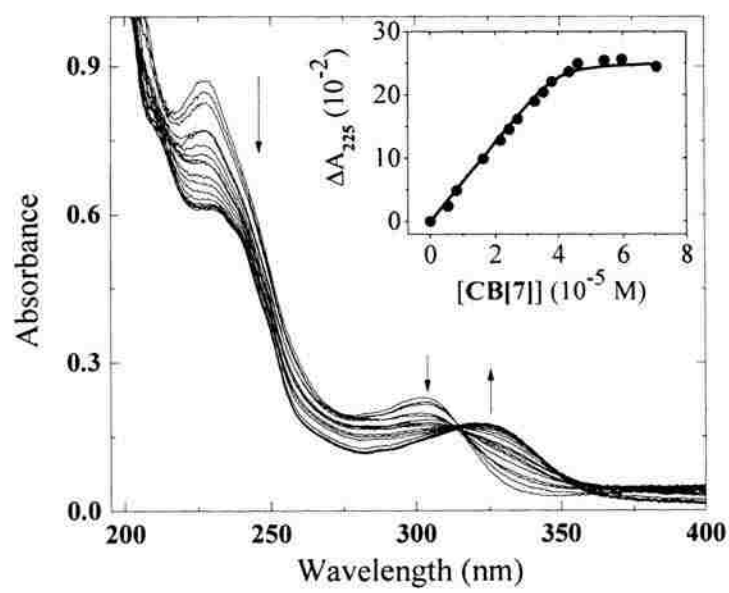

Figure 3.8. Spectrophotometric titration of **DAAQ** (3.96 10^{-5} M) with **CB[7]** in H_2O. Inset: non-linear fit (R^2=0.9936) of the absorbance at 225 nm versus total concentration of **CB[7]** (see Supporting Information).

3.4. CONCLUSIONS

Host–guest interactions of dicationic quinone **DAAQ** with **CB[7]** are reported for the first time. **DAAQ** exists in equilibrium with its *gem*-diol form in water, whereas it exists as a quinone in DMSO and aqueous acid (pH<1). In neutral pH, **DAAQ** shows line-broadening in ^{1}H NMR due to formation of aggregates which are supported by X-ray crystallography, as BF_4^- promotes electrostatic aggregate formation by holding together **DAAQ** dications which would have had otherwise electrostatic repulsions via their positively charged nitrogens. At low pH (<1), the aggregates break up and the equilibrium is shifted exclusively toward the quinone form. In the presence of **CB[7]**, the quinone form undergoes inclusion with **CB[7]** by slow exchange in both water and aqueous acid. Both free and **CB[7]**-intercalated quinone forms are observed by ^{1}H NMR. The resulting **DAAQ@CB[7]** complex is stable with a very high binding constant (3.61×10^6 M^{-1}), most probably because this complex is stabilized by two cation-dipole interactions.

3.5. EXPERIMENTAL

3.5.1.Materials. All starting materials and solvents were obtained from Sigma-Aldrich and used without further purification. **CB[7]** was prepared as described in our previous work.[13]

3.5.1.1. 5,10-dioxo-5,10-dihydropyrido[3,4-g]isoquinoline (or 2,6-diaza-9,10-anthraquinone). It was synthesized according to the literature.19 Mp 230-2320C (lit.19 mp 234-236 ^{0}C); ^{1}H NMR ($CDCl_3$) δ 8.11 (dd, J = 5.1 Hz, J = 0.8 Hz, 2 H), 9.20 (d, J = 5.1 Hz, 2 H), and 9.59 (d, J = 0.8 Hz, 2 H); ^{13}C NMR δ 119.0, 125.8, 137.9, 149.8, 156.4, 182.0.

3.5.1.2. 2,7-dimethyl-5,10-dioxo-5,10-dihydropyrido[3,4-g]isoquinoline-2,7-diium bis(tetrafluoroborate) (or N,N'-dimethyl-2,6-diaza-9,10-anthraquinonediium bis(tetrafluoroborate), DAAQ). 2,6-Diaza-9,10-anthraquinone (0.30 g, 1.43 mmol) was dissolved in nitromethane (20 mL) in a 50 mL round bottom flask. To this solution, under N_2, a solution of trimethyloxonium tetrafluoroborate (0.63 g, 4.26 mmol) in nitromethane (10 mL) was added dropwise under vigorous stirring at room temperature. The reaction mixture was stirred for 30 min at room temperature followed by the addition of diethyl

ether. The crude product thus precipitated was filtered and recrystallized in boiling water. Yield: 0.21 g (36%); mp 242-246 ^{0}C dec; ^{1}H NMR (DCl, 4.67 M in D_2O) δ 9.62 (s, 2H), 9.16 (d, J = 6.2 Hz, 2H), 8.60 (d, J = 6.4 Hz, 2H), 4.51 (s, 6H). The structure was confirmed by X-ray analysis (Figures S.3.1 and S.3.2).

3.5.2. General Methods and Equipment. ^{1}H NMR spectra were recorded on a Varian INOVA 400 MHz NMR spectrometer. UV-vis spectra were recorded with an Ocean Optics, Inc., model CHEM2000 miniature fiber optic spectrophotometer. Experimental data were analyzed with origin pro 8 software. Mass spectrometry was performed using a TSQ7000 triple quadruple mass spectrometer with electrospray ionization (ESI) at the University of Missouri-Columbia. PM3 semiempirical calculations using DFT-optimized structures (6-31G(d) basis set) were performed in windows XP with Gaussian '03 software. Melting points were uncorrected. X-ray crystallography was done on a Bruker Smart Apex diffractometer. A suitable crystal was selected and mounted on a glass fiber using epoxy-based glue. The data were collected at room temperature employing a scan of 0.3°in ω with an exposure time of 20 s/frame. The cell refinement and data reduction were carried out with SAINT, the program SADABS was used for the absorption correction. The structure was solved by direct methods using SHELXS-97 and difference Fourier syntheses. Full-matrix least-squares refinement against |F2| was carried out using the SHELXTL-PLUS suit of programs. All non-hydrogen atoms were refined anisotropically. Hydrogen atoms were placed geometrically and held in the riding mode during the final refinement.

3.5.2.1. NMR titrations of DAAQ with CB[7] in D_2O. DAAQ (3.4 mg, 0.0082 mmol) was dissolved in D_2O (0.5 mL) and equilibrated for about 30 min before its ^{1}H NMR spectrum was recorded. To this solution, an incremental amount of **CB[7]** (0.25, 1.25 mol ratio vs **DAAQ**) was added to form the inclusion complex. The ^{1}H NMR spectra were referenced versus residual H in D_2O.

3.5.2.2. NMR titrations of DAAQ with CB[7] in D_2O/DCl. DCl (0.25 mL, 40% v/v) was added to equal volume of D_2O. The resulting solvent mixture was added to **DAAQ** (2.5 mg, 0.0060 mmol). The sample was then transferred into a double jacket NMR tube (Wilmad LabGlass) in which the inner tube was filled with **DAAQ** and the

outer tube was filled with D_2O. The latter was used as an external reference. To the inner tube, was added an incremental amount of **CB[7]** (0.25, 0.75, 1.25 mol ratio vs. **DAAQ**).

3.5.2.3. NMR titrations of DAAQ with DCl. To a solution of **DAAQ** in D_2O (20 mM) were added progressively varied volumes of aq. DCl and the ^1H NMR spectra were recorded after each addition.

3.5.2.4. Determination of the binding constant of DAAQ with CB[7]. The binding constant was determined spectrophotometrically at 225 nm in H_2O. Stock solutions of **DAAQ** (3.96×10^{-4} M) and **CB[7]** (2.72×10^{-4} M) in H_2O were freshly prepared before each run. In a series of 10 mL volumetric flasks, a constant volume (1 mL) of the **DAAQ** solution was added, followed by the addition of varied volumes of the **CB[7]** solution. The mixtures were diluted to the 10 mL mark with H_2O. The absorbance of those solutions was recorded in a UV-Vis spectrophotometer. Plot of the change in absorbance at 225 nm was fitted using non-linear regression. The reported binding constant is the average of two such measurements. Data analysis is given in the supporting information.

3.6. ACKNOWLEDGMENT

We thank NSF for financial support (CHE-0809562). We are also grateful to Dr. Nathan D. Leigh at the University of Missouri-Columbia for obtaining the ESI/MS of **DAAQ** and Dr. Amitava Choudhury for the X-ray crystallographic analysis of **DAAQ**.

3.7. REFERENCES

1. Valderrama, J. A.; Gonzalez, M. F.; Pessoa-Mahana, D.; Tapia, R. A.; Fillion, H.; Pautet, F.; Rodriguez, J. A.; Theoduloz, C.; Schmeda-Hirschmannd, G. *Bioorg. & Med. Chem.* **2006**, *14*, 5003-5011.
2. Krapcho, P. A.; Petry, M. E.; Getahun, Z.; Landi, J. J.; Stallman, J.; Polsenberg, J. F.; Gallagher, C. E.; Maresch, M. J.; Hacker, M. P. *J. Med. Chem.* **1994**, *37*, 828-837.
3. Koyama, J.; Morita, I.; Kobayashi, N.; Osakai, T.; Usuki, Y.; Taniguchi, M. *Bioorg. & Med. Chem. Lett.* **2005**, *15*, 1079-1082.
4. Kim, S. H.; Choi, H. S.; Kim, J.; Lee, S. J.; Quang, D. T.; Kim, J. S. *Org. Lett.* **2010**, *12*, 560-563.
5. Kumar, S.; Luxami, V.; Kumar, A. *Org.Lett.* **2008**, *10*, 5549-5552.
6. Jung, H. S.; Kima, H. J.; Vicens, J.; Kima, J. S. *Tetrahedron Lett.* **2009**, *50*, 983-987.
7. Gomez, R.; Blanco, R.; Veldman, D.; Segura, J. L.; Janssen, R. A. J. *J. Phys. Chem. B* **2008**, *112*, 4953-4960.
8. Capitosti, G. J.; Cramer, S. J.; Rajesh, C. S.; Modarelli, D. A. *Org. Lett.* **2001**, *11*, 1645-1648.
9. Burckhardt, G.; Walter, A.; Triebel, H.; Storl, K.; Simon, H.; Storl, J.; Opitz, A.; Roemer, E.; Zimmer, C. *Biochemistry* **1998**, *37*, 4703-4711.
10. Sindelar, V.; Parker, S. E.; Kaifer, A. E. *New J. Chem.* **2007**, *31*, 725-728.
11. Kandoth, N.; Choudhury, S. D.; Mukherjee, T.; Pal, H. *Photochem. Photobiol. Sci.* **2009**, *8*, 82-90.
12. Rawashdeh, A. M. M; Thangavel, A.; Sotiriou-Leventis, C.; Leventis, N. *Org. Lett.* **2008**, *10*, 1131-1134.
13. Thangavel, A.; Rawashdeh, A. M. M; Sotiriou-Leventis, C.; Leventis, N. *Org. Lett.* **2009**, *11*, 1595-1598.
14. Guthrie, J. P. *J. Am. Chem. Soc.* **2000**, *122*, 5529-5538.
15. Connors, K. A. *Binding Constants, The Measurement of Molecular Complex Stability*; John Wiley and Sons, Inc.: New York, 1987; Chapter 4, p 141.
16. Kim, H.-J.; Jeon, W. S.; Ko, Y. H.; Kim, K. *Proc. Natl. Acad. Sci. U.S.A.* **2002**, *99*, 5007-5011.
17. Moon, K.; Kaifer, A. E. *Org. Lett.* **2004**, *6*, 185-188.
18. Ong, W.; Gomez-Kaifer, M.; Kaifer, A. E. *Org. Lett.* **2002**, *4*, 1791-1794.
19. Bolitt, V.; Mioskowski, C.; Reddy, S. P.; Falck, J. R. *Synthesis* **1988**, *5*, 388-389.

Appendix S.3.1, Absorption data for measurement of equilibrium constant of **DAAQ** with **CB[7]**; Appendix S.3.2, Calculation of the equilibrium constants for the **DAAQ / CB[7]** complex formation; Appendix S.3.3, XRD of **DAAQ**.

Appendix S.3.1: Absorption data for measurement of equilibrium constant of **DAAQ** with **CB[7]**

Table S.3.1. Absorption data for the **[DAAQ] / CB[7]** system.

Run-1			Run-2		
[DAAQ]	**[CB[7]]**	ΔA	**[DAAQ]**	**[CB[7]]**	ΔA
3.96E-05	0	0	3.96E-05	0	0
3.96E-05	5.43E-06	0.02381	3.96E-05	5.09E-06	0.0334
3.96E-05	8.15E-06	0.04823	3.96E-05	1.02E-05	0.07181
3.96E-05	1.63E-05	0.09859	3.96E-05	2.04E-05	0.12928
3.96E-05	2.17E-05	0.12736	3.96E-05	2.55E-05	0.15169
3.96E-05	2.45E-05	0.14508	3.96E-05	3.05E-05	0.17138
3.96E-05	2.72E-05	0.16162	3.96E-05	3.56E-05	0.1941
3.96E-05	3.26E-05	0.18922	3.96E-05	4.07E-05	0.21718
3.96E-05	3.53E-05	0.20371	3.96E-05	4.58E-05	0.22664
3.96E-05	3.80E-05	0.22074	3.96E-05	5.60E-05	0.22325
3.96E-05	4.35E-05	0.23594	3.96E-05	6.62E-05	0.22633
3.96E-05	4.62E-05	0.24907	3.96E-05	8.14E-05	0.22032
3.96E-05	5.43E-05	0.25414			
3.96E-05	5.98E-05	0.25576			
3.96E-05	7.06E-05	0.24431			
K_{eq} = 1.98E+06 M^{-1}		$b\Delta\varepsilon_{11}$ = 3.19E+03 M^{-1}	K_{eq} = 5.24E+06 M^{-1}		$b\Delta\varepsilon_{11}$ = 2.89E+03 M^{-1}

$$[\mathrm{L}] = L_t - \frac{\Delta A}{b\Delta\varepsilon_{11}}$$

Substituting now the last equation back into 4.5 we obtain a quadratic equation that can be solved into:

$$\Delta A = \frac{b\Delta\varepsilon_{11}\left[L_t + S_t + \frac{1}{K_{11}} \pm \sqrt{(L_t + S_t + \frac{1}{K_{11}})^2 - 4S_t L_t} \right]}{2}$$

The experimental data consist of measured absorption difference ΔA (A-A_o) versus added (total) concentration of **CB[7]** (L_t). S_t is a known constant for each titration, while $b\Delta\varepsilon_{11}$ and K_{11} are treated as adjustable parameters that are obtained by non-linear least square fitting of the ΔA versus L_t data. Table S1 provides the values obtained for K_{11} (which for the purposes of this paper is referred to as K_{eq}) and for $b\Delta\varepsilon_{11}$ for **DAAQ**.

Appendix S.3.3: XRD of **DAAQ**.

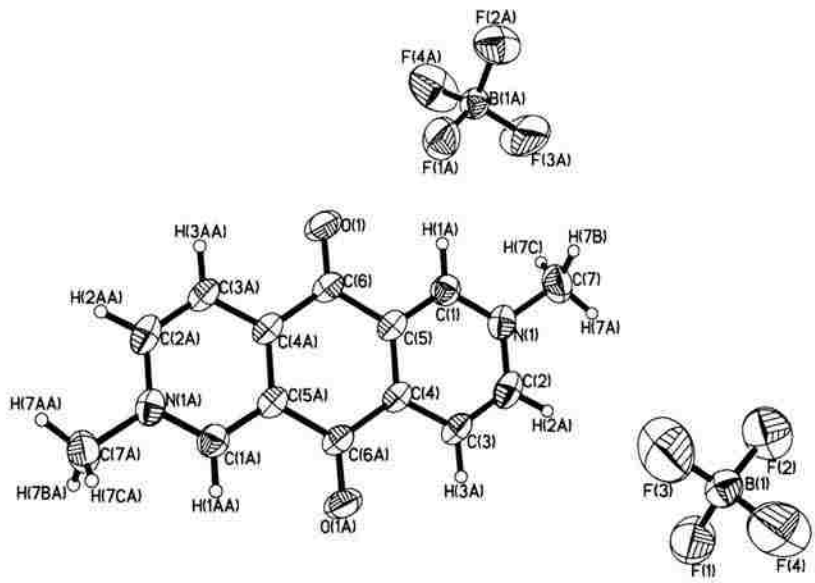

Figure S.3.1. ORTEP plot of *N,N'*-dimethyl-2,6-diaza-9,10-anthraquinonediium bis(tetrafluoroborate) (**DAAQ**). Thermal ellipsoids are drawn at the 35% probability level.

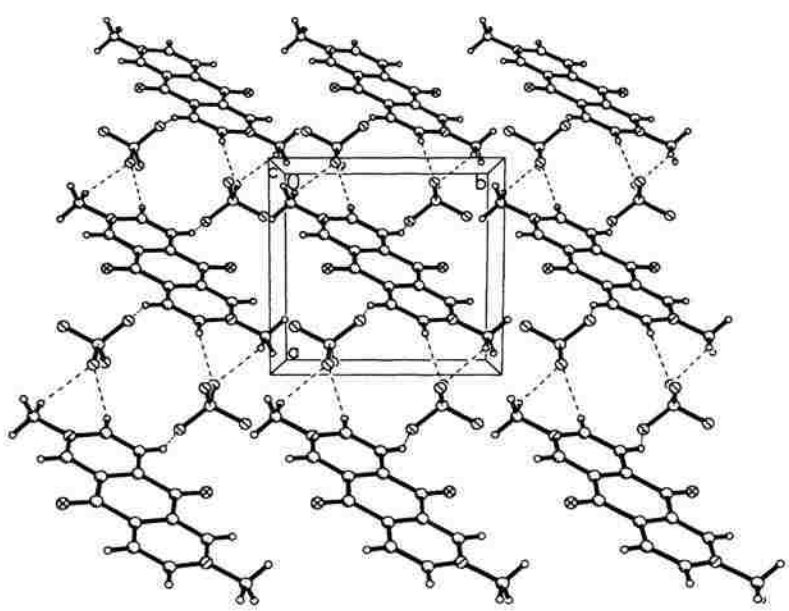

Figure S.3.2. Packing diagram for *N,N'*-dimethyl-2,6-diaza-9,10-anthraquinonediium bis(tetrafluoroborate) (**DAAQ**). Projection down the c axis.

4. THE FACTORS AT PLAY IN THE ORIENTATION OF PYRYLIUM GUESTS IN CUCURBITURIL HOSTS

Arumugam Thangavel, Chariklia Sotiriou-Leventis* and Nicholas Leventis*

Department of Chemistry, Missouri University of Science and Technology‡,

Rolla, MO 65409, U.S.A.

leventis@mst.edu; cslevent@mst.edu

4.1. ABSTRACT

Complexes of the pyrylium cation with cucurbit[x]urils (CB[x], x=7,8) show interesting photoluminescence that is related to their stereochemistry, however the latter has been debated. Here we report that in H_2O, 2,6-disubsituted-4-phenyl pyryliums form dimers, but they enter as such only in **CB[8]**. All guests insert their 4-phenyl groups in either cavity, except **(*i*Pr-Pylm)$_2$@CB[8]**, which inserts the *i*Pr-groups (Figure 4.1). Stereochemistry is interpreted by the size and hydrophobicity of the pyrylium substituents, out-of-cavity solvation effects, and size and flexibility of the hosts.

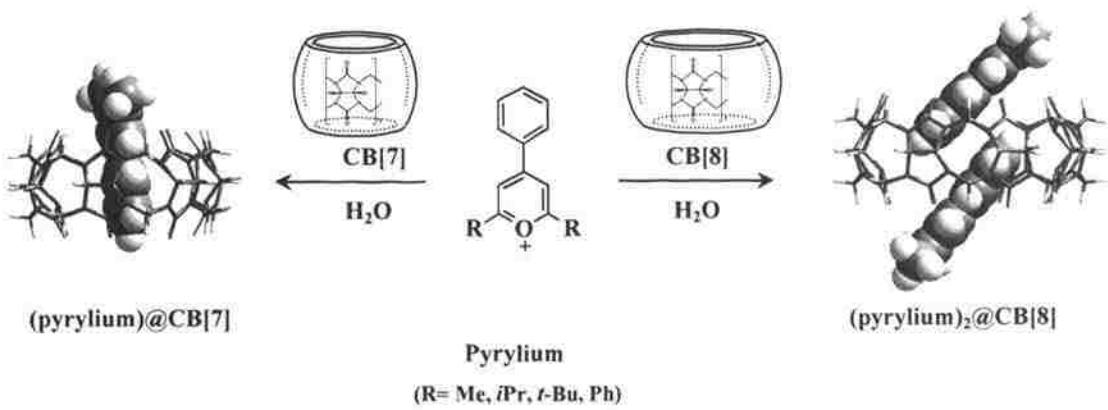

Figure 4.1. Schematic representation of inclusion of pyrylium with cucurbituril.

‡ Formerly, University of Missouri-Rolla.

4.2. INTRODUCTION

Cucurbit[x]urils (CB[x]) are water-soluble, barrel-shaped hosts prepared by condensation of x mol of glycoluril and 2x mol of formaldehyde.[1] The two rims, formed by the negative ends of the glycoluril carbonyl dipoles, are at a fixed distance (9.1 Å) for all x, while the portal/cavity diameters vary (e.g., 5.4 Å/7.3 Å for **CB[7]**, and 6.9 Å/8.8 Å for **CB[8]**). CB[x]s show an affinity for cationic guests, and intercalation of dications with a length matching the portal distance (e.g, dimethylviologen; 7.3 Å) has been studied extensively. The latter guest is stretched along the axis of the barrel, placing the positive N*s* near the negative rim O*s*.[2] On the other hand, monocationic *N*-substituted-4-benzoylpyridiniums can be oriented either *exo*- or *endo*-, placing the most hydrophobic group inside the hydrophobic cavity.[3,4] In fact, that driving force is so intense that those guests forfeit H-bonding with the solvent (H_2O), shifting their keto/*gem*-diol equilibrium towards the keto form in order to place the benzoyl group inside the cavity. Those results invite a global study for the intercalation of monocationic guests, not only as a function of their hydrophobic properties but also in terms of their shape and the size of the cavity. For this, the 4-phenyl pyrylium cation, whose size and hydrophobicity can be modified by 2,6-substitution, is a viable system:

Indeed, the 4-phenylpyrylium cation has been a suitable guest for studying intercalation in cyclodextrins, showing an increasing preference for the hydrophobic interior of the host as hydrophobic substituents at the c-position of the 4-phenyl ring become longer.[5] Further, owing to positive ion-dipole interactions, **Ph-Pylm** forms even more stable complexes with cucurbiturils placing the 4-phenyl group inside the cavity.[6] In this regard, the size of CB[x] plays a profound role in the relative mobility of the phenyl groups: in **CB[7]**, Ph-Pylm does not get as deep as in **CB[8]** and, once in the cavity, the tight fit restricts rotation of the 4-phenyl group while rotation of the 2- and 6-phenyl groups is free. On the other hand, once in **CB[8]**, rotation of the 4-phenyl group inside the cavity is free, while rotation of the 2- and 6-phenyl groups is inhibited by the portal oxygens that stand on the way of the H_d*s*. That restricted rotation slows relaxation of the excited state, and the guest shows long-wavelength room temperature emission, which has been attributed to phosphorescence and has been explored in electroluminescent devices.[6] Quite recently, this description has been revised as crystal

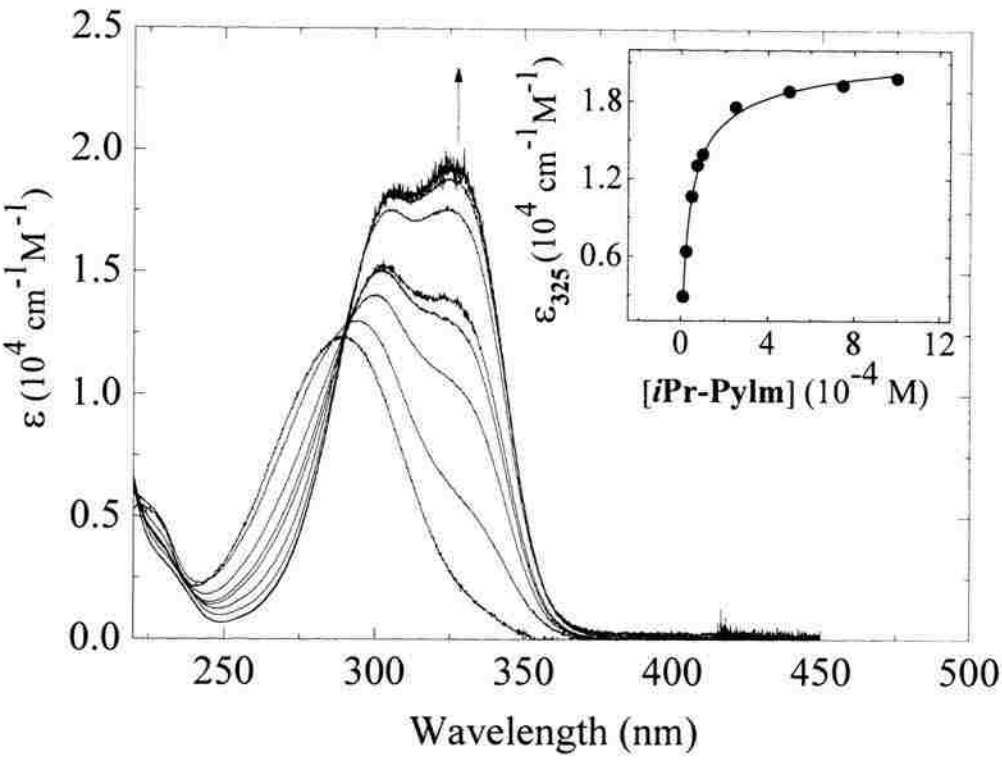

Figure 4.2. Typical absorption of a guest (***i*Pr-Pylm**) as a function of its concentration in H_2O. The red-shift is attributed to J-aggregation. Inset: non-linear fit (R^2=0.992) of ε at 325 nm versus concentration.

All four guests form 1:1 complexes with **CB[7]** (by Job's plots, see Supporting Information), and 2:1 complexes with **CB[8]** (by ESI-MS, Figure 4.3). In all cases, the 1:1 complexes with **CB[8]** are also present. The intercalation mechanisms with both hosts are summarized in Scheme 4.2.

Table 4.1. Dimerization constants for pyryliums in water.

	Me-Pylm	***i*Pr-Pylm**	***t*-Bu-Pylm**	**Ph-Pylm**
K_d (M^{-1})	1.0×10^4	3.2×10^4	1.2×10^5	3.9×10^5

Scheme 4.2. Intercalation mechanism of **Me-**, ***i*Pr-**, **t-Bu-** and **Ph-PyIm** in **CB[7]** and **CB[8]**.

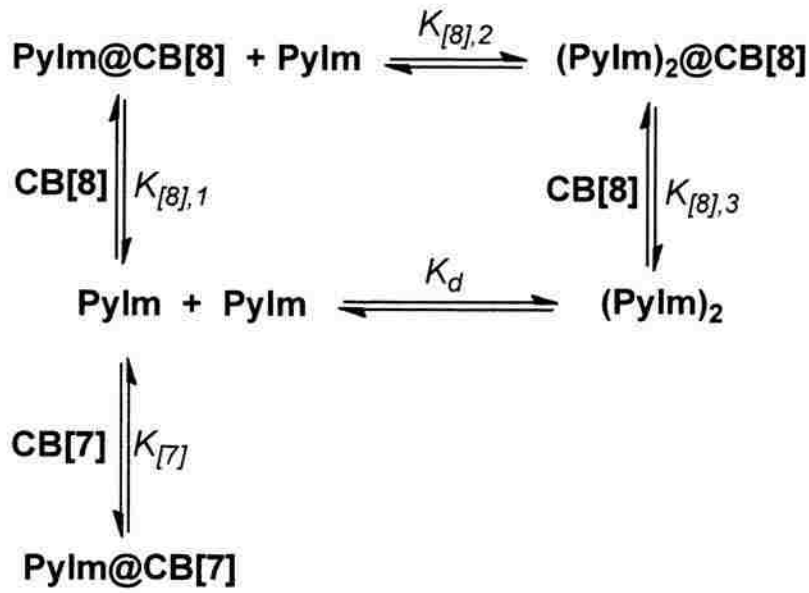

^{1}H NMR is a reliable tool for structural elucidation of host-guest complexes. Figure 4.5 shows the evolution of the spectra of **Me-PyIm** upon progressive addition of **CB[7]** or **CB[8]**. (For other guests see Supporting Information) The initial line-broadening is attributed to site-exchange between free and intercalated guest, and indirectly supports the stoichiometry of the complexes: the resonance lines become sharp again after addition of 1 mol equivalent of **CB[7]** and 2 mol equivalents of **CB[8]**, reflecting also the high equilibrium constants of intercalation (Table 4.2).

Table 4.2. Equilibrium constants (M^{-1}) per Scheme 4.2

	$K_{[7]}$	$K_{[8],1}$	$K_{[8],2}$	$K_{[8],3}$
Me-	$(3\pm1)\times10^5$	$(1.2\pm0.3)\times10^4$	5.6×10^6	6.7×10^6
***i*Pr-**	$(1\pm1)\times10^5$	$(8+8)\times10^4$	4.8×10^6	12×10^6
***t*-Bu-**	$(8\pm3)\times10^4$	$(4\pm4)\times10^4$	1.7×10^5	5.7×10^4
Ph-	$(6\pm2)\times10^4$	$(3\pm2)\times10^4$	1.5×10^5	1.2×10^4

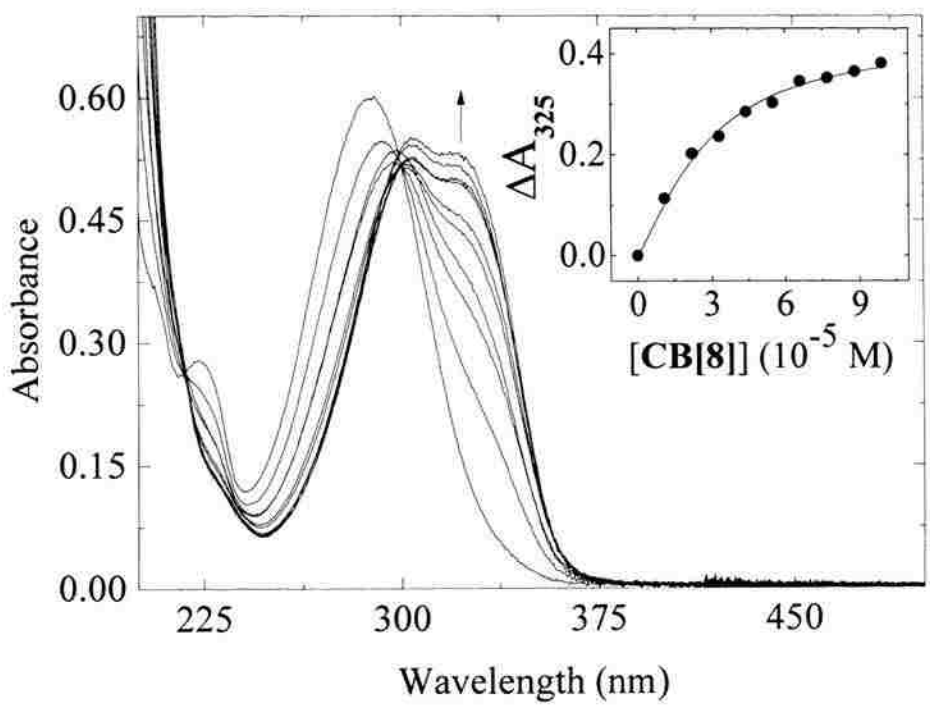

Figure 4.4. Spectrophotometric titration in H_2O of **Me-Pylm** ($4.74\ 10^{-5}$ M) with **CB[8]**. Multiple spectral inter-sections reflect the multistep processes of Scheme 4.2. Inset: non-linear fit (R^2=0.990) of absorbance as indicated.

Further, Figure 4.5 shows that all protons (aromatic and aliphatic) of **Me-Pylm** are shifted in the same direction with both hosts, implying that the guest monomer (case of **CB[7]**) and the guest dimer (case of **CB[8]**) are positioned similarly in the respective cavities. Thus, all aromatic Hs of **Me-Pylm** move upfield, signifying that they are located inside the cavity, while aliphatic Hs (CH_3) move downfield, signifying that they are located in the vicinity of the rim oxygens, just outside the cavity. In turn, Figure 4.6 shows and compares the ^{1}H NMR data for all guests with both hosts and Scheme 4.3 uses color-coding to summarize the results. Thus, first, we observe that all four guests are oriented similarly in **CB[7]** placing their 4-phenyl groups in the host. Further, ***t*-Bu-** and **Ph-Pylm** do not sit as deep as **Me-** and ***i*Pr-Pylm** in the **CB[7]** cavity. It is tempting to attribute those differences to the size of the 2,6-substituents, however, PM3 optimized structures (Supporting Information) show that all three ***i*Pr-**, ***t*-Bu-** and **Ph-Pylm** are able to sink at the same depth inside the host cavity. Therefore, the actual position of the guests is determined not only by their size/hydro-phobicity, but also by external factors, as for example solvation of the pyrylium oxygen that sits outside the cavity. In **CB[8]**, the dimers of **Me-**, ***t*-Bu-** and **Ph-Pylm** are oriented similarly as in **CB[7]**, namely with their 4-phenyl group in the cavity. ***t*-Bu-Pylm** enters deeper in **CB[8]** than in **CB[7]**, reflecting the relative sizes of the portals. On the other hand, **Me-** and **Ph-Pylm** seem to enter as deep in **CB[8]** as in **CB[7]**, which is rather surprising, and it should reflect that **Ph-Pylm** enters both hosts with similar orientation.

of **CB[8]** is preserved in **(Me-Pylm)$_2$@CB[8]** and **(*t*-Bu-Pylm)$_2$@CB[8]**, signify-ing that the two guests enter from opposite portals (Supporting Information). It is noted also that the same host distortion (by ^{1}H NMR – see Supporting Information) is observed in three of the four **CB[7]** complexes. Surprisingly, ***t*-Bu-Pylm@CB[7]** retains the symmetry of the host as apparently the width of ***t*-Bu-Pylm** is just large enough and cannot be accommodated even by stretching of the portal, thereby **CB[7]** prefers to retain its original minimum-energy cylindrical conformation.

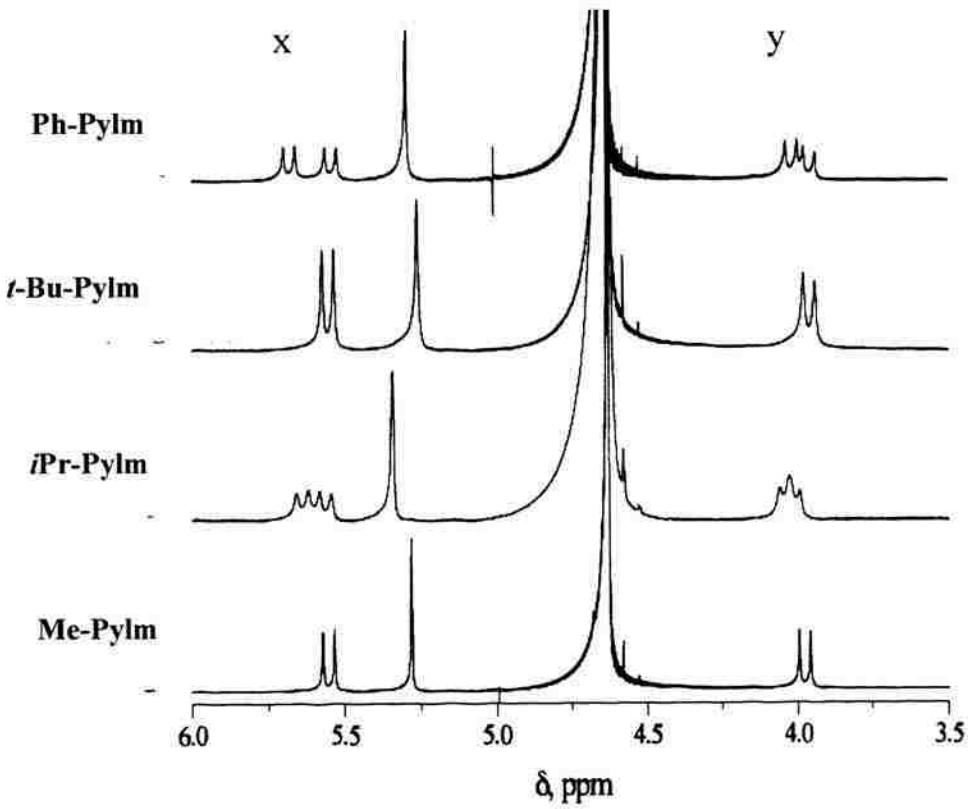

Figure 4.7. ^{1}H NMR (D_2O) of **CB[8]** after addition of 2 mol equivalents of the pyryliums shown at left. Upon asymmetric intercalation of ***i*Pr-** and **Ph-Pylm** the CH_AH_X protons at the two rims (x, y) are no longer equivalent.

Scheme 4.3. Color-coded ^{1}H NMR data

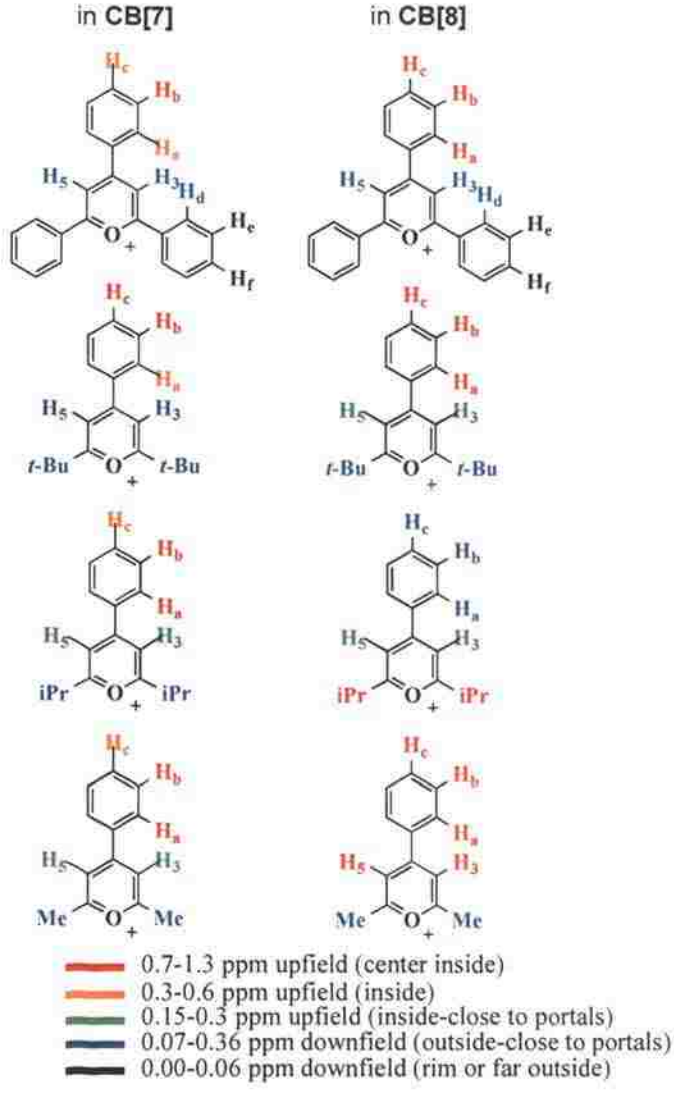

4.4. CONCLUSIONS

The stereochemistry of host-guest complexes is extremely important for supramolecular protection, separations and in general for technology based on molecular recognition. However, simple guest structure considerations may be poor predictors for the stoichiometry and strereochemistry of a complex, and reliance on modeling might be dangerous. In the case of the four pyrylium cations of this study, not only the size and shape of the substituents, but also the ability of the guest to dimerize as well as solvation effects and the flexibility of the host play important roles.

4.5. ACKNOWLEDGEMENT

We thank NSF for financial support (CHE-0809562).

4.6. REFERENCES

1. Lee, J. W.; Samal, S.; Selvapalam, N.; Kim, H.-J.; Kim, K. *Acc. Chem. Res.* **2003**, *36*, 621-630.
2. Kim, H.-J.; Jeon, W. S.; Ko, Y. H.; Kim, K. *Proc. Nat. Acad. Sci. U. S.A.* **2002**, *99*, 5007-5011.
3. Rawashdeh, A.-M. M.; Thangavel, A.; Sotiriou-Leventis, C.; Leventis, N. *Org. Lett.* **2008**, *10*, 1131-1134.
4. Thangavel, A.; Rawashdeh, A.-M. M.; Sotiriou-Leventis, C.; Leventis, N. *Org. Lett.* **2009**, *11*, 1595-1598.
5. Manoj, N. Gopidas, K. R. *Phys. Chem. Chem. Phys.* **1999**, *1*, 2743-2748.
6. Montes,-Navajas, P.; Teruel, L.; Corma, A.; Garcia, H. *Chem. Eur. J.* **2008**, *14*, 1762-1768.
7. Montes,-Navajas, P.; Garcia, H. *J. Phys. Chem. C* **2010**, *114*, 2034-2038.
8. Gadde, S.; Batchelor, E. K.; Weiss, J. P.; Ling, Y.; Kaifer, A. E. *J. Am. Chem. Soc.* **2008**, *130*, 17114-17119.
9. Connors, K. A. Binding Constants, The Measurement of Molecular Complex Stability, John Wiley and Sons, Inc.: New York, 1987.

Appendix S.4.1 Synthesis of the four 2,6-disubstituted-4-phenyl-pyryliums; Appendix S.4.2 Determination of the stoichiometry of the **Me-Pylm** and **Ph-Pylm** complexes with **CB[7]** via Job's plots; Appendix S.4.3 Determination of dimerization constants of **Me-Pylm**, ***i*Pr-Pylm**, ***t*-Bu-Pylm** and **Ph-Pylm** in water; Appendix S.4.4 Determination of equilibrium constants of the four pyryliums with cucurbiturils : 4.a in the presence of **CB[7]**; 4.b in the presence of **CB[8]**; Appendix S.4.5 ^{1}H NMR spectra of the four pyryliums / **CB[7]** or **CB[8]** systems; Appendix S.4.6 Crystal structure of **Me-Pylm**; Appendix S.4.7 Results from PM3 calculations:7.a **CB[7]** intercalation; 7.b **CB[8]** intercalation; Appendix S.4.8: References.

Appendix S.4.1: Synthesis of the four 2,6-disubstituted-4-phenyl-pyryliums.

Scheme S.2.1. Synthesis of 2,6-dimethyl-4-phenylpyrylium tetrafluoroborate (**Me-Pylm**)

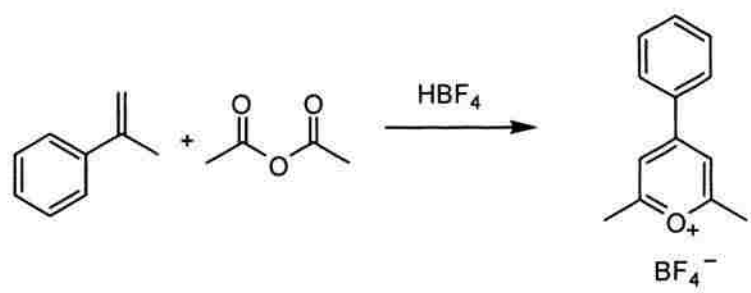

Me-Pylm was prepared according to reference S1. Acetic anhydride (20 mL) was added dropwise to tetrafluoroboric acid (50% w/w, 2.0 g, 0.0248 mol) under ice-cold conditions and the mixture was stirred till evolution of fumes ceased. To this homogenous, ice-cold mixture, α-methyl styrene (3.12 mL, 0.0248 mol) was added, and the new mixture was stirred for about 2 h, then it was let stand overnight at room temperature, and subsequently it was poured in to diethyl ether. The precipitate was collected, dried and further purified by recrystallization from hot water. Yield: 0.932 g (14 %); mp: 202-203 °C (lit.[S1] 196 °C; recrystallized from hot H_2O).

Scheme S.2.2. Synthesis of 2,6-diisopropyl-4-phenylpyrylium tetrafluoroborate (***i*Pr-Pylm**)

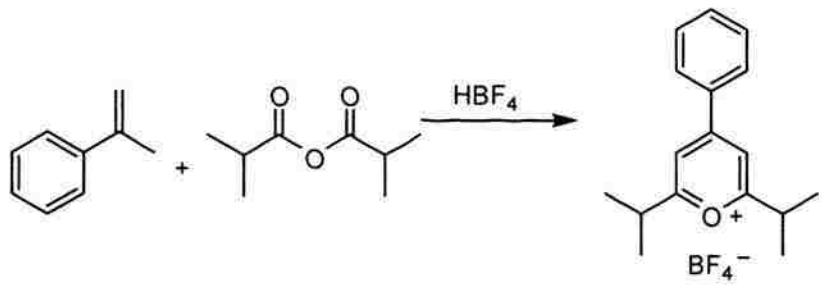

Isobutyric anhydride (10 mL, 0.060 mol) was added dropwise to tetrafluoroboric acid (50% w/w, 2 g, 0.024 mol) under ice-cold conditions and the mixture was stirred till evolution of fumes ceased. To this homogeneous, ice-cold mixture, α-methyl styrene (1.6 mL, 0.012 mol) was added, and the new mixture was stirred for 1 h at room temperature and then it was refluxed overnight. After cooling, the precipitate was collected, dried and further purified by recrystallization from methylene chloride/hexane at -10 ^{0}C. Yield: 1.64 g (41.6%); mp: 192-194 ^{o}C (lit.[S1] 178 ^{o}C; recrystallized from hot ether).

Scheme S.2.3. Synthesis of 2,6-di-*t*-butyl-4-phenylpyrylium tetrafluoroborate (***t*-Bu-Pylm**)

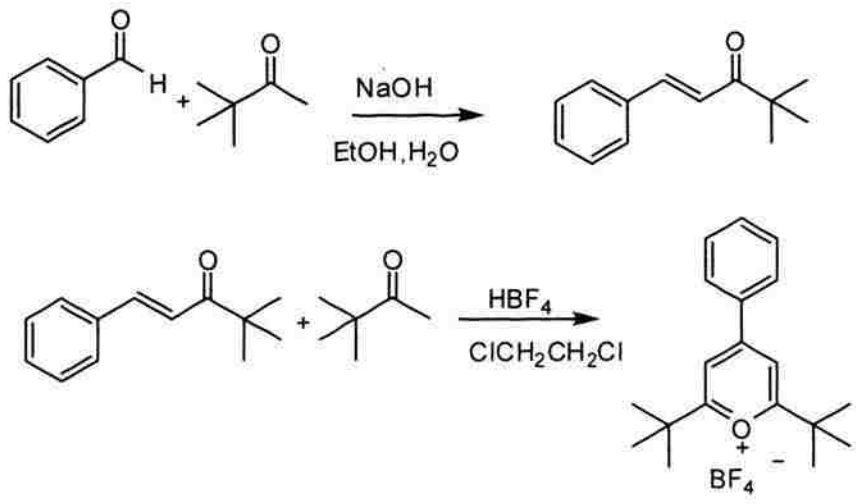

***t*-Bu-Pylm** was synthesized from benzylidenepinacolone and *t*-butyl methyl ketone. In turn, benzylidenepinacolone was synthesized according to reference 2 from benzaldehyde and *t*-butyl methyl ketone.

Benzaldehyde (2.34 mL, 0.023 mol) was added to the solution of *t*-butyl methyl ketone (2.86 mL, 0.023 mol) in 100 mL of ethanol. To the reaction mixture, NaOH (1 g, 0.0235 mol) dissolved in 5 mL of water was added dropwise at room temperature. After the addition of the NaOH solution was complete, the mixture was diluted with 25 mL of water and was stirred at room temperature for 5 h. Then ~75% of the solvent was removed with a rotary evaporator, and the remaining solution was extracted with methylene chloride. The extract was washed with water and dried with anhydrous sodium sulfate. Without further purification, the brownish liquid was used in the next step.

t-Butyl methyl ketone (2.86 mL, 0.023 mol) dissolved in 40 mL of 1,2-dichloroethane was added to the brownish liquid (benzylidenepinacolone) from the previous step. Tetrafluoroboric acid (50% w/w, 3.7 mL, 0.046 mol) in ether was added to the reaction mixture and the new mixture was refluxed for about 6 h. At the end of the period, it was cooled to room temperature and was poured into diethyl ether (~three fold in volume). The oil that was formed was separated and it was further purified by recrystallizion from dichloromethane/hexane at -10 °C, giving a light yellowish solid. Yield: 0.921 g (11 %); mp: 218-220 °C.

2,4,6-triphenylpyrylium tetrafluoroborate (Ph-Pylm)

Purchased from Acros. mp: 249-250 °C

Appendix S.4.2: Determination of the stoichiometry of the **Me-Pylm** and **Ph-Pylm** complexes with **CB[7]** via Job's plots.

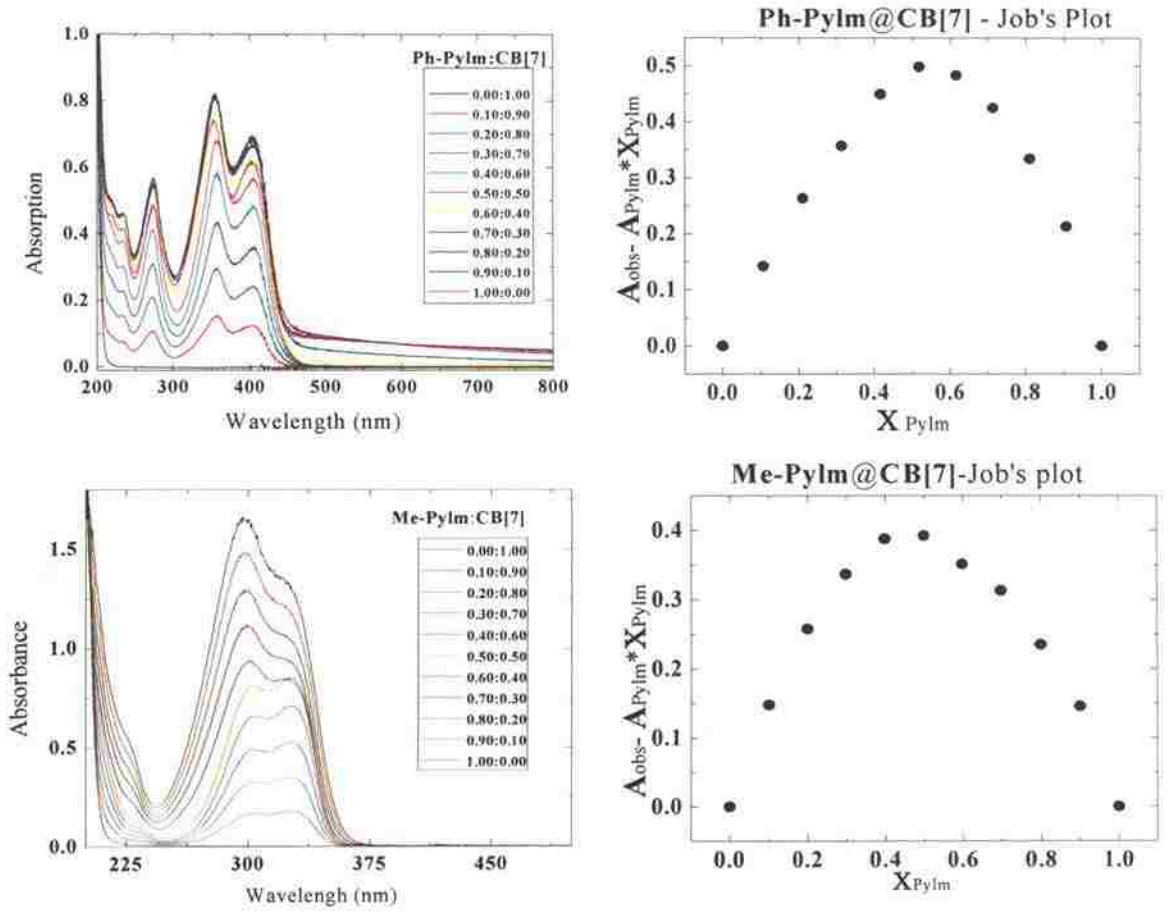

Figure S.4.1. Job's plots. X_{Pylm} = mole fraction of pyrylium: X_{Pylm} = mol Pylm / (mol Pylm + mol **CB[7]**). The maxima of the Job's plot are at X=0.5, therefore the complex stoichiometry is 1:1.

Appendix S.4.3: Determination of dimerization constants of **Me-Pylm**, ***i*Pr-Pylm**, ***t*-Bu-Pylm** and **Ph-Pylm** in water.

Those were determined spectrophotometrically from molar absorptivity (ε) at λ_{max} as a function of the concentration data (Figures 4.2 and S.4.1-S.4.3), using eqs S1-S4 (equations 6-8 of reference S3).

$$P + P \underset{}{\overset{K_d}{\rightleftharpoons}} P_2 \qquad \text{(S1)}$$

$$[P] = \frac{-1 + \sqrt{1 + 8K_d[P]_0}}{4K_d} \qquad \text{(S2)}$$

$$[P_2] = \frac{[P]_0}{2} + \frac{1 - \sqrt{1 + 8K_d}[P]_0}{8K_d} \qquad \text{(S3)}$$

$$\varepsilon_{app}(\lambda) = \varepsilon_P(\lambda)\frac{[P]}{[P]_0} + \varepsilon_{P_2}(\lambda)\frac{[P_2]}{[P]_0} \qquad \text{(S4)}$$

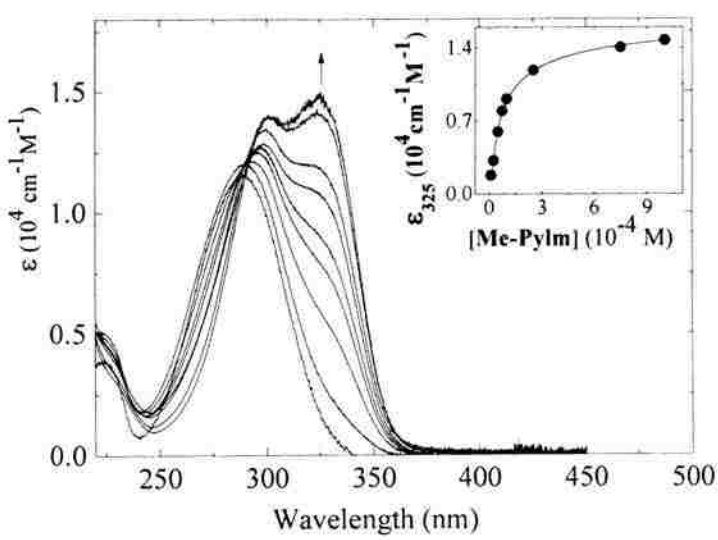

Figure S.4.2. Absorption of **Me-Pylm** as a function of its concentration in H_2O. Inset: non-linear fit (R^2=0.990) of ε at 325 nm versus concentration.

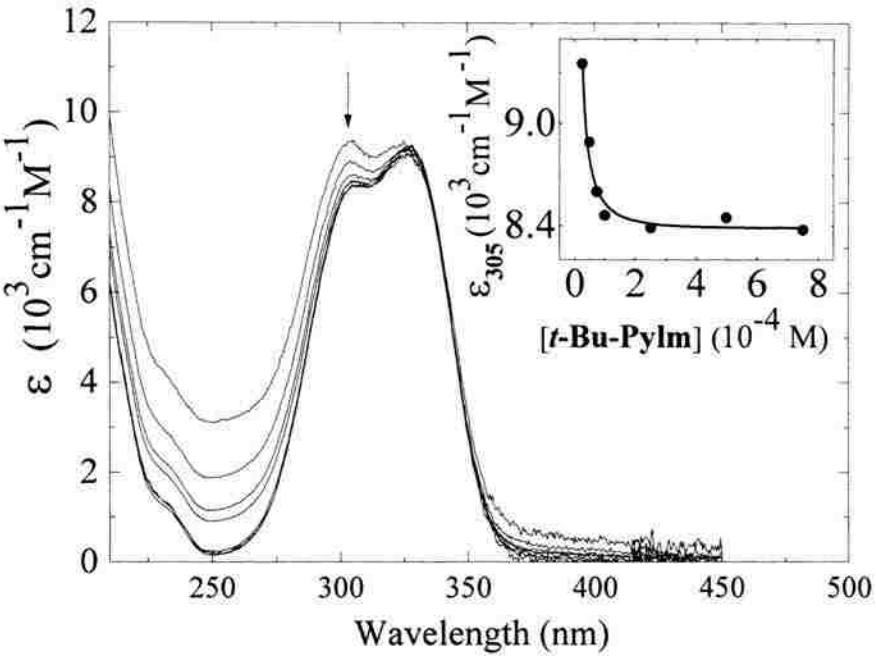

Figure S.4.3. Absorption of ***t*-Bu-Pylm** as a function of its concentration in H_2O. Inset: non-linear fit (R^2=0.961) of ε at 305 nm versus concentration.

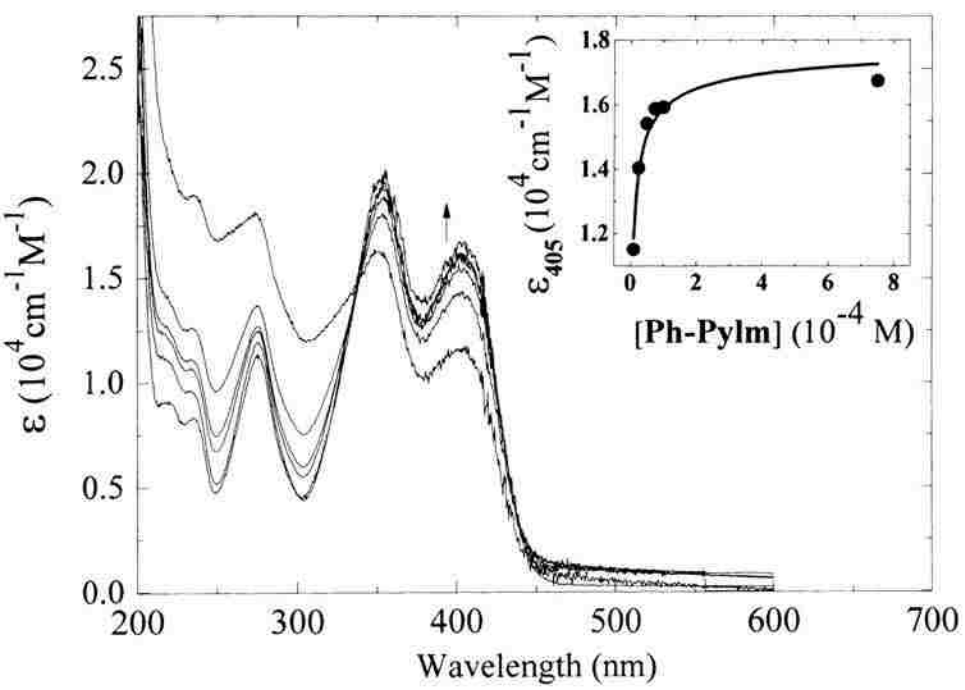

Figure S.4.4. Absorption of **Ph-Pylm** as a function of its concentration in H_2O. Inset: non-linear fit (R^2=0.937) of ε at 405 nm versus concentration.

Appendix S.4.4: Determination of binding constants of the four pyryliums with cucurbiturils.

Binding constants were determined spectrophotometrically, by keeping the pyrylium salt concentration constant and varying the concentration of the corresponding cucurbituril.

Stock solutions with known concentrations of the pyrylium salts and the corresponding cucurbituril were prepared freshly before each run. In a series of 10 mL volumetric flasks, a constant volume of the pyrylium solution was added, followed by the addition of varied volumes of the cucurbituril solution. The mixtures were diluted to the 10 mL mark. The absorbance of those solutions were recorded in a UV-Vis spectrophotometer. Plots of the change in absorbance at a specific wavelength were fitted using non-linear regression analysis and the appropriate mechanism.

Each titration was conducted twice and the reported equilibrium constants are averages. The concentration of the cucurbiturils was kept low (~10^{-5} M) to minimize dimerization. Nevertheless, the dimerization equilibrium was taken into consideration in the analysis.

Appendix S.4.4a: Determination of equilibrium constants of the four pyryliums with **CB[7].**

Intercalation of pyryliums in **CB[7]** is described adequately by:

$$\textbf{Pylm} + \textbf{CB[7]} \overset{K_{[7]}}{\rightleftharpoons} \textbf{Pylm@CB[7]}$$

The change in the absorbance (ΔA) owing to this equilibrium is given by equation S5 (eq 4.5, page 148, reference S4):

$$\frac{\Delta A}{b} = \frac{[P]K_{[7]}\Delta\varepsilon_{11}[L]}{1 + K_{[7]}[L]} \qquad \text{(S5)}$$

where:

b is the optical path length

$\Delta\varepsilon_{11}=\Delta(\varepsilon_{\text{P-monomer}}+\varepsilon_{\text{P-dimer}}-\varepsilon_{\textbf{PyIm@CB[7]}})$

$[P]$ is the monomer concentration, given by eq S2 above

$[L]$ is the concentration of free (uncomplexed) **CB[7]**, described by equation S6 (eq 4.9, page 149, reference S4):

$$[L]_{Total} = [L] + \frac{[P]K_{[7]}[L]}{1 + K_{[7]}[L]} \qquad \text{(S6)}$$

where $[L]_{Total}$ is the total concentration of free and complexed **CB[7]**.

Table S.4.1. Absorption data for the **Me-Pylm / CB[7]** system.

Run 1			Run 2		
[Me-Pylm]	**[CB[7]]**	$A-A_0$	**[Me-Pylm]**	**[CB[7]]**	$A-A_0$
2.87E-05	0.00E+00	0.0000	3.23E-05	0.00E+00	0.0000
2.87E-05	7.14E-06	0.0832	3.23E-05	7.52E-06	0.0639
2.87E-05	1.43E-05	0.1802	3.23E-05	1.20E-05	0.1419
2.87E-05	2.14E-05	0.2228	3.23E-05	1.50E-05	0.1655
2.87E-05	2.85E-05	0.2690	3.23E-05	1.81E-05	0.1870
2.87E-05	4.28E-05	0.3064	3.23E-05	2.26E-05	0.2177
2.87E-05	5.71E-05	0.3257	3.23E-05	3.01E-05	0.2548
2.87E-05	8.56E-05	0.3321	3.23E-05	3.76E-05	0.2790
2.87E-05	9.99E-05	0.3353	3.23E-05	5.27E-05	0.2876
2.87E-05	1.21E-04	0.3339	3.23E-05	6.02E-05	0.2929
			3.23E-05	6.77E-05	0.2928
$K_{[7]}$ =2.26E+05 M^{-1}			$K_{[7]}$ = 2.26E+05 M^{-1}		
$b\Delta\varepsilon$ =1.73E+04 M^{-1}			$b\Delta\varepsilon$ = 1.73E+04 M^{-1}		

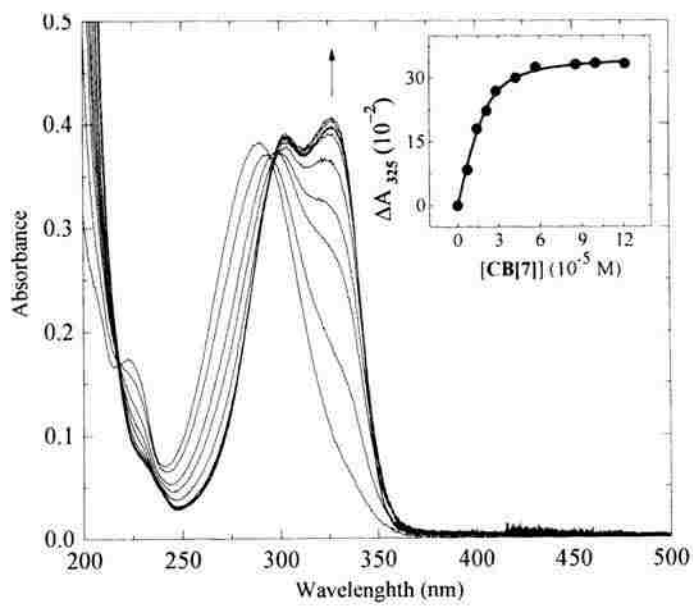

Figure S.4.5. Absorption of **Me-Pylm** (2.87×10^{-5} M) in water upon addition of **CB[7]**. Inset: non-linear fit (R^2=0.997) of the absorbance at 325 nm versus total concentration of **CB[7]**.

Table S.4.3. Absorption data for the ***t*-Bu-Pylm / CB[7]** system.

Run 1			Run 2		
[*t*-Bu-Pylm]	**[CB[7]]**	$A-A_0$	**[*t*-Bu-Pylm]**	**[CB[7]]**	$A-A_0$
2.61E-05	0.00E+00	0.0000	5.05E-05	0.00E+00	0.0000
2.61E-05	9.18E-06	0.0139	5.05E-05	9.65E-06	0.0192
2.61E-05	1.53E-05	0.0251	5.05E-05	1.61E-05	0.0246
2.61E-05	2.14E-05	0.0301	5.05E-05	2.25E-05	0.0535
2.61E-05	3.06E-05	0.0348	5.05E-05	4.82E-05	0.0945
2.61E-05	4.59E-05	0.0402	5.05E-05	6.43E-05	0.1152
2.61E-05	6.12E-05	0.0407	5.05E-05	8.04E-05	0.1311
2.61E-05	7.65E-05	0.0386	5.05E-05	9.65E-05	0.1359
2.61E-05	9.18E-05	0.0412	5.05E-05	1.13E-04	0.1333
2.61E-05	1.07E-04	0.0411	5.05E-05	1.45E-04	0.1281
2.61E-05	1.38E-04	0.0416			
K_{17} = 1.12E+05 M^{-1}			K_{17} = 5.17E+04 M^{-1}		
$b\Delta\varepsilon$ = 5.35E+03 M^{-1}			$b\Delta\varepsilon$ = 1.19E+04 M^{-1}		

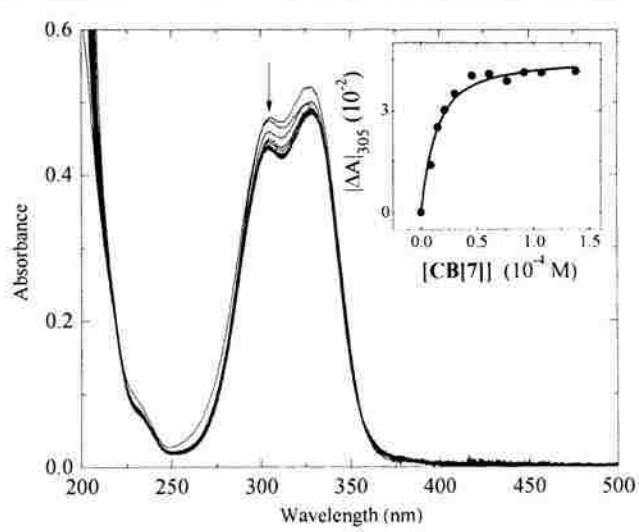

Figure S.4.7. Absorption of ***t*-Bu-Pylm** (2.61×10^{-5} M) in water upon addition of **CB[7]**. Inset: non-linear fit (R^2=0.978) of the absorbance at 305 nm. versus total concentration of **CB[7]**.

Appendix S.5.4b: Determination of equilibrium constants of the four pyryliums with **CB[8].**

At low concentrations (10^{-5} M) in water, pyryliums exist mostly as monomers and the intercalation in **CB[8]** is described adequately by:

$$\textbf{Pylm} + \textbf{CB[8]} \underset{}{\overset{K_{[8],1}}{\rightleftharpoons}} \textbf{Pylm@CB[8]}$$

$$\textbf{Pylm@CB[8]} + \textbf{Pylm} \underset{}{\overset{K_{[8],2}}{\rightleftharpoons}} \textbf{(Pylm)}_2\textbf{@CB[8]}$$

The change in the absorbance owing to this equilibrium is given by equation S7 (eq 4.28, case of multi equilibria, page 161, reference S4):

$$\frac{\Delta A}{b} = \frac{[P](K_{[8],1}\Delta\varepsilon_{11}[L]+K_{[8],1}K_{[8],2}\Delta\varepsilon_{12}[L]^2)}{1+K_{[8],1}[L]+K_{[8],1}K_{[8],2}[L]^2} \quad \text{(S7)}$$

where:

b is the optical path length

$\Delta\varepsilon_{11}=\Delta(\varepsilon_{\text{P-monomer}}+\varepsilon_{\text{P-dimer}}-\varepsilon_{\textbf{Pylm@CB[8]}})$

$\Delta\varepsilon_{12}=\Delta(\varepsilon_{\text{P-monomer}}+\varepsilon_{\text{P-dimer}}-\varepsilon_{\textbf{(Pylm)2@CB[8]}})$

$[P]$ is the monomer concentration, given by eq S2 above

$[L]$ is the concentration of free (uncomplexed) **CB[8]**, described by equation S8 (eq 4.29, page 161, reference S4):

$$[L]_{Total} = [L] + \frac{[P]([K]_{[8],1}[L]+2K_{[8],1}K_{[8],2}[L]^2}{1+K_{[8],1}[L]+K_{[8],1}K_{[8],2}[L]^2} \quad \text{(S8)}$$

A simplified solution of this equation is equation S9 (equation 2.43, page 45, reference S4):

$$[L] = \frac{[L]_{Total}+2K_{[8],1}K_{[8],2}[P][L]^2_{Total}}{1+[K]_{[8],1}[P]+4K_{[8],1}4K_{[8],2}[P][L]_{Total}} \quad \text{(S9)}$$

where $[L]_{Total}$ is the total concentration of free and complexed **CB[8]**.

Finally, the equilibrium constant $K_{[8],3}$, for direct intercalation of the dimer according to:

$$\mathbf{CB[8]} + \mathbf{(Pylm)_2} \overset{K_{[8],3}}{\rightleftharpoons} \mathbf{(Pylm)_2@CB[8]}$$

is given by equation S10:

$$K_{[8],3} = \frac{K_{[8],1}K_{[8],2}}{K_d} \quad \text{(S10)}$$

Table S.4.5. Absorption data for the **Me-Pylm / CB[8]** system.

Run 1			Run 2		
[Me- Pylm]	**[CB[8]]**	$A-A_0$	**[Me-Pylm]**	**[CB[8]]**	$A-A_0$
4.74E-05	0.00E+00	0.000	2.03E-05	0.00E+00	0.0000
4.74E-05	1.10E-05	0.113	2.03E-05	5.79E-06	0.0898
4.74E-05	3.30E-05	0.202	2.03E-05	1.16E-05	0.1307
4.74E-05	2.20E-05	0.236	2.03E-05	1.74E-05	0.1452
4.74E-05	6.61E-05	0.285	2.03E-05	2.32E-05	0.1498
4.74E-05	8.81E-05	0.302	2.03E-05	2.90E-05	0.1527
4.74E-05	9.91E-05	0.346	2.03E-05	3.48E-05	0.1539
4.74E-05	1.10E-04	0.352	2.03E-05	4.06E-05	0.1552
4.74E-05	4.41E-05	0.365	2.03E-05	4.63E-05	0.1527
4.74E-05	5.51E-05	0.381	2.03E-05	5.21E-05	0.1526
$K_{[8],1}$ = 9.33E+03 M^{-1} $K_{[8],1} \times K_{[8],2}$ = 2.11E+09 M^{-1} $b\Delta\varepsilon_{11}$ = 4.22E+04 M^{-1} $b\Delta\varepsilon_{12}$ = 1.22E+04 M^{-1}			$K_{[8],1}$ = 1.46E+04 M^{-1} $K_{[8],1} \times K_{[8],2}$ = 1.33E+11 M^{-1} $b\Delta\varepsilon_{11}$ = 1.24E+04 M^{-1} $b\Delta\varepsilon_{12}$ = 1.00E+04 M^{-1}		

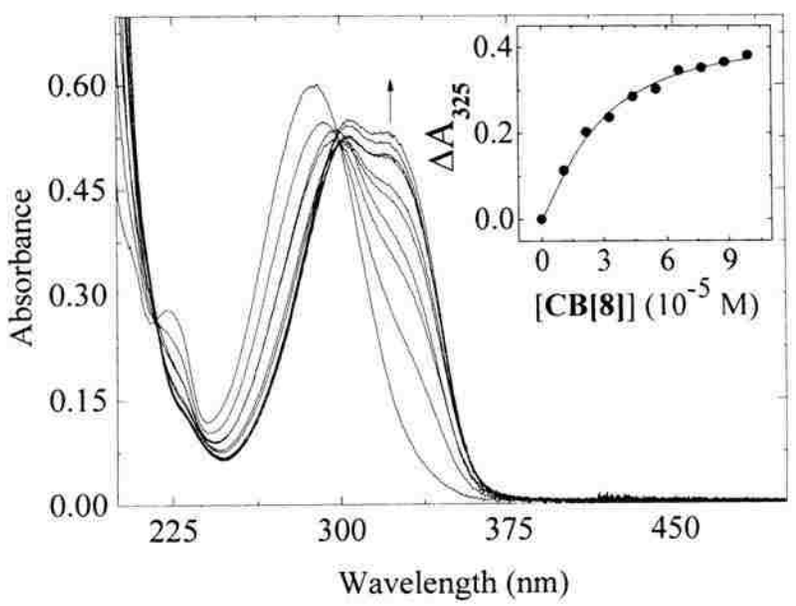

Figure S.4.9. Spectrophotometric titration in H_2O of **Me-Pylm** (4.74×10^{-5} M) with **CB[8]**. Multiple spectral inter-sections reflect the multistep processes of Scheme 1. Inset: non-linear fit (R^2=0.990) of absorbance as indicated.

Table S.4.6. Absorption data for the ***i*Pr-Pylm / CB[8]** system.

Run 1			Run 2		
[*i*Pr-Pylm]	**[CB[8]]**	$A-A_0$	**[*i*Pr-Pylm]**	**[CB[8]]**	$A-A_0$
3.78E-06	0.00E+00	0.0000	3.96E-06	0.00E+00	0.0000
3.78E-06	9.63E-07	0.0169	3.96E-06	8.58E-07	0.0186
3.78E-06	1.93E-06	0.0351	3.96E-06	1.72E-06	0.0326
3.78E-06	2.89E-06	0.0567	3.96E-06	2.57E-06	0.0483
3.78E-06	3.37E-06	0.0655	3.96E-06	3.43E-06	0.0630
3.78E-06	4.33E-06	0.0726	3.96E-06	4.29E-06	0.0769
3.78E-06	6.26E-06	0.0755	3.96E-06	5.15E-06	0.0843
3.78E-06	9.63E-06	0.0758	3.96E-06	6.00E-06	0.0860
3.78E-06	1.44E-05	0.0717	3.96E-06	6.86E-06	0.0864
			3.96E-06	7.72E-06	0.0878
			3.96E-06	8.58E-06	0.0854
			3.96E-06	9.44E-06	0.0853
$K_{18,1} = 1.64$ E+5 M^{-1} $K_{18,1} \times K_{18,2} = 1.09$E+11 M^{-1} $b\Delta\varepsilon_{11} = 9.02$E+4 M^{-1} $b\Delta\varepsilon_{12} = 1.36$E+4 M^{-1}			$K_{18,1} = 1.19$E+3 M^{-1} $K_{18,1} \times K_{18,2} = 6.83$E+11 M^{-1} $b\Delta\varepsilon_{11} = 6.26$ E+4 M^{-1} $b\Delta\varepsilon_{12} = 2.92$ E+4 M^{-1}		

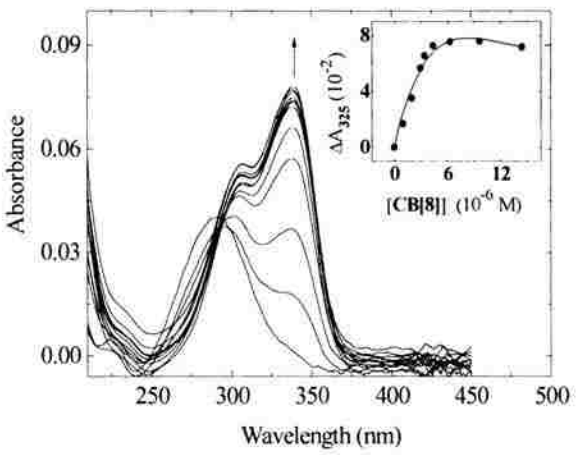

Figure S.4.10. Absorption of ***i*Pr-Pylm** (3.78×10^{-5} M) in water upon addition of **CB[8]**. Inset: non-linear fit (R^2=0.976) of the absorbance at 325 nm versus total concentration of **CB[8]**.

Table S.4.7. Absorption data for the ***t*-Bu-Pylm / CB[8]** system.

Run 1			Run 2		
[*t*-Bu-Pylm]	**[CB[8]]**	$A-A_0$	**[*t*-Bu-Pylm]**	**[CB[7]]**	$A-A_0$
3.23E-05	0.00E+00	0.0000	3.87E-05	0.00E+00	0.0000
3.23E-05	6.86E-06	0.0403	3.87E-05	8.79E-06	0.0389
3.23E-05	1.72E-05	0.0721	3.87E-05	1.32E-05	0.0532
3.23E-05	2.57E-05	0.0827	3.87E-05	2.20E-05	0.0843
3.23E-05	3.09E-05	0.0990	3.87E-05	3.08E-05	0.1044
3.23E-05	4.12E-05	0.1061	3.87E-05	4.39E-05	0.1254
3.23E-05	5.15E-05	0.1079	3.87E-05	5.27E-05	0.1369
3.23E-05	6.18E-05	0.1119	3.87E-05	6.59E-05	0.1491
			3.87E-05	7.47E-05	0.1525
			3.87E-05	8.79E-05	0.1570
			3.87E-05	1.10E-04	0.1649
$K_{[8],1}$ = 8.25 E+4 M^{-1} $K_{[8],1} \times K_{[8],2}$ = 1.12E+10 M^{-1} $b\Delta\varepsilon_{11}$ = 1.22 E+4 M^{-1} $b\Delta\varepsilon_{12}$ = 1.24 E+4 M^{-1}			$K_{[8],1}$ = 1.03 E+4 M^{-1} $K_{[8],1} \times K_{[8],2}$ = 4.72E+09 M^{-1} $b\Delta\varepsilon_{11}$ = 1.99 E+4 M^{-1} $b\Delta\varepsilon_{12}$ = 1.57 E+4 M^{-1}		

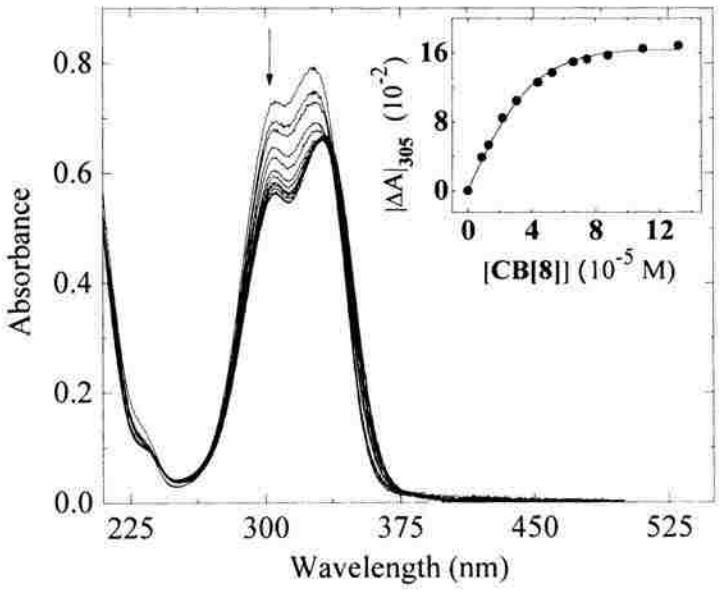

Figure S.4.11. Absorption of ***t*-Bu-Pylm** (3.87×10^{-5} M) in water upon addition of **CB[8]**. Inset: non-linear fit (R^2=0.997) of the absorbance at 305 nm versus total concentration of **CB[8]**.

Table S.4.8. Absorption data for the **Ph-Pylm / CB[8]** system.

Run 1			Run- 2		
[Ph-Pylm]	**[CB[8]]**	$A-A_0$	**[Ph-Pylm]**	**[CB[8]]**	$A-A_0$
4.09E-05	0.00E+00	0.0000	6.56E-05	0.00E+00	0.0000
4.09E-05	1.10E-05	0.1297	6.56E-05	1.11E-05	0.0162
4.09E-05	2.20E-05	0.2431	6.56E-05	2.23E-05	0.0444
4.09E-05	2.75E-05	0.2531	6.56E-05	2.78E-05	0.0638
4.09E-05	3.86E-05	0.2604	6.56E-05	3.34E-05	0.0746
4.09E-05	5.51E-05	0.2644	6.56E-05	3.90E-05	0.0782
4.09E-05	6.61E-05	0.2552	6.56E-05	5.01E-05	0.0943
4.09E-05	7.71E-05	0.2599	6.56E-05	6.68E-05	0.0984
			6.56E-05	7.79E-05	0.1028
$K_{[8],1}$ = 3.99 E+4 M^{-1} $K_{[8],1} \times K_{[8],2}$ = 2.90E+09 M^{-1} $b\Delta\varepsilon_{11}$ = 1.13 E+5 M^{-1} $b\Delta\varepsilon_{12}$ = 2.15.91 E+4 M^{-1}			$K_{[8],1}$ = 9.76 E+3 M^{-1} $K_{[8],1} \times K_{[8],2}$ = 4.34E+09 M^{-1} $b\Delta\varepsilon_{11}$ = 1.29 E+3 M^{-1} $b\Delta\varepsilon_{12}$ = 1.43 E+4 M^{-1}		

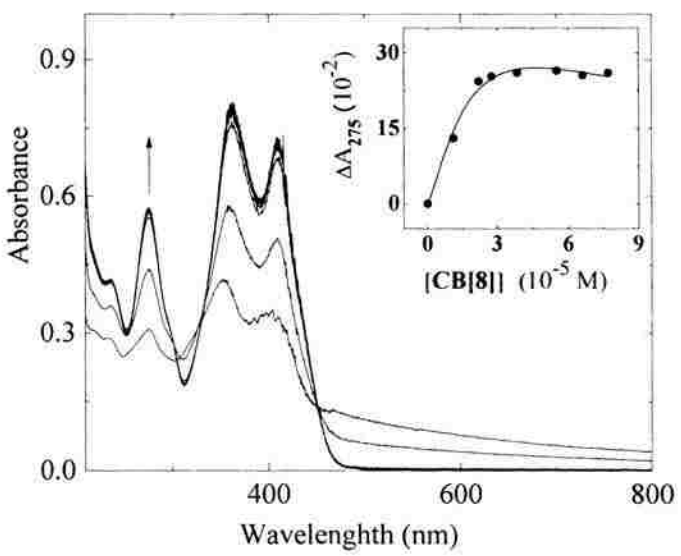

Figure S.4.12. Absorption of **Ph-Pylm** (4.09×10^{-5} M) in water upon addition of **CB[8]**. Inset: non-linear fit (R^2=0.977) of the absorbance at 275 nm versus total concentration of **CB[8]**.

Appendix S.4.5: ^{1}H NMR spectra of the four pyryliums / **CB[7]** or **CB[8]** systems.

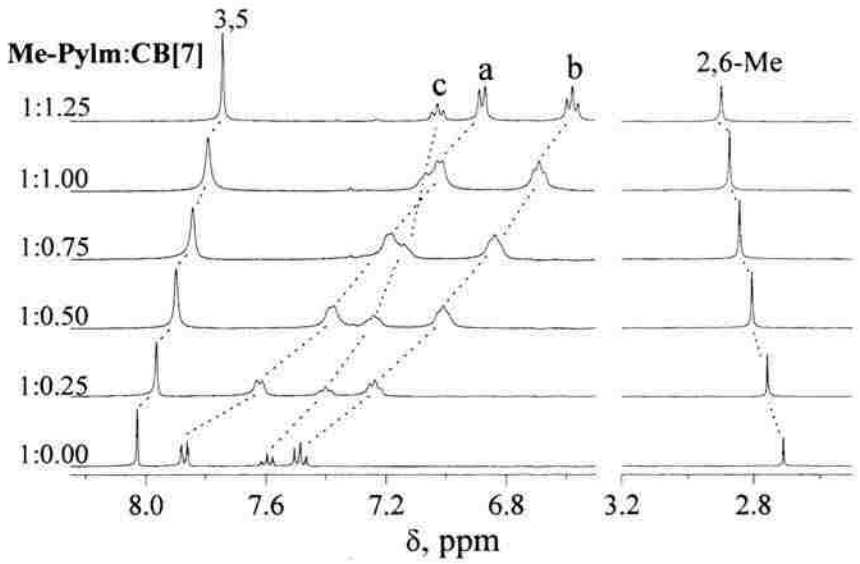

Figure S.4.13. Evolution of the ^{1}H NMR spectrum of **Me-Pylm** in D_2O by progressive addition of **CB[7]**. On the left, mol ratio of the pyrylium to **CB[7]**.

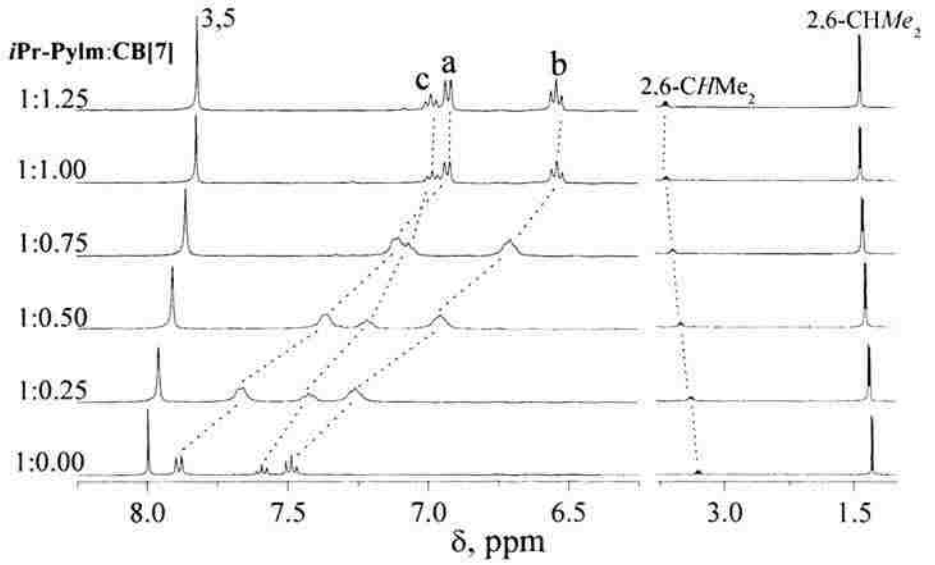

Figure S.4.14. Evolution of the ^{1}H NMR spectrum of ***i*Pr-Pylm** in D_2O by progressive addition of **CB[7]**. On the left, mol ratio of the pyrylium to **CB[7]**.

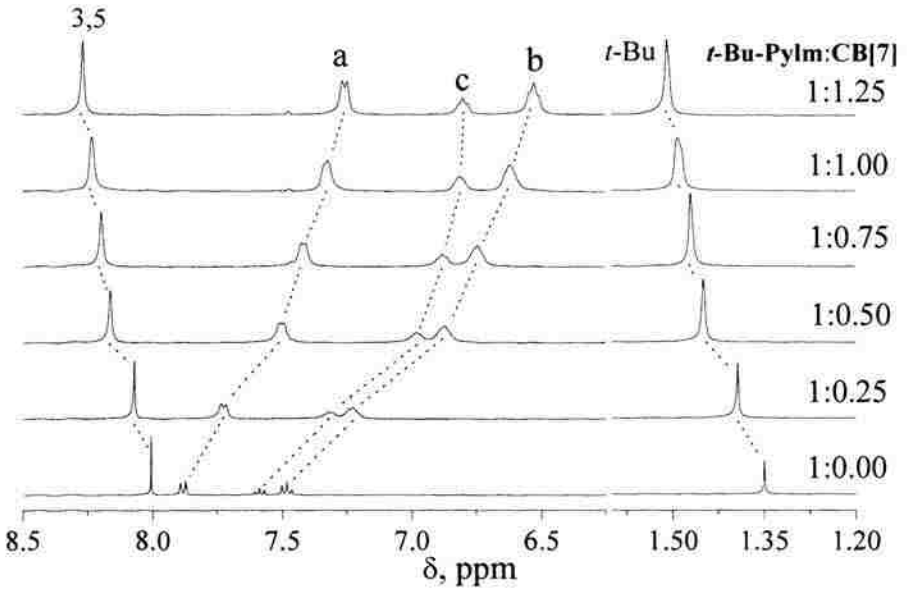

Figure S.4.15. Evolution of the ^{1}H NMR spectrum of ***t*-Bu-Pylm** in D_2O by progressive addition of **CB[7]**. On the left, mol ratio of the pyrylium to **CB[7]**.

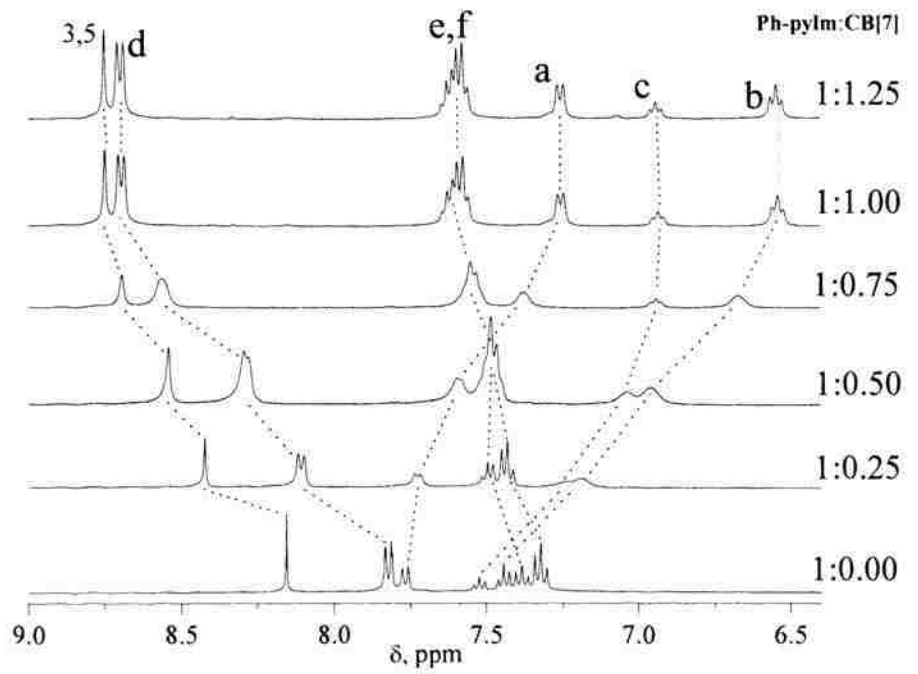

Figure S.4.16. Evolution of the ^{1}H NMR spectrum of **Ph-Pylm** in D_2O by progressive addition of **CB[7]**. On the left, mol ratio of the pyrylium to **CB[7]**.

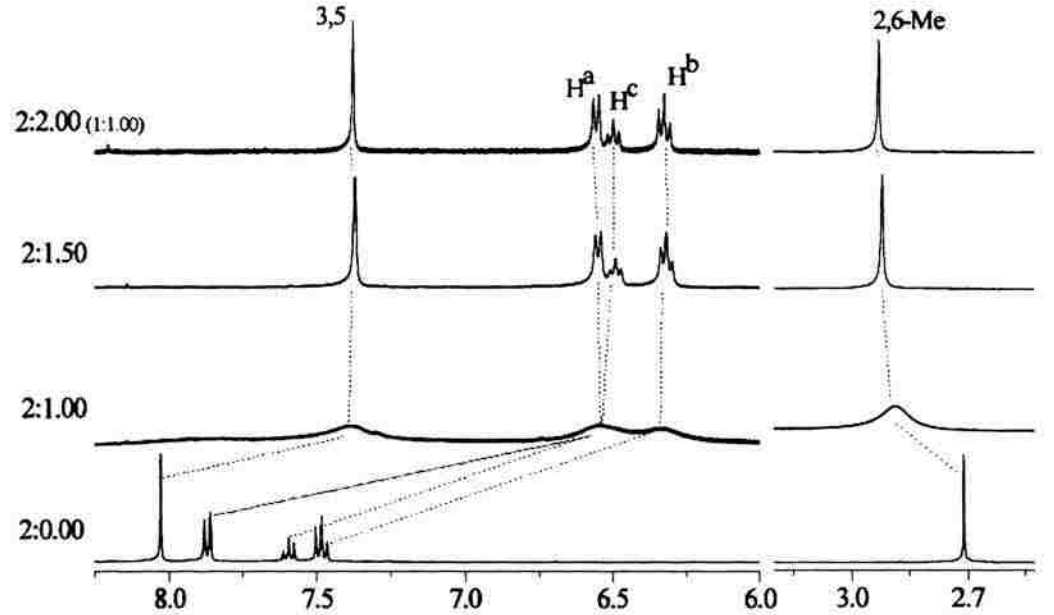

Figure S.4.17. Evolution of the ^{1}H NMR spectrum of **Me-Pylm** in D_2O by progressive addition of **CB[8]**. On the left, mol ratio of the pyrylium to **CB[8]**.

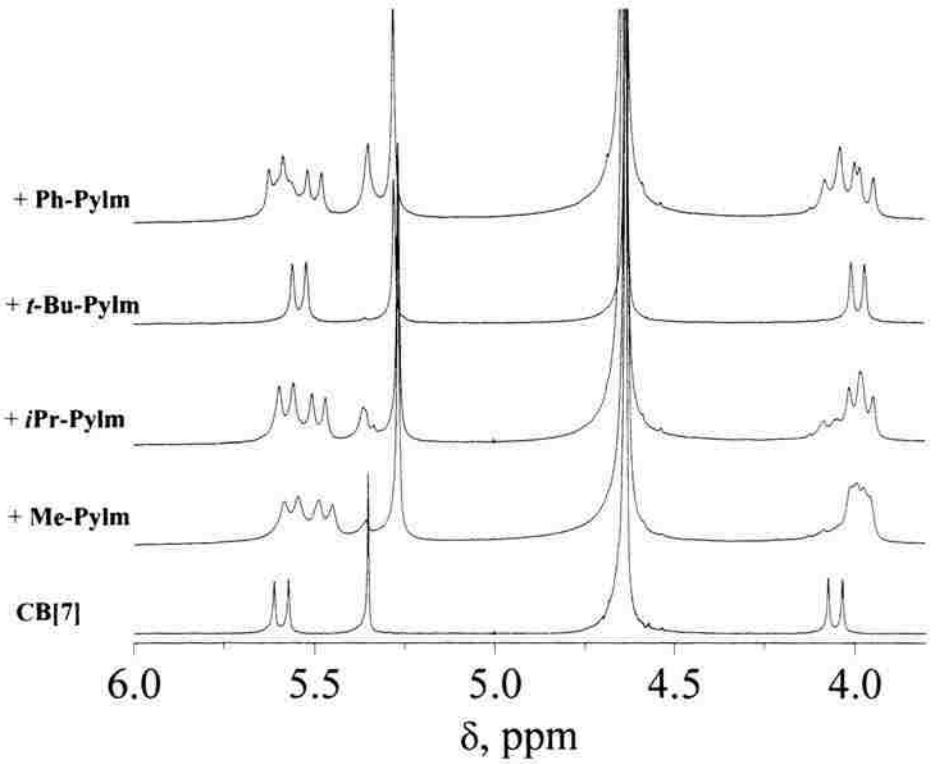

Figure S.4.18. ^{1}H NMR (D_2O) in the **CB[7]** range after addition of 1 mol equivalent of the pyryliums shown at left. Notice the symmetry brake-down of the CH_2 protons around the rim upon intercalation of **Me-Pylm**, ***i*Pr-Pylm** and **Ph-Pylm**.

Appendix S.4.6: Crystal structure of **Me-Pylm.**

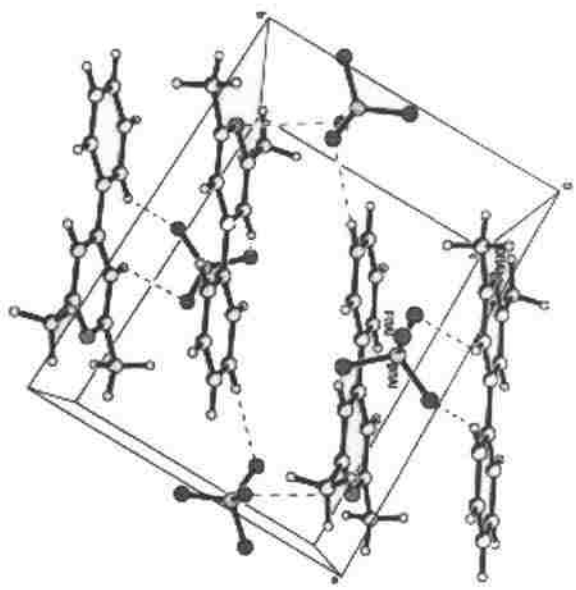

Figure S.4.19. Crystal structure of **Me-Pylm** showing formation of head-to-tail J-aggregates. Formation of similar structures in solution by increasing concentration is responsible for the red shift in the absorption spectra.

Appendix S.4.7: Results from PM3 calculations.

(A) **Me-Pylm@CB[7]** (-0.3745 a.u.)

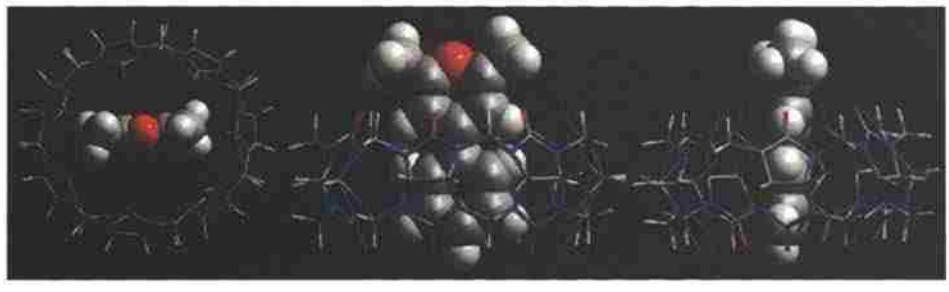

(B) ***i*Pr-Pylm@CB[7]** (-0.3957 a.u.)

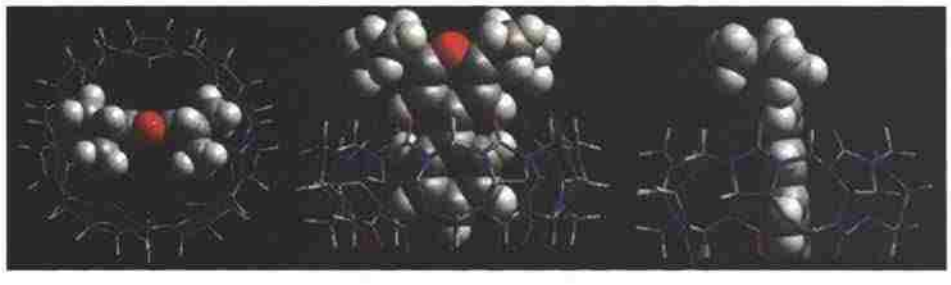

(C) ***t*-Bu-Pylm@CB[7]** (-0.4063 a.u.)

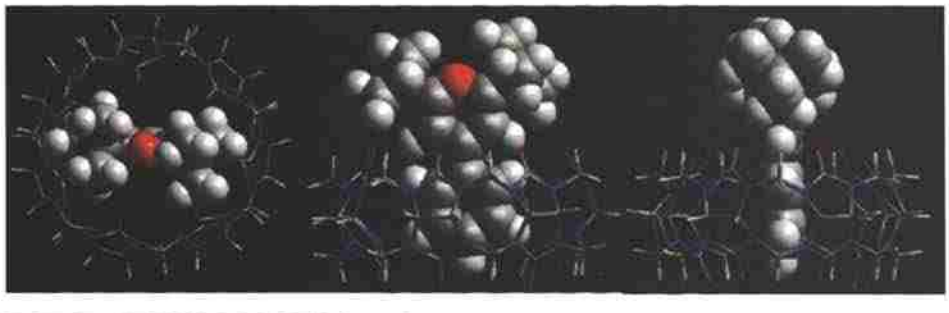

(D) **Ph-Pylm@CB[7]** (-0.2604 a.u.)

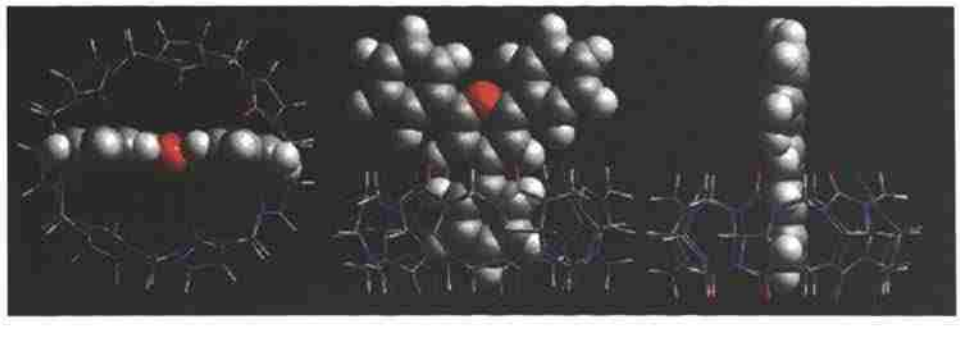

Figure S.4.20. Parts A-D: PM3 calculations for the **Pyrylium@CB[7]** systems as indicated.

7.b **CB[8]** intercalation.

(A) **(Me-Pylm)$_2$@CB[8]** (-0.1902 a.u.)

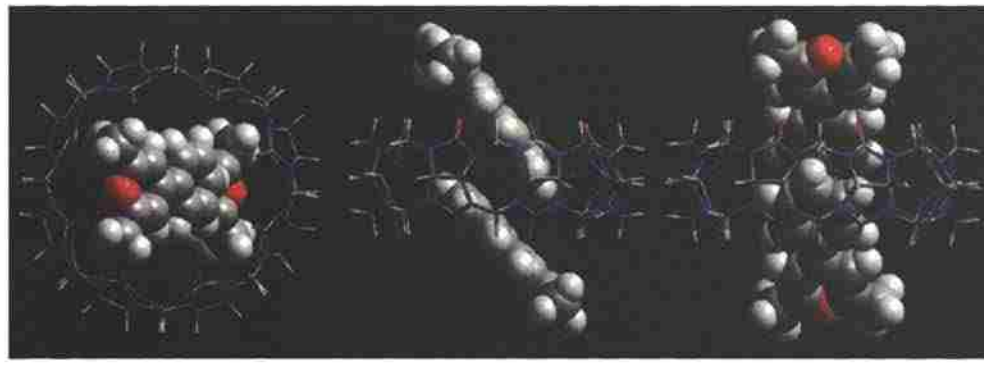

(B) **(*t*-Bu-Pylm)$_2$@CB[8]** (-0.2691 a.u.)

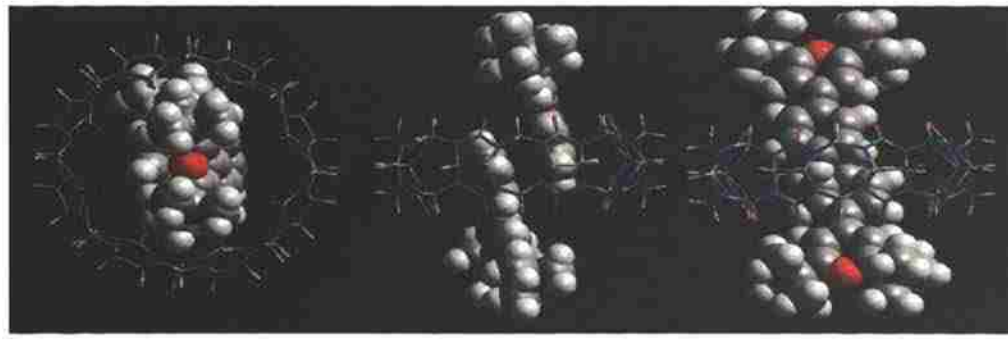

Figure S.4.21. Parts A, B: PM3 calculations for the **(Pyrylium)$_2$@CB[8]** systems as indicated.

Appendix S.4.8: References

S.5.1. Breit, B.; Winde, R.; Mackewitz, T.; Paciello, R.; Harms, K. *Chem. Eur. J.* **2001**, *7*, 3106-3121.

S.5.2. Garcia-Acosta, B.; Garcia, F.; Garcia, J. M.; Martinez-Manez, R. N.; Sancenon, F.; San-Jose, N.; Juan Soto, *Org. Lett.. 9*, **2007**, 2429-2432.

S.5.3. Bordello, J.; Reija, B.; Al-Soufi, W.; Novo, M. *Chem. Phys.Chem* **2009**, *10*, 931-939.

S.5.4. Connors, K. A. "Binding Constants. The Measurement of Molecular Complex Stability." John Wiley and Sons, New York, N.Y. 1987.

SECTION

3. CONCLUSIONS

In paper 1, it has been demonstrated that the hydrophobic cavity of cucurbit[7]uril (**CB[7]**) could be used to control the equilibrium between the ketone and its *gem* diol form. In water, *N*-methyl-4-(*p*-substituted benzoyl) pyridinium cations, **BP-X** exist in equilibrium with their *gem*-diols and concentration of the latter is determined by the nature of *p*-substituents (X). In the presence of **CB[7]**, the equilibrium is shifted towards the keto form which undergoes inclusion. This study reveals that the stabilization of benzoyl group inside the **CB[7]** cavity exceeds the hydrogen bonding stabilization of *gem*-diol in aqueous environment.

Paper 2 has been focused on studying the heterogeneous electron transfer on complexes of **CB[7]** with *N*-Methyl-, *N*-benzyl- and *N*-hexyl-4-benzoylpyridinium monocations (**Me-BP**, **Bz-BP** and **Hex-BP**, respectively). These guests, based on their hydrophobicity, orient either *endo*-or *exo*- and all the three complexes, irrespective of their orientations, show reversible simultaneous e-transfer from the free guest and quasi-reversible process from the complexes.

In Paper 3, *N,N'*-dimethyl-2,6-diaza-9,10-anthraquinonediium dication (**DAAQ**) was chosen as an extension of studying the keto to *gem*-diol equilibrium by host guest chemistry. This compound not only exists in equilibrium with its *gem*-diol form, but also forms aggregates in water. In strongly acidic media, the aggregates break up and equilibrium shifts exclusively towards the quinone form. Under both neutral and acidic conditions, the quinone form undergoes inclusion with **CB[7]** by slow exchange in which both free and **CB[7]**-intercalated forms were observed by ^{1}H NMR.

In Paper 4, in order to understand the role of guest's size, shape and size of cavity during the inclusion process, 2,6-disubsituted-4-phenylpyrylium cations **(Pylm)** were chosen as guests with **CB[7]** and **CB[8]** as hosts. The size and shape of the guest was modified by changing the nature of the substituents at 2 and 6 positions (**Me, *i*Pr, Ph, *t*-Bu**). These pyryliums exist as dimers in water and as such they enter the **CB[8]** cavity (2:1 complexes) whereas with **CB[7]**, the dimers break up forming 1:1 complexes. All pyrylium guests form inclusion complexes by inserting the 4-phenyl part of the molecule

with both hosts, expect the ***i*Pr-PyIm** guest which forms an inclusion complex with **CB[8]** by placing the isopropyl group inside the cavity. These studies reveal that intercalation is controlled by an interplay of size and hydrophobicity of guests, solvation effects, and size and flexibility of the hosts.

VITA

Arumugam Thangavel was born on November 13, 1977and raised in Pondicherry, a small, beautiful sea-side city in India. He got his Bachelor's and Master's degrees from Pondicherry Central University and came to Missouri S&T (UMR) to pursue a Ph.D. in organic chemistry in the fall of 2004. In the spring of 2005, he joined Prof. Chariklia Sotiriou–Leventis' group as a Ph.D. graduate student. During his stay at Missouri S&T (UMR), in addition to his research, he was responsible for teaching recitation for organic chemistry I&II, and general and organic chemistry laboratories. He has published 3 and submitted 2 papers from his Ph.D. work.